FRUCTOSE AFFECTS THE GROWTH OF LONG BONES IN MICE INDEPENDENT OF KETOHEXOKINASE

By

EDEK ALEX JOEL WILLLIAMS

A dissertation submitted to the

School of Graduate Studies

Rutgers, The State University of New Jersey

In partial fulfillment of the requirements

For the degree of

Doctor of Philosophy

Graduate Program in Biomedical Engineering

Written under the direction of

J. Christopher Fritton

And approved by

_____

_____

_____

_____

_____

New Brunswick, New Jersey

May 2019

ABSTRACT OF THE DISSERTATION

Fructose Affects the Growth of Long Bones in Mice Independent of Ketohexokinase

By EDEK ALEX JOEL WILLIAMS

Dissertation Director:

J. Christopher Fritton

Current trends in the Western-pattern diet are replacing bone-fortifying, calcium-rich beverages and foods with sweetened artificial alternatives. High-fructose corn syrup has only been used as a popular sweetener since 1970. Diet may impact growth by limiting the bioavailability of nutrients required for bone to reach its full genetic potential. The effects of reduced calcium, in animal models and man, have been studied extensively and in the work to be presented I uncovered that low calcium diet results in lower bone cellularity, i.e., fewer incorporating osteocytes per bone tissue volume. However, the current understanding of fructose and its effects on bone growth are varied, due to the absence of a standardized model and standard fructose administration regimen. Fructose is metabolized in the cytoplasm by the enzyme ketohexokinase (KHK), and excessive consumption may affect bone health. Specifically, previous work in calcium-restricted, growing mice demonstrated that fructose disrupted intestinal calcium transport. I hypothesized that the observed effects on bone were KHK-dependent and examined the effects of fructose on the long bones of growing mice in a series of studies. Congenic mice with intact KHK (wild-type, WT) or global knockout of both isoforms of KHK A/C (KHK-KO), were fed control diets or administered fructose either through diet or implanted osmotic pumps for 8 weeks. I found that dietary fructose increased by 40-fold plasma

fructose in KHK-KO compared to controls ($p < 0.05$). Plasma fructose was less effected due to pump administration. Obesity (no differences in epidydimal fat or body weight) or altered insulin, was not observed due to the fructose levels introduced. Longitudinal growth of the femur long-bone was inhibited in the KHK-KO mice fed 20% fructose. Unexpectedly, fructose feeding resulted in greater bone mineral density, percent volume and number of trabeculae in the distal femur of KHK-KO. Moreover, higher plasma fructose concentrations correlated with greater trabecular bone volume, greater work-to-fracture in three-point bending of the femur mid-shaft, and greater plasma sclerostin. Since the metabolism of fructose is severely inhibited in the KHK-KO condition, the new results combined with additional data generated during the completion of this dissertation suggests that fructose reaching the lower intestine may affect bone growth through an interaction with the microbiota. Future pursuit of this line of research is important as the effects of increased fructose consumption on bone during growth may influence the future risk for osteoporotic fracture.

DEDICATION

Dedicated to my mother and father

and the

Boys and Girls of:

Jamaica

New York

and

New Jersey

Acknowledgements

This document is an acknowledgment that no man is an island and that an individual's work is buoyed by the support of a great community. This work would not have been completed without the patience and guidance of my thesis advisor, Dr. J. Chris Fritton and collaborators Dr. Ronaldo Ferraris and Dr. Veronique Douard. I would like to thank the members of my committee: Dr. Patricia Buckendahl, Dr. Noshir Langrana Dr. Adrian Mann and Dr. Maribel Vazquez. I would like to thank my collaborators, Dr. Keiichiro Ishimoto, Dr. Kunihiro Kishada, Dr. Yves Sabbagh and Dr. Chirag Patel. I would like the acknowledge fellow lab members, past and present: Dr. Joseph Geissler, Dr. George Pellegrino, Dr. Devendra Bajaj and Brian Canter. Your support and objectivity have made the daily challenges of this thesis work less daunting. I would like to thank Dr. Phillip Payton, Dr. Mitchell Schaffler and Dr. Courtney St. Prix for creating the programs that introduced me to Biomedical Engineering at an early age. I would like to thank the undergraduate labs that were opened to me and for the valuable experiences in bone biomechanics and imaging. I would like to thank Dr. Ian Xu, Dr. Paolo Palachio and Dr. Ericka Calton for their mentorship. I would like to thank my graduate school classmates for levity during trying times. Namely, Dr. Emmanuel Ekeueme, Dr. Renea Faulknor, Dr. Antoinette Nelson, Dr. Joseph Kim, Dr. Brittany Taylor, Dr. Mathew Long, and Dr. Saurav De. I would like to thank the faculty and staff of Rutgers, Dr. David Schreiber, Dr. Joseph Freeman, Dr. Edouard Azzam, Linda, Stratos, Mayra Barreto, Beatrice Suffrant, Luke Fritzky, Ms. Diane, Ms. Annie, Ms. Gierve and security and animal facility personnel. Lastly, I would like to acknowledge the support of my family, my mother, my sister, niece, aunts and uncles and cousins. All I do has been for you.

Table of Contents

List of Tables

List of Illustrations

Chapter 1 : Introduction

The human diet has evolved as technology has allowed us access to different foods. The Western diet is a far departure from our most rudimentary food staples. The diets of pre-agrarian hunter-gathers are believed to have consisted of approximately 35% meat and 65% plant foods, with limited to no access to dairy products and cereal grains (1). Around 10,000 BCE our habits changed and we gave up nomadic life and attached ourselves to specific plots of land, and introduced dairy and we began consuming cereal grains, like corn (2). Though pre-history didn't record the effects of the agricultural revolution, today we see the effects of dairy consumption during growth, as it supports a larger bone structure, resistant to fracture. Around the 1800s and for the next 200 years, the Western diet has been refined. The unprecedented connectedness of the world facilitated by mercantile trade and the processing of food by the industrial revolution set forth the development of a diet that aimed to be palatable over being nutritive and supportive of health, especially during growth.

Changes in our utilization of natural and human resources have shifted our dietary patterns. During the 1800s, 95% of all Americans consumed foods produced primarily on their own farms, by the 1900s, only 60% of Americans lived on farms (2). By the end of the 2000s, approximately 75% of uniquely formulated consumer foods in the United States contain sweeteners (3). Of which 73.5% contain caloric sweeteners and 1.5% contain non-nutritive sweeteners (3).

Food science has allowed us to preserve, fortify and synthesize foods, replacing the land with supermarkets as our access points to metabolic energy. Today most Americans rely on others to produce, distribute and even prepare the food they consume; limiting their influence on what is going into their bodies. The work presented here aims to replace that limited influence with knowledge to inform better habits. Within the scope of bone health, we show that calcium is an integral part of bone growth, and that fructose consumption affects bone when systemic fructose concentrations are high.

Fructose

Glucose, galactose, fructose and mannose are the most important 6-carbon monosaccharides (hexoses) physiologically. These sugars serve as carbon sources for cellular respiration, the production of adenosine triphosphate (ATP, the energy currency of the body), and form the backbone of nucleic acids (see the section, *Bone and the Regulation of Energy Balance*, below. Free monosaccharides are found in significant amounts in fruits (4). Sucrose, a dimer of glucose and fructose, is found naturally in many plants. Sugarcane (Saccharum officinarum), is indigenous to New Guinea and one of the first natural sources, from which, humans have extracted sucrose (5). Western civilizations was first introduced to cane sugar and sugar refinement in 510 BC, by Persian soldiers invading the Indus River (5). Sugar was once considered a luxury item, reserved for peoples and occasions that afforded its use. It wasn't until the advent of New World plantations and sucrose extraction from beets in the 1800s, that sucrose use became more ubiquitous. (5). Sucrose was the dominant sweetener in the Western-Pattern Diet (western diet), until the 1970s, when advancements in biochemistry allowed for mass production of refined crystalline fructose

and High-Fructose Corn Syrup (HFCS) (6-8). Since the 1970s, refined sucrose consumption declined while HFCS use increased more than 700%. HFCS is produced by converting corn syrup, the 100% glucose containing product of breaking down corn starch. Corn syrup is then enzymatically converted to fructose by glucose isomerase. Each HFCS formulation contains a standardized percentage of fructose and is diluted with glucose and water before use in food products (Table 1-1).

Formula	% Fructose	Use
HFCS42	42%	Baked Goods (9).
HFCS55	55%	Beverages (9).
HFCS65	65%	Beverages (10).
HFCS90	90%	Mixed to create lower concentrations

Table 1-1 Formulations of High Fructose Corn Syrup, their respective fructose concentrations and uses.

The fructose content in beverages sweetened with nutritive sugars range between 7-15% (4). HFCS and crystalline fructose are now used extensively to enhance sweetness in soft drinks, baked goods, canned fruits, jams, jellies and dairy products (8, 11, 12). The widespread use of fructose in foods has increased overall use of sweeteners during that period (6-8, 11-13). Today, a person consuming the typical Western Diet ingests 49g fructose/day with about 12g coming from natural sources (14).

Sweetness is an innately attractive taste, a primordial indication of readily available energy. Taste perception begins on the tongue and soft palate, where taste receptors distributed

throughout the tongue sample the oral cavity. The sweet receptor is a dimeric G-protein coupled receptor composed of T1R2 and T1R3 subunits. Binding a single subunit elicits the sweet response, but the binding of both enhances it. These receptors interact with sugars (i.e. sucrose, fructose, galactose, glucose, lactose, and maltose), amino acids (i.e. alanine, glycine and D-tryptophan), sweet proteins (monellin and thaumatin), and non-nutritive sweeteners (i.e. acesulfame K, aspartame, cyclamate, dulcin, neotame, saccharin, and sucralose) (9). Sweetness is scaled relative to sucrose, and fructose is the sweetest (1.17 times more than sucrose) of natural sugars (Table 1-2).

Sweetener	***Type of Substance***	***Sweetness Relative to Sucrose***
Lactose	Disaccharide	0.16
D-Galactose	Monosaccharide	0.32
Maltose	Disaccharide	0.33-0.45
Sorbitol	Sugar Alcohol	0.54
Mannitol	Sugar Alcohol	0.56
D-Xylose	Monosaccharide	0.69
D-Glucose	Monosaccharide	0.74
L-Glycine	Amino Acid	0.76
Sucrose	Disaccharide	1.00
Xylitol	Sugar Alcohol	1.05
Alanine	Amino Acid	1.14
D-Fructose	Monosaccharide	1.17
D-Tryptophan	Amino Acid	49.11
Aspartame	Artificial Sweetener	180
Saccharin	Artificial Sweetener	300
Splenda	Artificial Sweetener	600
Thaumatin	Sweet Protein	~100000
Monellin	Sweet Protein	~100000

Table 1-2: Relative sweetness of biologically safe substances to sucrose.

Complex carbohydrates, such as starch and inulin, are digested through the process of hydrolysis into oligosaccharides, then into free di- and monosaccharides. The absorptive capacity for fructose is less than for glucose and sucrose and the addition of glucose

facilitates the absorption of fructose (8). Fructose enters the intestines at a rate twice that of glucose, with gastric emptying slowing with increasing fructose concentrations (15). Fructose is first absorbed by the small intestine via facilitated diffusion. Fructose transport across the cellular membrane is facilitated through glucose transporters (GLUTs). (Figure 1-1). Interestingly, the absorptive capacity of fructose derived from a sucrose load is greater than when fructose fed as a monosaccharide, though the mechanism is not fully understood (16).

GLUTs are transmembrane sugar transporters; GLUTs [2,5,7,8,9,11] in particular contain a common motif that facilitates fructose transport (17). These transporters are found in a variety of cells and are involved in transport of multiple sugars and molecules. The main GLUTs involved in fructose transport are GLUT2 and GLUT5. GLUT2 transports both glucose (Km = 17mM) and fructose (Km = 16 mM) and is found in kidney, liver and pancreas beta cells (14). GLUT5 is primarily expressed by the enterocytes of the jejunum and hepatocytes, but also expressed in kidney, skeletal muscle, hypertrophic chondrocytes, adipocytes and cilial cells (11, 18). GLUT5 is the only member of the GLUT family which has specificity for fructose and no other sugars (17), with a high Km of 6-10Mm (14). Radiolabel tracing with 6-Deoxy-6-[^{18}F]fluoro-D-Fructose (6-FDF), has shown that fructose is present in the blood, lung, liver, small intestine, kidney, heart, bone, pancreas and brain within two minutes after ingestion (19). For most of these tissue sites where fructose accumulates, fructose specific GLUTs are present.

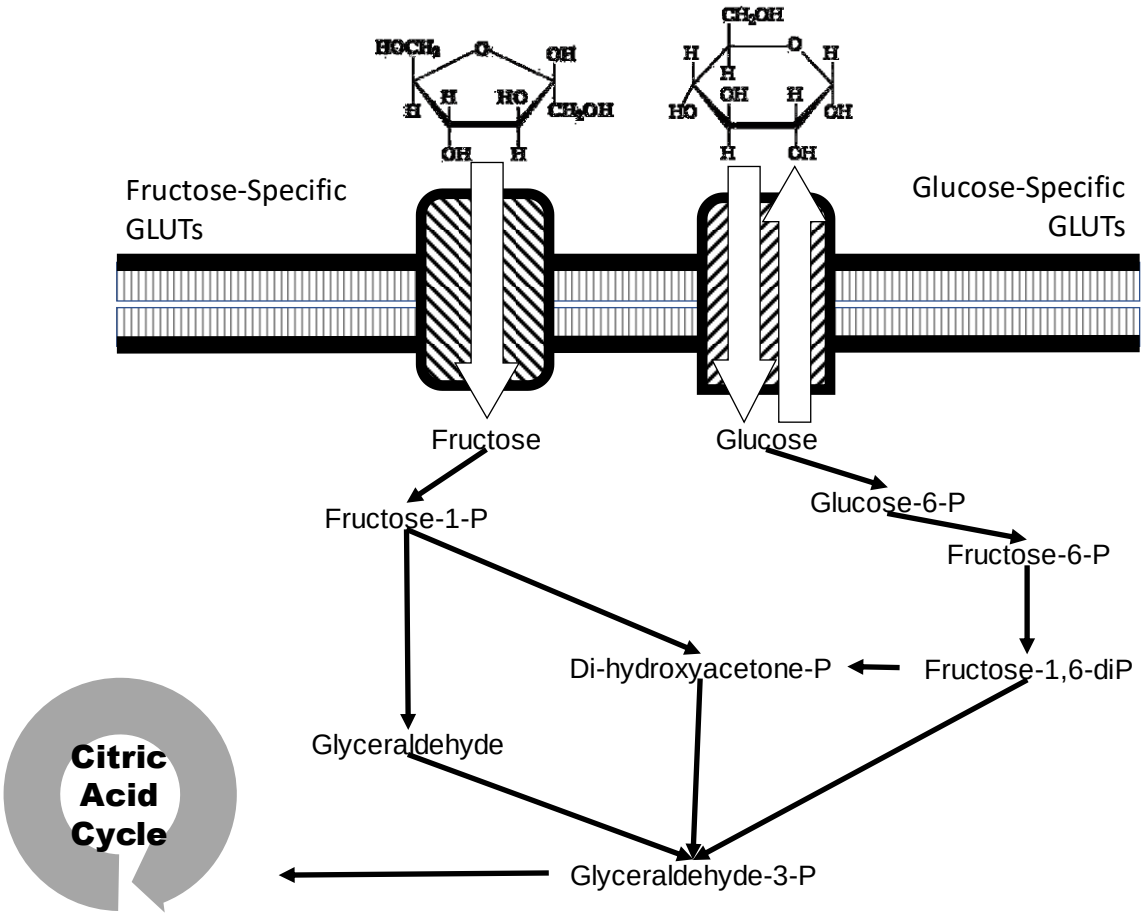

Figure 1-1: Fructose and glucose are initially metabolized differently. Glucose has an extra metabolic intermediate and is more tightly regulated than fructose. The Citric Acid Cycle liberates energy in the form of ATP from sugars.

Glucose and fructose are metabolized differently (Figure 1-1). Both sugars are primarily metabolized by the liver. However, KHK is most abundant in the liver, constituting between 0.04-0.06% of the total organ protein (20), and gene expression is found in the kidney, intestine, brain, pancreas, lung, muscle and optic nerve (21). Hexokinases that metabolize glucose exclusively are ubiquitous and glucose is the primary energy source of most cells. Glucose metabolism is limited by phosphofructokinase in a key regulatory step

of glycolysis; however, fructose is not. This allows carbons to readily and continuously enter the glycolytic pathway and uncontrollably produce glucose, glycogen, lactate and pyruvate (7, 8, 11, 13).

Fructose metabolism provides a free-flowing source of carbons to produce pyruvate, lactate, Acetyl-CoA and triglycerides (11, 12). D-fructose, the naturally found enantiomer of fructose, is primarily converted to D-fructose-1-phosphate by fructokinase/ketohexokinase (KHK), in organs such as liver, gut and kidneys after which the phosphate is cleaved by aldolase B to glyceraldehyde and dihydroxyacetone phosphate (DHP). Human hepatic KHK has an apparent Km for fructose of 0.86 mM; its high V_{max} allows very rapid metabolism while bypassing a regulatory step, as seen in glycolysis (22). These two metabolites, the favored products of fructose metabolism, lead to glycolysis, gluconeogenesis, glyconeogenesis and lipogenesis. D-fructose is also, though with lower affinity, phosphorylated to D-fructose-6-phosphate, an intermediate of D-glucose catabolism, by KHK (8, 11, 19). Unlike glucose metabolism, which is regulated by insulin, glucagon and phosphofructokinase, fructose availability is the rate-limiting step in conversion of d-fructose to fructose-1-phosphate by KHK in the liver and kidney. Due to the lack of a feedback mechanism, all the fructose entering the cell is rapidly phosphorylated, which can rapidly deplete ATP stores and lead to uric acid formation (23, 24). Energetically spent ATP, in the form of AMP, is degraded to hypoxanthine and then to uric acid by XOR (24).

There are multiple enzymes that can convert fructose into other products (Table 1-3). Fructose can also be converted to fructose-6-phosphate by hexokinase I, II, and III though this is believed to occur only in the absence of glucose. Other enzymes that are reactive to fructose include fructose dehydrogenase (Km = 5mM), fructose 3-phophokinase (Km = 30mM), sorbitol dehydrogenase (Km = 100mM) and hexokinase IV/glucokinase (Km > 100 mM). (21)

Enzyme	Reactivity to Fructose [Km]
Ketohexokinase-A (KHK-A)	7.0 mM
Ketohexokinase-C (KHK-C)	0.80 mM
Hexokinase I,II,III	~3 mM
Hexokinase IV/Glucokinase	~420 mM
Fructose Dehydrogenase	5mM
Fructose 3-phosphokinase	30mM
Sorbitol Dehydrogenase	100mM

Table 1-3: Reactivity of metabolic enzymes with fructose.

KHK is highly specific for fructose, but is able to break down other furan ring sugars, (20) including: L-sorbose, n-tagatose, 2,5-anhydro-n-mannitol, 2,5-anhydro-n-glucitol, 2,5-anhydro-n-lyxitol, and 2,5-anhydro-n-mannose (25). Rodent and human KHK genes are identical and alternative splicing is a feature of both (20). The human KHK gene is located on chromosome 2p23, has 9 exons and spans 14 kb (26, 27). Two exons of the KHK gene, referred to as 3a and 3c, arose by an intragenic duplication and are mutually exclusively spliced into mRNA (21, 26). KHK-C, expressed primarily in liver, kidney and intestine, is well characterized biochemically and is encoded by the mRNA that includes exon 3c (26-28). KHK-A biochemically active and is found in a wide range of tissues, but probably has

lower physiological function due to is low Km (7mM). The two isoforms (KHK-A, KHK-C) differ at 32 positions between amino acid residues 72-115. (26)

Fructose is used minimally by extra-hepatic tissues, though these tissues express the proper metabolic enzymes (8, 19). Fructose is transported from the intestinal lumen to the liver via the portal vein, where 50-75% of the fructose load is metabolized before reaching the systemic blood supply (16, 23, 24). Fasting levels of fructose are on the order of 10^{-5} – 10^{-4} Mol/L (5, 29, 30) . Upon ingestion of 1g of fructose per kg body weight, fructose levels in plasma increase to about 10^{-3} Mol/L; orders of magnitude less than the peak serosal concentrations of glucose, roughly 10^{-2} Mol/L, after ingestion of similar amounts of glucose (11, 23). Fructose absorption appears to be enhanced in the presence of glucose, as would be present during the digestion of sucrose (11, 31).

Fructose enters the bloodstream slower, at lower levels and remains elevated for longer than glucose, when consumed together. When healthy adults were given 24oz soft drink beverages (Dr. Pepper) sweetened with 69g sucrose (34.5, fructose), fructose levels spiked ~50-fold from fasting levels of 5 µM to peaks of 240 µM. Those given the same beverage sweetened with 69.4g HFCS (39.2g fructose), fructose levels rose significantly higher than individuals given sucrose to about 300 µM. Fructose levels were elevated for 3hrs after soft-drink consumption in both groups, while glucose levels rose from 5.5mM to 6.8mM and returned to baseline in 90-minutes (32).

Renal KHK expression in rodents is predominately localized to the straight segments of the proximal tubules, where the largest levels of fructose-1-phosphate and fructokinase activity was found (21). The kidneys metabolize about 20% of an intra venous fructose load, whatever remains after first pass through the liver (33, 34). Though glucose is known to be reabsorbed in the proximal tubules, the low levels of fructose in systemic blood indicate that fructose reabsorption is minimal. Fructose is reabsorbed in the S3 segment of the proximal tubule at a slower rate than glucose (Figure 1-2). It should be noted that the S3 segment lies within the outer medullary stripe and is a common site for chronic renal injury, due to low amounts of oxygen in this region of the kidney (23).

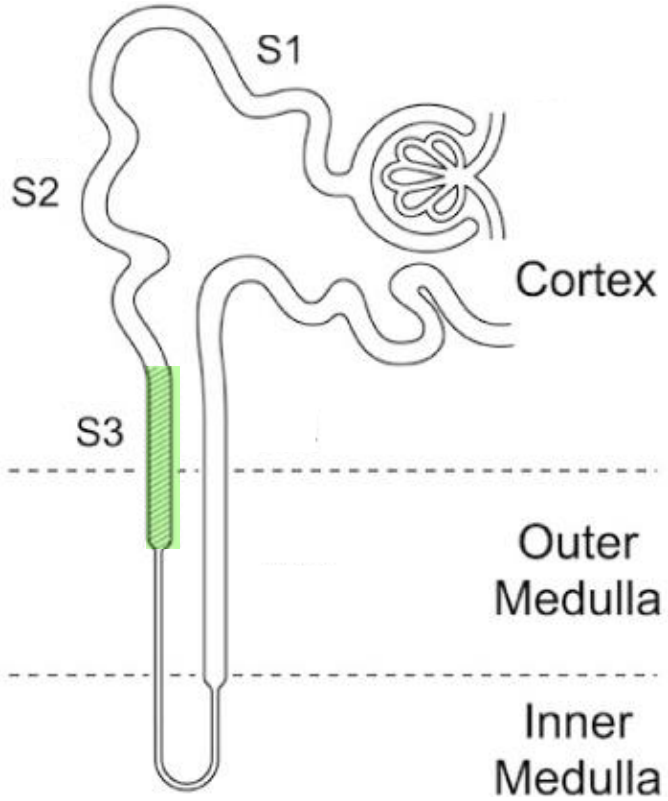

Figure 1-2: Schematic of the nephron. Area shaded represents the S3 segment of the proximal tubule, the site where fructose is reabsorbed.

Fructose impacts the energy control pathways differently than glucose. The chief difference is that fructose does not illicit the insulin response and that increased lipogenesis from rapid metabolism disrupts leptin signaling. Fructose reduces the satiety signal of ghrelin and peptide YY (PYY), increasing total caloric intake due to dysregulation of food intake regulation (35). Acute fructose intake has been shown to increase plasma glucagon-like peptide (GLP-1), but not gastric inhibitory peptide GIP (36-38). The palatability and the reduced ability for fructose to satiate, make over-consumption an inevitability in an environment where fructose is ubiquitous.

The increased fructose load of Western diets has been implicated as a cause of the development of the Metabolic syndrome (MS); a disease state characterized by glucose intolerance, hyperlipidemia, obesity, insulin resistance, diabetes and gout (21, 23, 28). Studies in humans show that fructose intake can induce hypertriglyceridemia, hypertension, hyperuricemia and increased body weight (23). Metabolic syndrome may induce or exacerbate other diseases such as, chronic kidney disease (CKD). Fructose has been shown to accelerate the progression of CKD in a remnant kidney rodent model fed 60% fructose for 6-weeks (23, 39). In this study, accelerated CKD is induced by surgical removal of 5/6ths of the kidney and characterized by: increased protein excretion, elevated plasma BUN and creatinine, decreased creatinine clearance, greater renal hypertrophy and higher mortality (23, 39). Chronic hyperinsulinemia, due to insulin resistance, appears to prevent central leptin signaling, resulting in leptin resistance (35).

Fructose-feeding of rodents has been successfully used to model the effects of insulin insensitivity on bone. Felice et al recently used a young, fructose-fed rat to model the effects of metabolic syndrome on bone. Fructose feeding is a common method of inducing metabolic syndrome and is characterized by elevated plasma glucose, insulin and triglycerides (40). Marrow-derived cells from animals fed fructose had decreased Runt-related transcription factor 2 (RUNX2) expression, a transcription factor associated with osteoblast differentiation, and preferential adipogenic commitment from marrow-cultured cells. Additionally, histology revealed that fructose fed animals had decreased osteocytes density at the growth plate during growth as well as during endochondral bone repair (41).

The fructose-induced metabolic disease model is an effective model for the prolonged utilization of fructose. Studying the effects of fructose on bone is impactful; fructose consumption has never been greater and the effects of prolonged consumption during bone growth are not yet known. Work by Cheeseman et al reveal that fructose travels to bone, as demonstrated by positron emission topography (PET). 6-FDF is a modification of fructose that allows for uptake of the sugar into the cell, but incomplete metabolism leads to enhanced uptake in metabolically active cells. Radioactive 6-FDF is synthesized with standard ^{18}F-fluorination (42). Bone is involved in regulating energy and mineral metabolism and disruption in energy or mineral source could result in poor tissue construction. Targeted evaluations of fructose effects in animal models, including specific bone measures, are needed to determine the role this sugar plays in bone activity (43).

Bone

Movement and support are facilitated by the long bones; which are found in the appendicular skeleton and they are both light-weight and resistant to large static and dynamic forces. Bending and torsional loads are resisted by the diaphysis which consist of a cortical shell around a medullary cavity. Axial forces, compressive, are absorbed by the cancellous bone of the epiphysis and metaphysis. Long bones grow in length by endochondral ossification, in size by modelling and regulate bone mass and tissue density by remodeling (44). Longitudinal growth occurs at the growth plate where proliferative chondrocytes create cartilage that serves as a template for new bone. Circumferential growth is a result of periosteal bone formation and endosteal resorption and remodeling (44, 45). Although longitudinal growth ends in early adulthood, circumferential adaptation to mechanical loads continues throughout life (44).

Bone is a metabolically active organ; with bone cells constituting 2-5% of the organic matter in bone. Within this cell population, 95% are embedded osteocytes (46-48), and the remaining 5% are bone forming osteoblasts, the bone resorbing osteoclasts, and their progenitors from mesenchymal and hematopoietic stem cell niches. Cell-mediated remodeling and cell signaling allow bone to accomplish its primary functions of structural support and protection for soft tissues, the secondary role of storage of microminerals and tertiary role of feedback to the Vitamin D cascade (49).

The osteoblast lineage begins when stems cells in the marrow begin exhibiting a phenotype that supports bone building. Pre-osteoblasts are MSCs that have committed to become bone forming cells. Mature osteoblasts are typically cuboidal cells with a round nucleus and an

abundance of protein production and transport machinery. They arrange themselves as a continuous mono-layer on the bone surface, like the confluent nature of primary and cell-line derived osteoblasts in culture. Their niches are in bone marrow, typically at the interface of marrow and bone. Mature osteoblasts richly express collagen 1 (Col1); selectively express the mineralization aid, alkaline phosphatase (ALP); the matrix proteins: bone sialoprotein (BSP), osteopontin (OPN); and signaling hormone, osteocalcin (OCN) (50-53). They participate in bone formation by producing primarily collagen and non-collagenous proteins (NCPs), generating matrix vesicles and transporting calcium ions (50, 51). Hydroxyapatite (HA), the mineral phase of bone, crystal nucleation occurs within matrix vesicles that bud from osteogenic cells and migrate to the extracellular matrix (ECM) (54). ALP helps recruit inorganic phosphate and allows for the compound to pass through the cell membrane (54). Once in the matrix, calcium influxes into the vesicle allows for the growth of HA crystals and the subsequent association with collagen fibrils (54). Along quiescent bone surfaces are thin elongated, bone-lining cells that are thought to represent an inactive, in terms of mineralization, post-proliferative phenotype of osteoblasts.

During bone formation a small proportion of osteoblasts (10-20%) incorporate into the matrix, lose many of their organelles and experience a reduction in metabolic activity. This final differentiated state of the osteoblast is the bone-resident osteocyte (50). The osteoblast-osteocyte transition is an organized process that includes specific changes in the gene expression pattern (48).

The osteoblast-osteocyte transition is a dramatic change in morphology and function. The cuboidal osteoblast, optimized to produce collagen and mineralize matrix becomes trapped in its own new formed bone, called osteoid. The osteoblast becomes more stellate and begins producing the dendritic processes characteristic of osteocytes. These processes aid in the mineralization of the ECM as well as locate other osteocytes, surface osteoblasts and nutrition sources (55, 56). Osteocytes embed into pockets called lacunae and connect to each other and bone lining cells through cytoplasmic processes passing through the mineralized matrix in thin tunnels called canaliculi (46, 48, 52). In situ analysis of osteocytes function proved difficult due to the cells being entombed in mineralized matrix. Making early theories on the role(s) of osteocytes limited, and mostly controversial.

Osteocytogenesis is not a fully understood process (57); however there is evidence that the process is active. Osteoblasts undergo a number of changes that show active interaction with the cells environment, as it incorporates into the matrix: 1) Active formation of polarized dendritic processes, with cytoplasmic volume reduction which is a dynamic process (55). 2) The osteoid osteocyte, a transient phase, is believed to be responsible for mineralizing the matrix around the embedding cell and not from surface osteoblasts (55, 58). 3) MMP9 is utilized by the transitioning osteocyte to cleave collagen matrix and to 'remodel' its own lacunae (55, 57, 59).

Advances in animal models and imaging modalities have expanded our understanding of the role osteocytes play as endocrine regulator of bone matrix. Bone is directly involved in calcium metabolism through the action of fibroblast growth factor 23 (FGF23). FGF23 is

a feedback mechanism used by bone to regulate plasma 1,25-Vitamin D3 and phosphate. FGF23 is a 251 amino-acid protein secreted by osteoblasts and osteocytes with a putative N-terminal signal peptide (60). FGF23 decreases the expression of NaPi2 in the kidney, reducing the excretion of phosphate (60, 61). FGF23 decrease renal production of 1α-hydroxylase and increases 24-hydoxylase, independent of parathyroid hormone (PTH) and Vitamin D (60, 61). FGF23 works in feedback to vitamin D signaling by decreasing 1,25-Vitamin D3 production and increase breakdown (60, 61). Bone is directly involved in glucose metabolism through the action of osteocalcin. Osteocalcin, also known as bone Gla protein is a secreted 5kDa protein that is the most prevalent non-collagenous protein in the bone extra-cellular matrix (62). Vitamin-K dependent carboxylation of three Gla residues of OCN allow it to tightly bind to HA (62-64). Vitamin-K is a cofactor for glutamate carboxylase, the enzyme required for the carboxylation of OCN (62). OCN with fewer than three carboxylated residues, have a lower affinity for bone and can be found in the plasma; though carboxylated and uncarboxylated forms are found in both bone and plasma (62-64). Uncarboxylated OCN affects travels to the pancreas and alters the proliferation of β-cells (63).

Though the primary task of orchestrating matrix apposition through osteoblasts and matrix resorption through osteoclasts, osteocytes also fulfill their secondary role by readily making available the macromolecules trapped in bone matrix. Osteocytes produce factors that directly regulate remodeling locally, and calcium homeostasis systemically (Figure 1-3). Osteocytes synthesize several factors that modulate osteoblast and osteoclast function, including prostaglandins, nitric oxide (NO), adenosine triphosphate (ATP),

fibroblast growth factor-23 (FGF23), receptor for nuclear factor κ ligand (RANKL), macrophage-colony stimulating factor (M-CSF), sclerostin, matrix extracellular phosphoglycoprotein (MEPE), phosphate-regulating endopeptidase homolog, X-linked (Phex), and dickkopf 1 (DKK1). Osteocytes use these factors to modulate the formation or resorption of bone due to factors such as: mechanotransduction of loads and tissue damage (46, 48, 65). The osteocytic production of FGF23 and the subsequent translocation and activity of this hormone in the kidney, gives bone endocrine functionality.

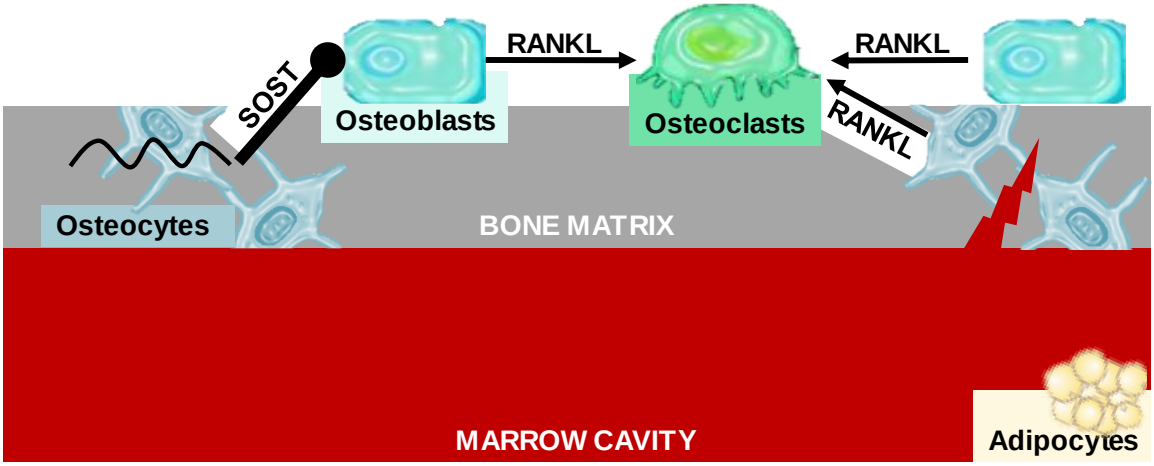

Figure 1-3: Schematic of the interrelation of bone cells. Osteocytes sense mechanical loads and matrix defects and coordinate osteoblast driven bone apposition and osteoclast driven resorption by sclerostin and RANKL secretion respectively.

Cell number depends on two factors, cell division and cell death, and in the case of differentiated cells there is a compound effect of these two factors from each progenitor generation. In the case of osteocytes, they are terminally differentiated cells and do not divide. Between 19%-29% of bone forming osteoblasts, become osteocytes (66). Osteoblast precursors can be affected by age, or disease state. Osteoblast recruitment can

be affected by precursor pool, osteocyte signaling and anabolic signaling. Osteocyte density therefore is a function of the available osteoblast precursor pool, the amount recruited for bone formation and the stimulus for an osteoblast to transition into an osteocyte; in addition to cell death. Osteocyte density can be determined through histology, backscattered electron imaging, confocal microscopy, or corrosion casting followed by SEM and mercury infiltration (67).

A lucky osteocyte will spend its life, of several decades (68), communicating with neighboring cells, metering interstitial fluid flow and interstitial fluid constitutions. While alive, osteocytes sense mechanical signals, by deformation of the cell body due to flow of interstitial fluid through the lacuna-canalicular system. Eukaryotic cells in general are sensitive to mechanical forces (69). In osteocytes and osteoblasts specifically, mechanical strain is transduced to biochemical signals via membrane proteins, integrins, connexins and stretch-activated ion channels. Integrin signaling activates mitogen-activated protein kinase (MAPK) via β1 integrin and focal adhesion kinase (FAK) dependent tyrosine phosphorylation in endothelial cells. FAK brings about MAPK activation via interaction with proto-oncogene tyrosine-protein kinase (c-src), growth factor receptor-bound protein 2 (Grb2) and small GTPase, Ras. FAK activates the γ1 isoform of phospholipase C (PLCγ1), leading to intracellular calcium mobilization. Mechanical stimulation upregulates integrin subunit expression, calcium mobilization and connexin expression.

In response to mechanical loading, osteocytes reduce expression of sclerostin (SOST) and Dickkopf-related protein 1 (DKK1), which antagonizes wingless-related integration site

(Wnt)/β-Catenin signaling in osteoblasts(57, 69, 70). DKKs and allosteric SOST sequester LRP5/6 into complexes with the transmembrane protein Kremens (Kringle-containing protein marking the eye and the nose) and are believed to promote lysosomal destruction(57, 69). Knockout of SOST in mice increased bone mass, cortical bone area, and cortical thickness. Thus, mechanical loading removes the inhibitory force of SOST and DKK1 and stimulates down-stream transcription of RUNX2 (69).

For metabolism to occur in any living tissue, molecular transports must be insured. Molecular diffusion through interstitial spaces is the primary mode of transport in soft tissues and organs. Bone cells do not have this luxury and are limited spatially to nutrient supplies; osteocytes are dependent on the lacunar-canalicular system (71). Osteocytes are washed in a flowing fluid that clears waste, delivers nutrients and humoral information from the systemic circulation. They are sensitive to a variety of systemic hormones with a rapid and efficient communication between osteocytes and systemic circulation (70). Increased contact with the interstitial fluid amplifies the sensitivity of the osteocyte network. The lacuno-canalicular system has approximately 215 m^2 of surface area, filled with osteocytes and their chemo- and mechano-sensitive dendritic processes. Osteocyte density is variable between sampling sites, species, races, ages, as well as other factors. Osteocyte density can decrease with age, disease state and diet. Humans have approximately 42 billion osteocytes embedded in 1.75 x 10^6 mm^3 of bone tissue. (66) Large systemic responses could be made when many individual osteocytes receive the same signal and respond in concert. The scalability of this signal transduction is strongly

dependent on density of osteocytes, their cell processes and fluid flow within the lacuna-canalicular network.

Osteocytes may be signaled to undergo apoptosis through chemical signaling or damage to the extracellular matrix. When osteocytes die, they may trigger the remodeling cascade or their lacunae may simply be filled in with calcium salts (72). It is approximated that 5% of total lacunae are empty and approximately 9.1 million osteocytes turnover each day. This indicates that there is inherent discontinuity to the osteocyte network, however redundancies in dendritic processes mitigates any compromises to signal transduction (73). Histological observations of the fractured hips from patients with osteoporotic fractures showed a reduction in the number of osteocytes (48). Osteocyte density is both an effector of bone quality as well as a readout for bone health.

Osteoporosis is a systemic skeletal disease characterized by low bone mass and deterioration the microstructure of bone tissue. Consequently this deteriorated bone is fragile and susceptible to fracture (74). Osteoporosis is determined from either areal or volumetric bone mass scans, and the diagnosis given when density is greater than -2.5 standard deviations below healthy adult reference population (74). Osteoporosis is a growing global epidemic characterized by increased fracture risk due to poor bone quality. Data from the National Osteoporosis Foundation suggests that 9 million adults in the United States have osteoporosis and 48 million have low bone mass; states of increased susceptibility to fracture. In 2005, incident fracture was estimated at >2million, with women being the greater at-risk population. It is estimated that 1 in 3 women and 1 in 5

men aged 50+ will experience a fracture in their lifetime (75). If current trends of osteoporosis prevalence continue, by 2020, the number of adults 50+ with osteoporosis or low bone mass will grow to 64.4 million and by 2030, the number will increase to 71.2 million (a 29% increase from 2010); with fractures expected to increase as well (76). European figures show that 1 in 8 European Union (EU) citizens 50+yrs fractured their spines in 2006 and that by 2050, hip fracture incidences should increase 135% (74).

Growth

In mammals, the growth and development of an individual determines initial body plan from the whole-organism level fully down to sub-cellular detail. Growth occurs through the enlargement of unitary cells, cell division (proliferation) and development of the extracellular matrix by the growing cell population (77). In large animals, limits on the diffusion of nutrients and waste cause bone tissue to grow through increased cell number.

The endochondral skeleton helped to ameliorate the new stresses that were caused when animals started to first colonize land during the late Devonian period, ~300M years ago (78). Chondrocytes in growth cartilage facilitate longitudinal growth through genetically regulated cell proliferation and maturation. Chondrocyte proliferation and matrix secretion during the hypertrophic phase cause the elongation of bone (79). There are marked differences in cell kinetics and growth rate between humans and small laboratory animals. In the rat, particularly, the growth rate is faster (250 μm/day vs. 35 μm/day); the number of cells produced daily is greater than in humans (80). Humans however, have longer

growth periods (14-15 years) and the life span and inter-mitotic period of the proliferating cells are longer than in rats, which creates a larger organism (80).

Bone growth is greatest during neonatal bone formation and pubertal growth; during these two periods bone is formed and remodeled to accommodate the growing organism. Annual height velocities increase from ~2 inches per year in childhood to a peak of 3.25-3.27 inches per year in adolescence. The end of puberty generally signals the completion of skeletal development, with closure of growth plates at the ends of long bones and in the vertebral column. At this point in time, the "modeling" of new bone tissue, including both longitudinal growth and the addition of new tissue on existing surfaces, becomes limited (81).

Bone mineral stores almost double during puberty, through the increase in skeletal size with minor changes in volumetric bone density. Bone mass accrued during longitudinal growth is accomplished by the converting the cartilaginous growth plate to mature bone tissue. When bone reaches the appointed, genetically determined, length, two things happen: 1) longitudinal growth ceases 2) the epiphysis fuses with metaphysis, as the growth plate disappears (82). This is due to depletion of growth plate chondrocytes by maturation and the cessation of proliferation. By the end of the second decade of life, most of the body mineral capital has been accumulated, though a very small proportion of bone consolidation may occur during the third decade, primarily in males. There are no sex differences in the volumetric trabecular bone density at the end of the period of maturation (83).

During puberty, growth hormone (GH) secretion from the somatotropic cells of the pituitary gland stimulates insulin-like growth factor 1 (IGF-I) in the liver and other tissues (84, 85). Pulsate secretion of growth hormone increases (1.5-3-fold) along with greater than three-fold spikes in IGF-I (84, 86). The changes in body fat distribution, skeletal muscle mass and bone mass seen during puberty are dimorphic and are mediated by GH and IGF and the additive effects of androgenic hormones (86). In mice, the pubertal period lies between 4-8 weeks of age, and is marked by peaks in GH and rapid changes in femoral size and shape are observed (85). After secondary sexual development is complete, GH and IGF-I levels fall to prepubertal levels (84). The pubertal phase contributes 15-20% of final height and precedes senescence of the growth plates (84).

Longitudinal bone growth is influenced directly by several systemic hormones, GH, IGF-1, glucocorticoids, thyroid hormone, sex hormones, vitamin D and leptin. GH enhances the recruitment of resting zone chondrocytes and local IGF-I production in the growth plate (84). In adolescents, the peak of longitudinal growth precedes peak bone mass accrual by 2-3 years, highlighting some dissociation between longitudinal growth and bone mass accumulation (87). Vitamin D status was not found to be a predictor of bone mass, however an increase in 1,25VitD3 in the early stages of puberty may be in anticipation of an incipient calcium demand (88). Loss of GH during puberty appears to hinder both transverse and longitudinal growth (85). *In vitro*, IGF-1 has been observed to be a mitogen for preosteoblasts and promotes their ability to mineralize in culture (89). In a mouse model, knockout of liver IGF-1 (LID) longitudinal long-bone length is unaffected but the

bone is slender bone with reduced cortical bone area. Conversely, growth hormone receptor knockout (GHRKO) mice have both reduced femoral length, and cortical bone area (85).

Puberty is the period during which the sex difference in bone mass become expressed (87). Males have greater mean areal BMD values than females due to a more prolonged period of pubertal growth rather than greater maximal rate of bone accretion (87). In boys, GH increases are seen later than girls, at Tanner genital Stage 4 (G4) (84). An observational study of 107 boys and girls between the ages of 9 and 17 showed that GH status correlated strongly with both bone formation (P1NP) and resorption markers (CTX), independently of IGF-I (81).

Fractures during childhood are common among healthy children (90, 91), with approximately 30-50% experiencing fractures (91). Forearm, hand and foot are the most common sites of fracture in children from the US, Europe and Asia (91, 92). The overall incidence of pediatric fracture is more pronounced in boys and occurs during the growth spurt (between the ages of 12-15y) (91). Global estimates are variable; however, boys are estimated to be at a risk of 42-64% fracture incidence and girls 27-40% (90, 92, 93). This variability may depend on the child's condition, age and social and environmental factors (90). Though boys fracture more frequently, girls sustain fracture at an early age (90). It has also been demonstrated that fracturing a bone at a young age increases the incidence of recurring fracture (90-92). It is important to study the etiology of injuries and circumstances and settings in which they occur in the various stages of development to identify risky behavior or an unsafe environment which can be corrected (90). Fracture

rates in children and adolescents are currently increasing, particularly in the forearm. Between 1969-1999 child fracture rates in the US increased by 56% in girls and 32% in boys (92). Between 1986-1995, total fracture rate in children rose by 14% in Japan and 45% in Australia. The magnitude and velocity of these increases suggest an environmental effector (92).

Bone and the Regulation of Mineral Balance

Bone strength is determined by the amount of bone accumulated and the structure developed by the end of skeletal growth (i.e. peak bone mass), and the amount of bone lost and the microstructure degradation occurring afterwards. Peak bone mass is attained, in most parts of the skeleton, by the end of the 2nd decade. There is no evidence of gender difference in bone mass of both the axial and appendicular skeleton at birth (87). It is estimated that 10% increase in peak bone mass could reduce the risk of osteoporotic fractures during adult life by 50%.(83, 87) From a life-course perspective, poor dietary patterns, that tract into adulthood may constitute for fractures seen later in life (91).

Age-adjusted fracture incidence of fracture exponentially increases during the 7th decade (87). Menopause and loss of ovarian function lead to an increase in the prevalence of osteoporosis (87). Quantitative bone traits change over time under the influence of genetic, hormonal, nutritional and other external factors (87). Genetic determinants appear to be the most important, accounting for more than 70% of the variance in bone parameters (87, 94). Nutrition is able to modulate this genetic potential, with effects starting as early as in utero (87). Nutrients that support bone health include calcium, vitamin D, protein, phosphorus,

magnesium, zinc, copper, manganese, vitamin C, vitamin B-12, vitamin K and potassium. Some of these nutrients are essential for skeletal growth and development, some are involved in the formation of collagen or cartilage and some support calcium and phosphate homeostasis (95).

Bone is sensitive to nutritional calcium deficiencies in different periods of life and under some physiological conditions or pharmacological treatments (96). The cells of bone tissue regulate 99% of the body's stores of calcium (97). Calcium and phosphate are fundamental building blocks for hydroxyapatite [$Ca_{10}(PO_4)_6(OH)_2$] (HA), which constitutes 80-90% of bone volume. The intake of these micronutrients is necessary for achieving peak bone mass in the first 20-30yrs of life and maintenance of bone mass, later in life (96, 98). The diet is the only external source of these micronutrients (**Error! Reference source not found.**) and the appropriate intake levels are dependent on age and sex (96). Calcium is considered a threshold nutrient, meaning that bone mass is linearly related to intake below the threshold, but not above it (98). As such, phosphate intake would be reliant on calcium intake to form HA and impose a similar threshold relationship to bone mass.

Calcium-Rich Foods	Serving	Calcium (mg)	Phosphorus-Rich Food	Serving	Phosphorus (mg)
Cheddar Cheese	1.5 oz	303	Yogurt, plain nonfat	8 oz	385
Milk	8 oz	300	Fish, salmon	3 oz, cooked	252
Yogurt	8 oz	300	Milk, skim	8 oz	247
Fruit Punch w/ Calcium Citrate Malate	8 oz	300	Lentils	½ cup, cooked	178
Tofu, Calcium set	½ cup	258	Beef	3 oz, cooked	173
Rhubarb	½ cup, cooked	174	Chicken	3 oz, cooked	155
Spinach	½ cup, cooked	115	Almonds	1 oz (23 nuts)	134
White Beans	½ cup, cooked	113	Cheese, mozzarella; part skim	1 oz	131
Bok choy	½ cup, cooked	79	Egg	1 large, cooked	104
Kale	½ cup, cooked	61	Bread, whole wheat	1 slice	57

Table 1-4: Common foods that are known to be rich in calcium and phosphorus. Dairy products are rich in both.

The tight control of plasma calcium and phosphate is important to the performance of many physiological functions. Calcium is an essential nutrient required for physiological processes such as: nerve conduction, muscle contraction, cell adhesion, mitosis, blood coagulation, and secretory activity (96, 99-102). Failure to maintain calcium stasis appears to be a common factor linking conditions such as hypertension, insulin resistance and obesity, as well as risk of breast and colon cancer (96). Phosphate is vital to intracellular signaling (IP3, cAMP, cGMP), oxidative and protein phosphorylation, as a component of membrane lipids and to build the backbone of DNA and RNA (102-107). Phosphate stasis in vertebrae animals is maintained through a set of highly conserved sodium-dependent phosphate co-transporters NaPi-IIa,b,c (NaP2a,b,c) (104). Plasma phosphate levels are maintained through activation of these pumps by hormones, which efficiently prevent hypo/hyper-phosphatemia in response to phosphate intake and either condition is an indication of overall dietary deficiency (98, 104, 108). Dysregulation of phosphate may lead to hypophosphatemia, the effects of which include: anemia, cardiomyopathy, muscle weakness, bone pain, rickets/osteomalacia, diminished immunity, or even death (7).

Metabolism of calcium and phosphate within the body is controlled by a four-tissue axis of parathyroid gland, intestine, kidney and bone that keeps plasma concentrations of calcium within a narrow range (102, 109). The principle calcium sensors that regulate bone calcium uptake are in the parathyroid gland which produces parathyroid hormone (PTH), in periods of low plasma calcium to phosphorus ratio (97). PTH regulates calcium indirectly by increasing bone resorption through RANKL production in osteoblasts. While

directly acting on kidney by increasing calcium and phosphate reabsorption, and triggering secondary signaling of 1,25-Vitamin D3 (1,25VitD3) (104). Vitamin D is first synthesized from 7-dehydrocholesterol in skin, when exposed to ultraviolet light (290-315nm) and is hydroxylated by the hepatic cytochrome P-450s (CYPs) in the liver to 25-hydroxyvitamin D (25VitD3) (110, 111) (Figure 1-4).

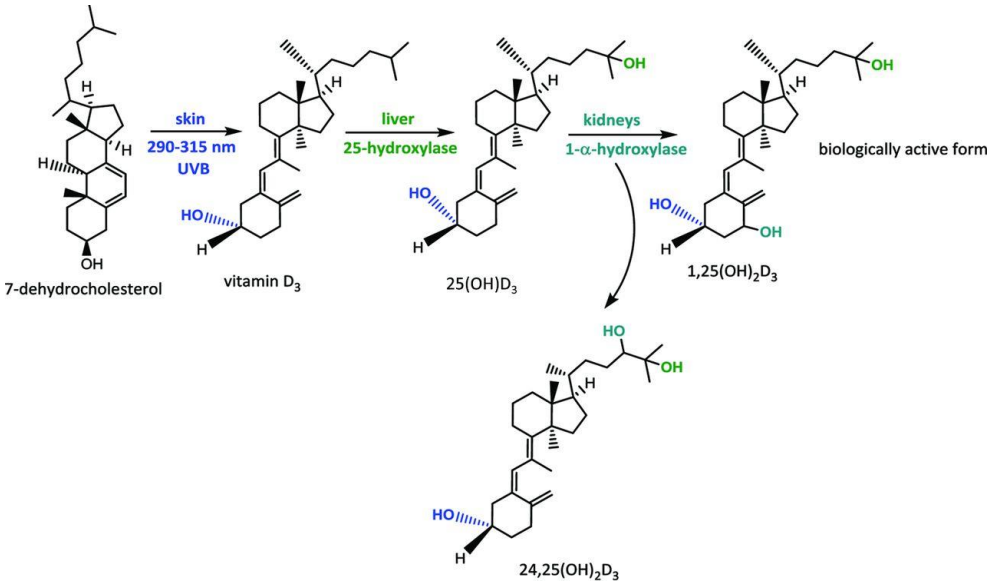

Figure 1-4: Vitamin D is synthesized from 7-dehydrocholesterol which is converted to Vitamin D3. Hepatic 25-hydroxylase converts Vitamin D3 to 25VitD3, the most abundant form systematically. The kidneys coverts 25VitD3 to 1,25VitD3 using1-α-hydroxylase at which point it is biologically active. When no longer needed 1,25VitD3 is deactivated to 24,25VitD3.

Renal CYPSs (CYP24a1 and CYP27b1), which degrade and activate the hormone respectively, expressed by cells in the proximal tubule tightly regulate plasma 1,25VitD3 concentrations (110). The activation of 1,25VitD3 by the CYP27b1 is affected by PTH, Vitamin D and FGF23 and rate limits 1,25VitD3 production (110). Clinically, it is easier to measure 25VitD3 than the activated 1,25VitD3 due to the binding to the vitamin D

binding protein (VDBP) and the much higher levels of 25VitD3 (nM) than 1,25VitD3 (pM) (110).

The Vitamin D cascade is a multi-organ feedback loop that efficiently keeps plasma Ca^{2+} concentrations stable (Figure 1-5). 1,25VitD3 acts directly on bone by increasing bone remodeling activity, by inducing osteoblast and osteoclast differentiation and secondarily activating FGF23. 1,25VitD3 also acts directly on the intestine by increasing calcium absorption from the intestinal lumen through the increased expression of Transient Receptor Potential Cation Channel Subfamily V member 6 (TRPV6) and Calbindin D9k (CaBP9k) (112-116). 1,25VitD3 binds to the Vitamin D response element (VDRE) a promoter region on vitamin D regulated genes, like TRPV6 and CaBP9k. Increased TRPV6 and CaBP9k expression, facilitates calcium transport through the epithelium of the small intestine. FGF23 increases phosphate clearance by decreasing NaPi2c expression and reduces the activation of 1,25VitD3. FGF23 regulates Vitamin D activation by the MAP kinase signaling pathway (117). When FGF23 binds to a FGF receptor, FGFR isoforms 2c and 3c, in the presence of its co-receptor Klotho, serine phosphorylation through extracellular signal-regulated kinase (ERK1/2) and plasma glucocorticoid-regulated kinase-1 signaling (SGK1) (61, 117). FGF23 also acts directly on the parathyroid gland by reducing PTH levels (104). Recently, in work that I helped conduct and outlined in Chapter 2, increased levels of the dietary sugar fructose were shown to interfere with calcium (Ca^{2+}) and phosphate metabolism in adult mice through 1,25VitD3/FGF23 dysregulation (114, 115, 118). Specifically, the normal adaptive increases in intestinal and renal Ca^{2+} transporter expression and activity (through CYP27B1 coding for 1a-hydroxylase in

kidney) during low Ca^{2+} feeding was not exhibited in mice fed high fructose diet. Thus, serum 1,25VitD3 levels did not compensate for the low availability of Ca^{2+}.

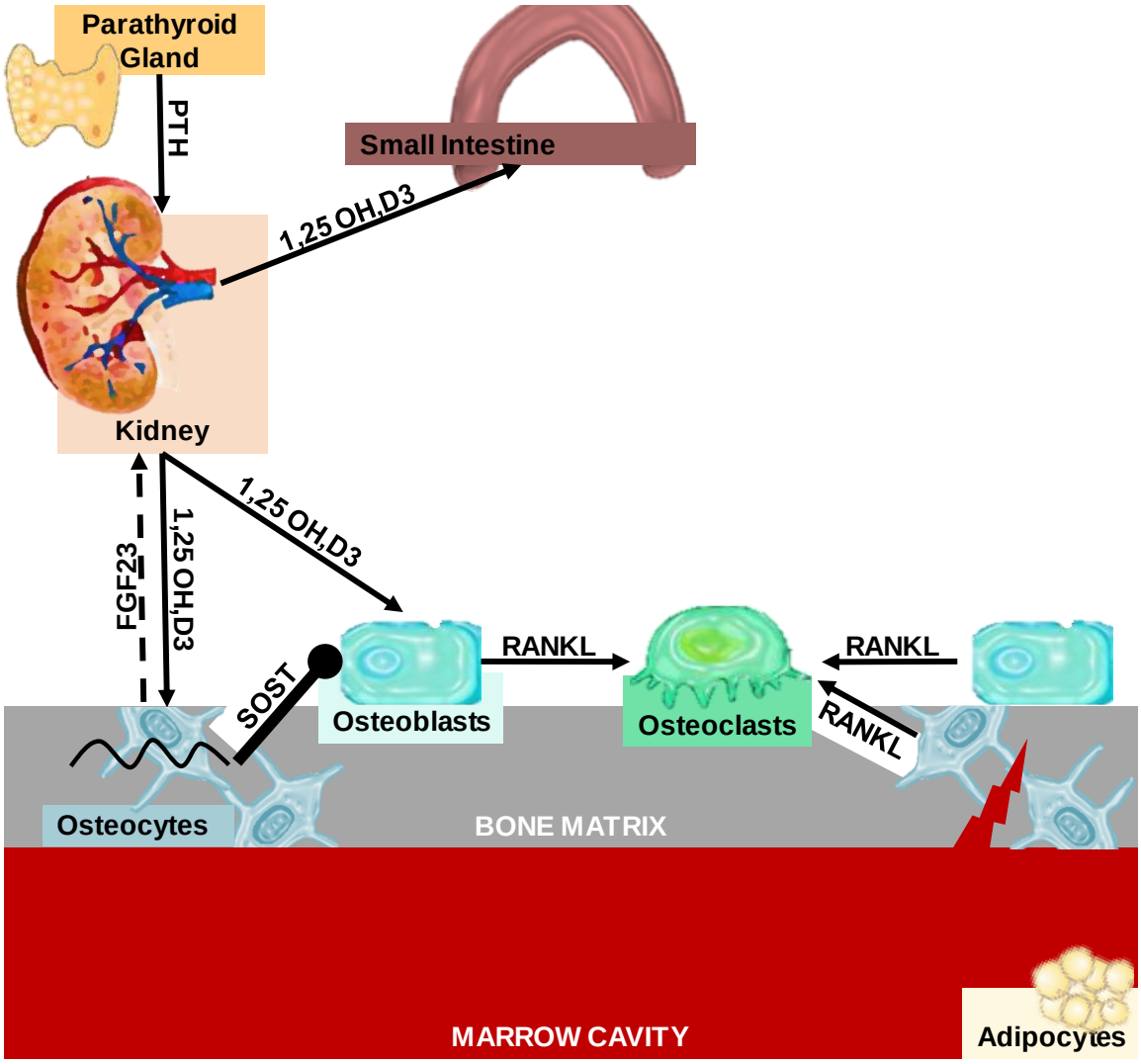

Figure 1-5: Bone cells are involved in calcium regulation as part of a 4-organ axis that utilizes PTH, 1,25OH,D3 and FGF23 to regulate the storage, reabsorption and clearance of calcium.

In Western countries, more than two-thirds of dietary calcium intake is derived from consumption of milk and dairy products (119). Milk and dairy products provide an efficient vehicle for energy, protein, micronutrients and bioactive compounds that support bone growth and development (107). Calcium-fortification, supplementation and natural sources account for the remaining third (107). Calcium supplementation is used by 30-50% of older women in the western world for preventive treatment against osteoporotic fracture (120).

Milk is a liquid produced by mammals to nourish their young but has become a staple within the human diet at all ages. The composition of the milk from placental mammals (humans, rodents bovines and canines) reflects maternal nutritional habits and lactation durations (121). Milk is an energy-packed nutritive colloid of sugar, protein, fat, minerals and vitamins suspended in water, needed to support the energy intensive process of neonatal growth (122). The addition of milk from other mammals, particularly ungulates like goats, sheep and cows, has given the human phenotype greater stature and stronger bones.

Milk fat is present primarily as globules and contains more than 400 different fatty acids, making it among the most complex fats (107). Milk fatty acids are either derived from feed or from the microbial activity in the rumen. Approximately 70% of fat fraction is composed by saturated fatty acids (SFAs) and 30% unsaturated fatty acids. Short-chain fatty acids (SCFA) make up about 11% of SFAs, consisting mainly of butyric (4.4%) and caproic (2.4%) acids (107, 122).

Calcium is the mineral most identified with milk, representing the greatest fraction of 20 essential minerals. In children and adolescents from the US, milk contributes 50% or more of total calcium intake (107). A typical serving size of milk (200mL) provides about 22% of the US recommended daily allowance (RDA) for 19-50 year-old individuals (74). The average concentration of calcium in milk is 1200mg/L, distributed between the micellar and aqueous phases. In the micellar phase, it is associated with phosphoseryl residues of casein, whereas in the aqueous phase, calcium can bind to whey proteins or inorganic forms of phosphate-forming salts (122).

Phosphorus is abundant in milk, with a typical serving size providing 25% of the US RDA for 19-50 year-old individuals (74). The average concentration of phosphorus in milk is about 950mg/L in both organic and inorganic forms. Organic phosphate is bound to organic molecules like proteins, phospholipids, organic acids and nucleotides, which are present in the micellar phase. Inorganic phosphate corresponds to the ionized phosphate, which depends on pH levels and is in the aqueous phase (122). Dietary phosphorus intake has risen in the past 30 years, by 10-15% due to the addition of phosphate salts and cola (phosphoric acid) to our diets. It is believed that low calcium to phosphorus ratios, the order of 1:4, can elevate PTH levels, inducing the Vitamin D cascade (74). Bone has a Ca/Pa ratio between 1.7 and 2.2, which is like the ratio found in human milk (2.2) and much higher than cow-milk (~1.3), making milk an adequate source for both macrominerals.

Though considered a good source of Vitamin D, milk itself does not present considerable amounts unless fortified (122). Milk contains trace amounts of Vitamin D (2 IU/100g);

however, milk is voluntarily fortified by producers with 41-51 IU/100g of Vitamin D (107). Vitamin D is obtained from the diet as cholecalciferol (vitamin D3) from animal sources and to a much lesser extent as ergocalciferol (vitamin D2) from plant sources (75).

Many interventions have found varying effects of dairy consumption on bone, but the strongest effects are believed to be seen during growth (107). Interactions between genes and environmental factors could explain part of the heterogeneity of the results of calcium intervention studies (87). An NHANES III follow-up study found that women 50+yrs who recalled low milk intake during childhood and adolescence had twice the risk of fracture (75, 123). Intervention studies with food have shown that adding dairy foods to the diets of post-menopausal women raised calcium intake and significantly lowered bone loss (75, 124). Milk and calcium enriched foods enhanced the gain of both mean scanned bone area and height in pre-pubertal girls who were spontaneously low calcium consumers, to the levels of high calcium consumers (83, 125). In growing children, long-term milk avoidance is associated with smaller stature, lower bone mineral density (83, 87) and increased risk of fracture before puberty and possibly later in life (83, 126).

In the US, fructose consumption decreased significantly in children aged 2-18yrs old which was concomitant with increased consumption of sweetened beverages. Between 1977-2001 the proportion of children who drank milk decreased from 94-84%, with daily consumption being reduced from 3.5-2.8 servings per day (107). Soft drink consumption substituted for milk and for every 30mL reduction in milk consumption was replaced by 126mL of

sweetened drink (107). This substitution increases caloric intake 31kcal and reduces calcium intake by 34 mg for each 30mL of milk replaced (107).

Milk consumption on the individual level may factor in individual taste preference, ethics, inability to digest milk, milk protein allergy or replacement by other beverages. Certain vegetarians, in accordance to their practice of avoiding animal products, do not ingest milk from mammals. Diets high in fruits and vegetables provide plenty of bone-promoting nutrients like: magnesium, calcium, potassium, vitamin K and vitamin C (95). Milk and dairy products have the highest bioavailability for calcium but are not the only sources. Bioavailability refers to the proportion of the nutrient which is absorbed from the diet and utilized by the body (127). Fractional mineral absorption varies over a wide range (<1% to >90%) depending on the amount of mineral in the diet, the oxidative state and chemical form of the mineral, as well as the presence of enhancers and inhibitors (127). Another factor that influences mineral bioavailability is the nutritional status of the individual (127). In order for intake of the same amount of absorbable calcium from 1 cup of cow milk, a vegetarian would need to consume 1.3 cups of calcium-fortified soy milk or 0.6-1.0 cups of calcium-fortified juice (95). Studies in children who consume low amounts of milk are able to recover any decreases in BMD with calcium supplementation (119). In lactose intolerant and milk-protein allergic children, milk avoidance is associated with decreased bone quality (119). Dietary calcium can be supplemented from several sources: calcium citrate-malate, calcium carbonate, calcium phosphate, calcium lactate-gluconate, calcium phosphate milk extract or milk minerals. Calcium supplementation positively influenced total body bone mineral content (83, 128). Whereas, calcium supplementation could

influence volumetric BMD and thus the remodeling process, dairy products may have an additional effect on bone growth and periosteal bone expansion and thus primarily affect modelling (83).

Bone and the Regulation of Energy Balance

Growth is an energy intensive process and tight control of food intake and appetite regulation is necessary to ensure that bone cells can facilitate growth. Adenosine triophosphate (ATP) is the universal energy currency for all living organism. Animals do not store energy as ATP, instead they use lipids, carbohydrates and to a lesser extent protein as energy reserves (129). Cytoplasmic breakdown of monosaccharides provides a large amount of ATP in the absence of oxygen. Metabolic intermediates can be converted to lipids or returned to a carbohydrate to store ATP (129). Glucose is the primary monosaccharide of choice and glycolysis, is the main energy pathway. Progenitor cells utilize enhanced glycolysis to maintain proliferative populations and sacrifice efficient ATP generation from oxidative phosphorylation for rapid breakdown by anaerobic glycolysis (130). During periods of active growth, within 24- to 72-hrs chondrocytes, that produce the cartilaginous template for bone, progress from a proliferative state to terminal differentiation and subsequent death (131). Chondrocytes are glycolytic and utilize this rapid energy pathway to synthesize large amounts of ECM (131). Osteoblasts have the enzymatic machinery to accomplish both glycolysis and oxidative phosphorylation (OXPHOS) and during mineralization ATP levels peak to facilitate the increased cellular activity (78, 132). Mature osteocytes utilize either glycolysis or OXPHOS depending on their location within cortical bone. The number of mitochondria is greater on the periosteal

and endosteal surfaces, compared to endocortical bone; however, the osteocytes closer to the endosteum function poorly and are susceptible to apoptosis (133). Bone is not only an energy sink, but also plays a role in the endocrine signaling of energy balance.

Appetite regulation is achieved by hormone signals produced peripherally and centrally. Peripheral signals come from the stomach (ghrelin), pancreas (insulin), intestines (PYY, GLP1, GIP) and white adipose tissue (WAT) (Leptin) (4, 134) (Figure 1-6). These peripheral signals act on the hypothalamus, which serves as a sensor of metabolic status and is referred to as the apatite center (28). Hypothalamic neurons, located in the arcuate nucleus, produce the hunger peptide neuropeptide Y (NPY) and the satiety peptide pro-opiomelanocortin (POMC). The neurons that produce NPY also produce agouti protein related peptide (AgRP) (4). These neurons that produce POMC are also involved in the cocaine and amphetamine signaling and produce the cocaine- and amphetamine-regulated transcript protein (CART) (4).

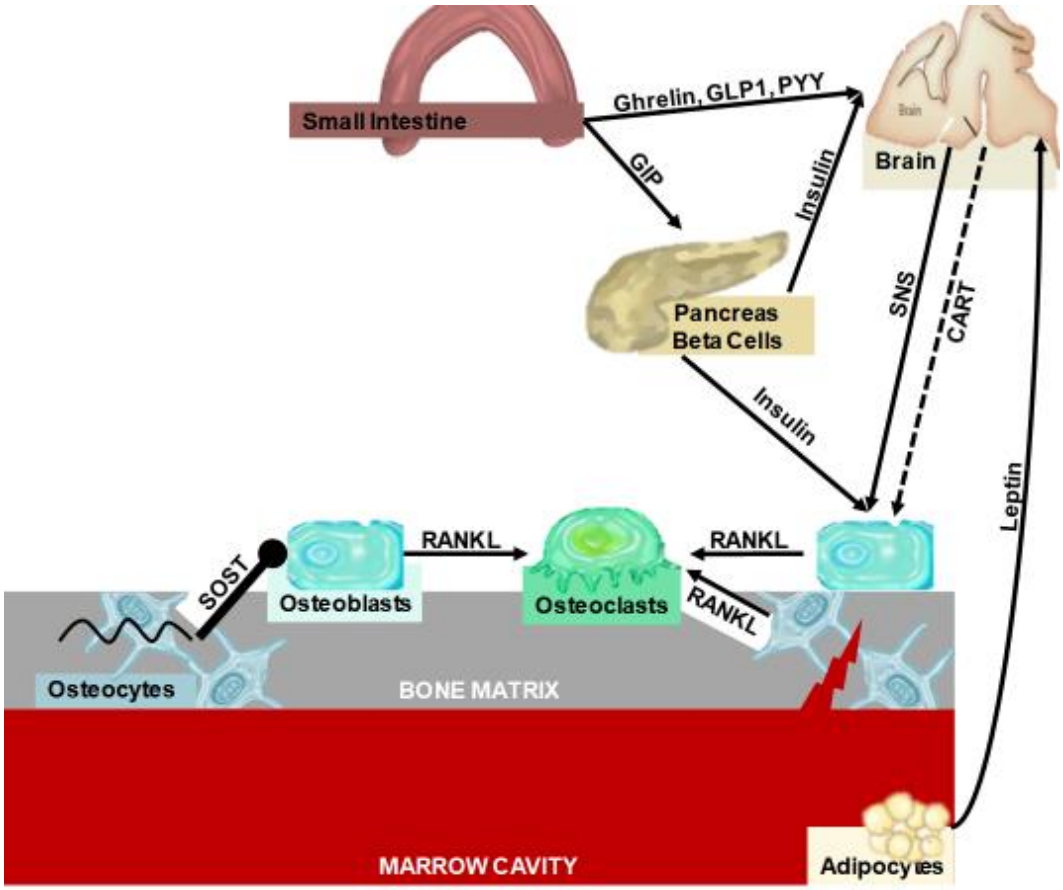

Figure 1-6: Bone cells are involved in the regulation of energy balance. Signals for appetite are interpreted by the brain and using sympathetic nervous system or CART signaling can activate osteoblasts or indirectly activate osteoclasts. Resorption of bone matrix

Insulin was the first hormone discovered to be involved in the control of body weight by the central nervous system. Pancreatic β cells, produce and secrete insulin and act as glucose sensors which regulate blood glucose (135). Hexokinase, the first step of glycolysis, regulates glycolytic activity and glucose oxidation in pancreatic β cells (135). Insulin acts centrally on energy metabolism through the inhibition of NPY and AgRP

neurons and the stimulation of POMC neurons (134, 136). Insulin signaling in osteoblasts appears to be a feedforward mechanism by which bone can affect systemic glucose homeostasis. Insulin signaling stimulates osteoblasts to proliferate and differentiate by suppressing Twist2 (63). Insulin also control osteoclasts indirectly by inhibiting OPG production and increasing recruitment of multi-nucleate osteoclasts (63). Osteoclasts use an acid environment to break down bone tissue, but this also activates OCN by de-carboxylation. The release of uncarboxylated OCN in the plasma then enhances the effect of insulin by promoting insulin sensitivity and production by the pancreas.

Leptin is a 16kDa glycoprotein and one of the most important adipokines in the control of energy homeostasis. It is produced primarily by subcutaneous differentiated adipocytes in direct relation with triglyceride content; although, leptin is produced by several other tissues (64, 134, 137). Leptin is released into the circulation in a pulsatile manner with diurnal variation (137). Leptin crosses the blood-brain barrier and reaches the cerebrospinal fluid and finally its central targets. Those targets are the leptin receptor (ObRb) populated nuclei of the hypothalamus: the arcuate (Arc), the ventromedial hypothalamic (VMH) and paraventricular (PVN) nuclei (64, 137). Leptin mainly controls energy homeostasis through the activation of neurons producing POMC and CART and inhibition of those producing NPY and AgRP (134, 137). Leptin inhibits appetite and bone mass through two different hypothalamic pathways. Leptin deficient ob/ob mice have high bone mass due to an increase in bone formation that outweighs increases in osteoclast activity (64). Deletion of leptin receptor in osteoblasts alone did not have the same effect as the ob/ob mice, but deletion of the leptin receptor in neurons replicated the ob/ob model (64, 138). This

indicates that leptin uses a central neuronal relay to regulate bone mass (64). Under the control of leptin, the sympathetic tone acts through the β2 adrenergic receptor in osteoblasts, which inhibit bone mass accrual through: decreased bone formation and increased resorption (64). The increased resorption from the leptin signal would excavate and uncarboxylate embedded OCN and trigger the insulin response.

Growth during puberty is a metabolically intensive process and bone is an influencer of energy status. Energy requirements increase to support rapid physical changes and are compensated by increased food intake (139). Disruption of energy balance, such as in patients with anorexia nervosa, malnutrition and other wasting disorders associated with low body weight, increases susceptibility to fracture due to secondary osteoporosis (130). Inflammatory cytokines, such as IL-6 and TNF-α produced by macrophages, lymphocytes, monocytes, epithelial cells, endothelial cells and other cells at the site of inflammation have been shown to stimulate osteoclast formation. (130)

Work in animal models that try to link fructose to obesity and diabetes often use fructose at higher-than-physiological or higher-than-clinical concentrations (

Author	***Year***	***Model***	***Method of Administration***	***Age***	***Duration***	***Dosage***	
Tzanzi et al	*2008*	*Rats*	*Solid Diet*	*5-Wk*	*8 Wk*	*13%*	• *Incre and B*
Douard et al	*2010*	*Rats*	*Solid Diet*	*3-Mo*	*4 Wk*	*60%*	• *Reduc dihyd nephr* • *Incre protei*

Douard et al	*2012*	*Rats*	*Solid Diet*	*~2-Mo*	*6 Wk*	*63%*	• *Reduc* • *Reduc*
Douard et al	*2013*	*Rats*	*Solid Diet*	*21-D*	*4 Wk*	*63%*	• *Reduc dry w* • *Reduc CYP2* • *Increa* • *Increa*
Bass et al	*2013*	*Rats*	*Solid Diet*	*60-D*	*12 Wk*	*40%*	• *Reduc* • *Increa Ultim*
Felice et al	*2014*	*Rats*	*Water*	*YA*	*28 d*	*10% w/v*	• *Reduc activi activi*
Yarrow et al	*2016*	*Rats*	*High Fat Solid Diet*	*7-Wk*	*12 Wk*	*40% kcal*	• *Recov High* • *Reduc*
Jatkar et al	*2017*	*Mice*	*Water*	*7-Wk*	*15 Wk*	*10% w/v*	• *Fructo effects*
Felice et al	*2017*	*Rats*	*Water*	*8-Wk*	*5 Wk*	*10% w/v*	• *Reduc Area* • *Increa Fructo*

Table 1-5). While providing valuable information about excessive fructose consumption, they fail to give an understanding fructose metabolism at low levels, as a minor component of a well-balanced meal (14). Fructose is rarely consumed as the only carbohydrate and glucose often present in the same meal is metabolized together with fructose (14). When consumed alone or in great excess, many people experience fructose intolerance due to malabsorption (14). Experiments that use sucrose or fructose with glucose, and limit

plasma fructose concentrations to physiological levels are likely to reveal the most information about normal fructose metabolism. (14).

Author	*Year*	*Model*	*Method of Administration*	*Age*	*Duration*	*Dosage*	*Findings*
Tzanzi et al	*2008*	*Rats*	*Solid Diet*	*5-Wk*	*8 Wk*	*13%*	• *Increased Femoral and Tibial BMD and BMC;*
Douard et al	*2010*	*Rats*	*Solid Diet*	*3-Mo*	*4 Wk*	*60%*	• *Reduced 25-hydroxy and 1,25-dihydroxy vitamin D with nephrectomy;* • *Increased: 1-alpha-hydroxylase protein abundance*
Douard et al	*2012*	*Rats*	*Solid Diet*	*~2-Mo*	*6 Wk*	*63%*	• *Reduced Body BMC; Shear Stress* • *Reduced 1,25-dihydroxyvitamin D*
Douard et al	*2013*	*Rats*	*Solid Diet*	*21-D*	*4 Wk*	*63%*	• *Reduced Femur length; Humerus dry weight and ash weight* • *Reduced 1,25-dihyroxyvitamin D; CYP27b1* • *Increased: Cortical thickness* • *Increased: CYP24a1;*
Bass et al	*2013*	*Rats*	*Solid Diet*	*60-D*	*12 Wk*	*40%*	• *Reduced: BS/BV* • *Increased: Tb.BV/TV; TbTh; Ultimate Load*

Felice et al	*2014*	*Rats*	*Water*	*YA*	*28 d*	*10% w/v*	• *Reduced: Runx2 expression; ALP activity; Col1 production; TRAP activity; Osteocyte density;*
Yarrow et al	*2016*	*Rats*	*High Fat Solid Diet*	*7-Wk*	*12 Wk*	*40% kcal*	• *Recovered deleterious effects of High fat diet;* • *Reduced: Serum Osteocalcin*
Jatkar et al	*2017*	*Mice*	*Water*	*7-Wk*	*15 Wk*	*10% w/v*	• *Fructose Diet did not have adverse effects seen in high fat diet*
Felice et al	*2017*	*Rats*	*Water*	*8-Wk*	*5 Wk*	*10% w/v*	• *Reduced Osteocyte density; TRAP Area* • *Increased: Glucose and Fructosamine*

Table 1-5: Rodent studies that have examined the effects of fructose on bone and calcium metabolism.

Excessive fructose feeding elicits a rodent metabolic response like the one seen in humans, within a short time. Fructose effects are demonstrated in rodents given human equivalent (<20% of diet being from carbohydrate) proportions of sugar, however the order of time needed to see metabolic effects extends from weeks to months (118). Preliminary work for this study and others demonstrated that KHK-KO mice are unable to tolerate 40%, or greater, fructose diets, and decrease food intake after a few days (140). In my work at 20% fructose, WT animals metabolized and regulated fructose at levels near glucose-fed (~0.5mM). For comparison, in healthy humans, systemic fructose levels are relatively low (10-60µM) but post-prandial levels can reach as high as 2.2mM (23).

A convention of using fructose in animal models is that chronic supraphysiologic fructose exposure equates to high-dose acute consumption. A goal of studies that evaluate the effects of fructose-feeding in rodent models, is to replicate the chronic effects of fructose feeding in humans in an acute model. In the study design of my work, I decided on an amount of fructose that better reflects the caloric contributions of fructose to humans in America. Before 1900, Americans consumed approximately 15 g/day (4% of total calories), by 1977 fructose consumption more than doubled to 37 g/day (7% of total calories). Estimates from the new millennium have adolescents consuming 73 g/day (12% of total calories) of fructose (35). The Institute of Medicine recommended that intake of added sugar, in humans, shouldn't exceed 25% of energy while a more conservative figure by the World Health Organization recommends that <10% of energy be provided by added sugars (9). In the US, it is estimated that over 70% of adults consume >10% of calories from added sugars, with approximately 10% getting >25% from those sources (141).

Experimental diets used in rodent models range between 20-60% fructose and growth studies typically last less than 3 months. Work done in mouse and rat models is limited in their length of study. The goal of fructose-feeding for bone research should be to identify direct effects of fructose on bone, not confounding effects from excessive consumption.

Fructose has infiltrated our diets aggressively in only a few generations, the effects of which have not been fully realized. Increased consumption of this sugar has been shown to illicit morbidities affecting organ systems that form an axis with bone to maintain homeostasis. Experimentally or clinically, there have not been any conclusive findings demonstrating that fructose consumption critically impacts bone quality. However, those interventions have not been able to bridge the gap in the knowledge regarding whether fructose affects bone directly, and/or by indirect means. Direct interaction between fructose and bone matrix/cells or metabolism by the latter could alter bone quality. Fructose effects on non-osseous tissues that drive mineral and energy balance could have deleterious effects on bone. The work presented tests the hypothesis that fructose, fed at moderate levels will affect bone quality by alterations in bone formation, bone composition and evidenced through changes in bone strength.

The endocrine role of the osteocyte network in mineral homeostasis and energy metabolism are becoming increasingly clear in recent years. The fructose-fed mouse highlights bone's role as an endocrine organ as changes in energy source have consequences on material properties and hormonal output. I hypothesize that the bone cells of mesenchymal origin are sensitive to fructose concentrations and are unable to maintain proper growth with

chronic exposure. The experiments detailed within addressed the following aims: 1) Determine the effects of fructose on pre-osteoblasts, osteoblasts and osteocytes. 2) Characterize the effects of fructose metabolism on cellular, structural and mechanical bone indices of growing mice.

Chapter 2 : Bone Quality Assessment in Fructose Feeding Experiments

Introduction

In my collaborative work with the labs of Dr. Ronaldo Ferraris and Dr. Veronique Douard I have characterized the effects of high fructose load and low calcium on wild-type C57BL/6 (B6) mice as well as moderate fructose loads on KHK-KO mice. Analysis of the bones from these studies provide additional observations on how fructose affects mouse bones.

I analyzed the bones from a five-week evaluation of the effects of 43% glucose or fructose and normal (0.5%) or restricted calcium (0.02%) on calcium metabolism in growing mice (118). Calcium restriction was used to elicit the Vitamin D cascade, to show how fructose inhibits the action of Vitamin D on calcium homeostasis. In this model, fructose inhibited the upregulation of CYP27b1 in the kidney, in response to low calcium and this reduced the amount of active Vitamin D produced in response to calcium restriction. Downstream effects of this inhibition included: decreased expression of intestinal calcium transporters TRPV6 and Calbindin9k and reductions in calcium transport across the epithelium. These perturbations to calcium homeostasis did not however alter serum calcium and phosphate drawing the question of how calcium status was maintained despite deficiency.

I also performed mechanical analysis of bone from a study that evaluated the effects of 25% fructose (20% fructose with 10% sucrose) on growing wild-type and KHK-KO mice for 12-weeks (140). KHK-KO animals, like individuals with Essential Benign Fructosuria (EBF), have elevated fructose concentrations without consuming fructose. This elevated

baseline was due to accumulation of fructose synthesized by the sorbitol pathway. Fructose concentrations were not affected by the diet in the wild-type, but fructose significantly raised the fructose concentrations in KHK-KO mice. Additionally, this diet did not raise HbA1c or glucose concentrations in KHK-KO mice, showing an inert insulin response. PCR data from homogenized kidneys found that fructose feeding to KHK-KO mice reduced the expression of CYP27b1 and increased CYP24a1 expression. A similar trend was seen in WT animals but not significantly. This confirms the previous findings in fructose feeding studies of reduced CYP27b1 expression with a consequential reduction in activated 1,25-Vitamin D_3.

Materials and Methods

Animals. **Study 1)** Thirty-six 3-week-old C57BL/6 mice (n=9/group) were fed a combination of normal- (0.5 %) /low-calcium (0.02%) and glucose/fructose (43%) diets for 5 wks. Mice were housed in a clean mouse facility, fed their designated diets and water ad libitum and kept on a 12-h light/dark cycle. Animal care and maintenance provided through IACUC approved protocol. **Study 2)** Twenty-one 7-week-old C57BL/6 mice (n=5-6/group) were fed a starch or 20% fructose with 10% sucrose diets for 12 wks. Mice were housed in a clean mouse facility, fed their designated diets and water ad libitum and kept on a reverse 12-h light/dark cycle. Animal care and maintenance provided through IACUC approved protocol.

Tissue Sampling. **Study 1)** At 10d and 3d prior to sacrifice, all mice were administered calcein (20 mg/kg BW). Left humerus and femur were excised and cleaned of soft tissue.

The humerii were stored at -80°C until used for mechanical testing and femurs were fixed in formalin before being prepared for staining and plastic embedment.

Study 2) Left humerus was excised and cleaned of soft tissue. The humerii were stored at -80°C until used for mechanical testing.

Whole Bone Mechanical Testing. Frozen humerii were gradually thawed (~80°C, ~20°C, ~20°C) and tested to failure in the three-point bending configuration. Bones were pre-loaded at -0.4N and tested at a displacement rate of -0.05 mm/s until failure. Humerus remained under hydrated conditions prior to testing on ElectroForce system (LM1 Test Bench, Bose). All tests were conducted at room temperature in a controlled lab environment. Load and displacement signals were bridge amplified, with the same gain in each test. These signals, comprising the load-deflection curves, were digitally sampled with the Bose WinTest software (Version X).

Load-deflection curves were analyzed in MATLAB (Version R2016b, MathWorks, Natick MA) for stiffness (the slope of the initial linear portion of the curve), strength (maximum load), post-yield deflection (deflection at failure minus deflection at yield, PYD) and work-to-failure (area under the curve prior to failure). Yield was defined as a 10% reduction of secant stiffness (load range normalized for deflection range) relative to the initial (tangent) stiffness. Moments of inertia were calculated as elliptical shells.

Histomorphometry. **Study 1)** Femurs were dehydrated, bulk stained in basic fuchsin and embedded in poly-methyl-methacrylate, sectioned at the mid-shaft using precision saw (Isomet 5000 Buehler) and finely polished. Calcein labels, differentiated from the fuchsin background were visualized using confocal microscopy (A1, Nikon) at 20X magnification and digital images of each cross section were saved at .63 µm/px. Histomorphological features were outlined with interactive pen and tablet display (21UX, Wacom Cintiq) in Photoshop (Adobe) and analyzed in NIH Image. Nomenclature was standardized using Dempster et all 2013 (142). Measurements of bone morphology including areas enclosed by the periosteal (T.Ar) and endosteal (Ec.Ar) perimeters, and lengths of the perimeters (Ps.Pm and Ec.Pm, respectively). Cortical thickness (Ct.Th) is measured on posterior, anterior, medial, and lateral perimeters of the femur mid-diaphysis cross sections.

µCT

Study 1) After microscopy, the embedded distal end of the femur was wrapped in paraffin film and scanned with high-resolution µCT scanner (SkyScan 1172, Bruker) at an excitation voltage of 80kV through .5mm thick aluminum and copper filters. Images were acquired using the equipped 10-megapixel cooled CCD camera, at ~8 µm to gain histomorphometric parameters. Using packaged software, scanned images were reconstructed, phantom calibrated for density and analyzed. Trabecular regions were designated as a 1.72mm region that was 0.215mm distal from the growth plate. Cortical regions were designated as a 0.5 mm region that were 2.15mm proximal to the growth plate of the distal femur.

Statistical Analysis. Differences between groups were evaluated by one-way ANOVA tests ($p<0.05$). Post-hoc analysis was completed with Tukey adjustment for multiple comparisons.

Results

Study 1) Neither fructose or low calcium affected body weight or the length of the humerus or femur (Table 2-1). The reduced calcium and chronic fructose diet affected the mineral metabolism, structural and mechanical bone quality in our model. In bone, reduced calcium reduced endosteal bone formation while increasing periosteal growth. Fructose causes a positive trend in endosteal formation, while reducing periosteal adjustments to low calcium (Table 2-2). Cortical mineral density was significantly reduced with calcium deficiency (Table 2-4). Calcium restriction also reduced trabecular BMD, trabecular thickness, and number of trabeculae (Table 2-5). Significant fructose effects were not detected by histological or computed tomography.

		Calcium	Glucose	Fructose
Body Weights				
		Normal	23.50 ± 1.52	22.70 ± 2.38
		Low	24.60 ± 2.15	22.55 ± 1.79
Bone Lengths				
	Femur	Normal	14.03 ± 0.35	13.87 ± 0.30
		Low	13.80 ± 0.66	13.94 ± 0.38
	Humerus	Normal	11.66 ± 0.18	11.68 ± 0.17
		Low	11.72 ± 0.20	11.66 ± 0.08

Table 2-1: Body weights and lengths of humerus and femurs from C57BL/6 mice (n=9/group) fed a combination of normal- (0.5 %) /low-calcium (0.02%) and glucose/fructose (43%) diets for 5 wks. No significant differences were found between groups.

				Statistics	
	Calcium	**Glucose**	**Fructose**	**Sugar**	**Sugar X Calcium**
Femoral Periosteal Histomorphometry					
Perimeter (mm)	Normal	$7.32 \pm 2.17^{a,b}$	$7.06 \pm 2.02^{a,b}$	ns	ns
	Low*	5.81 ± 2.29^{a}	7.77 ± 3.28^{b}		
Mineralizing Surface (%)	Normal	0.25 ± 0.10	0.23 ± 0.08	ns	ns
	Low	0.29 ± 0.09	0.24 ± 0.08		
Mineral Apposition Rate (µm/day)	Normal	3.13 ± 1.60	3.72 ± 1.82	ns	ns
	Low	3.14 ± 1.79	2.91 ± 1.22		
Bone Formation Rate ($\mu m^3/\mu m^2$/day)	Normal	0.86 ± 0.61	0.90 ± 0.69	ns	ns
	Low	0.87 ± 0.50	0.65 ± 0.27		

Table 2-2: Dynamic histomorphometric parameters measured on the periosteal surface of femurs from C57BL/6 mice (n=9/group) fed a combination of normal- (0.5 %) /low-calcium (0.02%) and glucose/fructose (43%) diets for 5 wks. Asterisk (*) represent differences between normal calcium and low calcium group. Similar superscripts indicate values that are not significantly different from each other by Tukey post-hoc test. Significant differences between groups determined by ANOVA with Tukey Test correction ($p < 0.05$).

				Statistics	
	Calcium	**Glucose**	**Fructose**	**Sugar**	**Sugar X Calcium**
Femoral Endosteal Histomorphometry					
Perimeter (mm)	Normal	4.39 ± 0.34	4.39 ± 0.25	ns	ns
	Low	4.25 ± 0.40	4.30 ± 0.39		
Mineralizing Surface (%)	Normal	0.52 ± 0.17	0.51 ± 0.15	ns	ns
	Low	0.32 ± 0.13	0.48 ± 0.27		
Mineral Apposition Rate (µm/day)	Normal	3.39 ± 1.50	4.09 ± 1.66	ns	ns
	Low	3.59 ± 1.22	4.06 ± 3.04		
Bone Formation Rate ($\mu m^3/\mu m^2$/day)	Normal	1.59 ± 0.45^{a,b}	2.21 ± 0.85^{a}	0.007	ns
	Low	1.09 ± 0.45^{b}	2.06 ± 1.05^{a,b}		

Table 2-3: Dynamic histomorphometric parameters measured on the endosteal surface of femurs from C57BL/6 mice (n=9/group) fed a combination of normal- (0.5 %) /low-calcium (0.02%) and glucose/fructose (43%) diets for 5 wks. Statistical significance determined by one-way ANOVA tests ($p<0.05$). Post-hoc analysis was completed with Tukey adjustment for multiple comparisons.

				Statistics	

	Calcium	Glucose	Fructose	Sugar	Sugar X Calcium
Femoral Cortical MicroCT					
Ct.BMD (g/cm^3)	Normal	1.38 ± 0.14^{a}	1.32 ± 0.33^{a,b}	ns	ns
	Low*	1.20 ± 0.07^{b}	1.28 ± 0.13^{a,b}		
Ct.B.Ar (mm^2)	Normal	0.62 ± 0.15^{a}	0.70 ± 0.03^{a}	ns	ns
	Low*	0.46 ± 0.13^{b}	0.49 ± 0.06^{b}		
Ct.M.Ar (mm^2)	Normal	2.08 ± 1.87	1.26 ± 0.64	ns	ns
	Low	1.75 ± 1.35	1.56 ± 0.79		
Ct.Tt.Ar (mm^2)	Normal	1.70 ± 0.11	1.75 ± 0.15	ns	ns
	Low	1.71 ± 0.05	1.55 ± 0.10		
%Ct.Ar (%)	Normal	40.55 ± 1.11^{a}	39.91 ± 3.00^{a}	ns	ns
	Low*	28.38 ± 2.29^{b}	31.67 ± 3.01^{b}		

Table 2-4: Cortical µCT parameters measured from femurs from C57BL/6 mice (n=9/group) fed a combination of normal- (0.5 %) /low-calcium (0.02%) and glucose/fructose (43%) diets for 5 wks. Asterisk (*) represent differences between normal calcium and low calcium group. Similar super scripts indicate values that are not significantly different from each other by Tukey post-hoc test. Significant differences between groups determined by ANOVA with Tukey Test correction ($p < 0.05$).

				Statistics	
	Calcium	**Glucose**	**Fructose**	**Sugar**	**Sugar X Calcium**
Distal Femur Trabecular MicroCT					
Tb.BMD (g/cm^3)	Normal	0.18 ± 0.05^a	0.18 ± 0.02^a	ns	ns
	Low*	0.10 ± 0.03^b	0.09 ± 0.07^b		
Tb.BV/TV (%)	Normal	79.61 ± 3.44	89.34 ± 5.46	ns	ns
	Low	82.32 ± 6.67	81.18 ± 7.05		
Tb.Th (mm)	Normal	34.82 ± 2.50^a	35.23 ± 1.00^b	ns	ns
	Low*	30.25 ± 2.00^a	29.85 ± 1.68^a		
Tb.N (#)	Normal	23.00 ± 2.02^a	22.80 ± 1.26^b	ns	ns
	Low*	27.23 ± 1.81^a	27.23 ± 2.45^b		
Tb.Sp (mm)	Normal	0.023 ± 4.79^{a,b}	0.025 ± 4.47^a	ns	ns
	Low*	0.019 ± 2.08^b	0.020 ± 4.18^{a,b}		
Tb.Conn.Dn (mm^4)	Normal	5103.50 ± 1250.87	4802.82 ± 795.80	ns	ns
	Low*	6476.30 ± 1306.16	7239.32 ± 2196.47		

Table 2-5: Trabecular µCT parameters measured from femurs from C57BL/6 mice (n=9/group) fed a combination of normal- (0.5 %) /low-calcium (0.02%) and glucose/fructose (43%) diets for 5 wks. Asterisk (*) represent differences between normal calcium and low calcium group. Similar super scripts indicate values that are not significantly different from each other by Tukey post-hoc test. Significant differences between groups determined by ANOVA with Tukey Test correction ($p < 0.05$).

Diminished cortical parameters attributed to poorer quality bone, which was supported with mechanical testing. Calcium deficient animals had weaker bones than those animals on the normal calcium diet (Table 2-6). The post-yield deflection in fructose-fed bones were reduced compared to glucose-fed animals, resulting in less pliable bone.

				Statistics	
	Calcium	**Saline**	**Fructose**	**Sugar**	**Sugar X Calcium**
3-Point Bending Parameter					
Ultimate Load (N)	Normal	8.92 ± 0.35[a]	13.87 ± 0.30[a]	ns	ns
	Low*	4.44 ± 1.01[b]	5.20 ± 1.06[b]		
Yield Load (N)	Normal	7.19 ± 0.98[a]	6.68 ± 1.14[a]	ns	ns
	Low*	3.26 ± 1.08[b]	3.58 ± 1.13[b]		
Maximum Displacement (mm)	Normal	0.27 ± 0.04[a]	0.23 ± 0.06[a]	ns	0.04
	Low*	0.45 ± 0.19[b]	0.34 ± 0.04[a,b]		
Yield Displacement (mm)	Normal	0.11 ± 0.03	0.10 ± 0.03	ns	ns
	Low	0.13 ± 0.07	0.10 ± 0.04		
Post-Yield Displacement (mm)	Normal	0.16 ± 0.05[a]	0.14 ± 0.05[a]	ns	ns
	Low*	0.32 ± 0.16[b]	0.24 ± 0.07[a,b]		
Stiffness (N/mm)	Normal	111.97 ± 14.06[a]	119.26 ± 15.36[a]	ns	0.03
	Low*	43.47 ± 13.21[b]	55.968 ± 4.89[b]		

Total Work (N*mm)	Normal	1.70 ± 0.47	1.35 ± 0.49	ns	ns
	Low	1.39 ± 0.56	1.25 ± .20		
Yield Work (N*mm)	Normal	0.31 ± 0.09	0.26 ± 0.10	ns	ns
	Low	0.19 ± 0.14	0.16 ± 0.09		
Post-Yield Work (N*mm)	Normal	1.39 ± 0.48	1.09 ± 0.42	ns	ns
	Low	1.20 ± 0.54	1.09 ± 0.21		

Table 2-6: Mechanical testing parameters of femurs from C57BL/6 mice (n=9/group) fed a combination of normal- (0.5 %) /low-calcium (0.02%) and glucose/fructose (43%) diets for 5 wks. Asterisk (*) represent differences between normal calcium and low calcium group. Similar superscripts indicate values that are not significantly different from each other by Tukey post-hoc test. Significant differences between groups determined by ANOVA with Tukey Test correction ($p < 0.05$).

Fructose reduced the number of osteoblasts that transitioned into osteocytes after they finished depositing matrix. Calcium restricted, fructose-fed mice saw a 60% reduction in osteocyte density (Table 2-7).

				Statistics	
	Calcium	**Saline**	**Fructose**	**Sugar**	**Sugar X Calcium**
Osteocyte Densities					
Endosteal Osteocyte Lacunar Density	Normal	5.08 ± 2.71^{a}	$4.44 \pm 1.69^{a,b}$	ns	ns
	Low*	$2.51 \pm 1.36^{a,b}$	1.67 ± 0.39^{b}		
Periosteal Osteocyte Lacunar Density	Normal	8.33 ± 5.27	6.47 ± 5.46	ns	ns
	Low	2.94 ± 0.27	3.71 ± 1.15		
Total Osteocyte Lacunar Density	Normal	6.68 ± 3.10^{a}	$5.22 \pm 2.32^{a,b}$	ns	ns
	Low*	$2.52 \pm 1.03^{a,b}$	2.69 ± 0.47^{b}		
Osteocyte Lacunar Density / Length of Calcein Label	Normal	1.54 ± 0.79^{a}	$1.04 \pm 0.50^{a,b}$	ns	ns
	Low*	0.57 ± 0.24^{b}	0.56 ± 0.10^{b}		
Osteocyte Lacunar Density / Average Bone Formation Rate	Normal	5.63 ± 3.52	3.53 ± 1.09	ns	ns
	Low	3.09 ± 2.36	2.36 ± 1.20		

Table 2-7: Direct measurement and ratios of osteocyte lacunar densities on periosteal and endosteal growth regions in femurs from C57BL/6 mice (n=9/group) fed a combination of normal- (0.5 %) /low-calcium (0.02%) and glucose/fructose (43%) diets for 5 wks. Asterisk (*) represent differences between normal calcium and low calcium group. Similar super scripts indicate values that are not

significantly different from each other by Tukey post-hoc test. Significant differences between groups determined by ANOVA with Tukey Test correction ($p < 0.05$).

Study 2) Fructose had no effect on the length of the long bones of either WT or KHK-KO animals (Table 2-8). I found that there was a sugar and gene interaction ($p < 0.05$) that caused the ultimate load of KHK-KO animals fed fructose to resist a greater load (Table 2-9). There were no other significant findings from mechanical testing.

	WT		KHK-KO		Statistics		
	Starch	**Fructose**	**Starch**	**Fructose**	**Sugar**	**Genotype**	**Interaction**
Long Bone Lengths							
Femur	15.90 ± 0.58	16.19 ± 0.33	15.86 ± 0.45	15.95 ± 0.14	ns	ns	ns
Humerus	18.36 ± 0.18	18.48 ± 0.39	18.41 ± 0.27	18.59 ± 0.24	ns	ns	ns

Table 2-8: Femur and humerus length for WT and KO mice fed either starch or 20% fructose with 10% sucrose, for 12 weeks; starting after weaning at 4 weeks of age (n=5-6 mice per group; mean ± SD). No significant differences were found.

	WT		KHK-KO		Statistics		
	Starch	**Fructose**	**Starch**	**Fructose**	**Sugar**	**Genotype**	**Interaction**
3-Point Bending Parameter							
Ultimate Load (N)	$11.92 \pm 1.06^{a,b}$	12.00 ± 0.39^{b}	10.78 ± 0.77^{a}	12.59 ± 0.96^{b}	ns	0.028	0.041
Yield Load (N)	10.63 ± 1.16	11.30 ± 0.94	9.63 ± 0.95	10.53 ± 0.79	ns	ns	ns
Maximum Displacement (mm)	0.44 ± 0.11	0.44 ± 0.06	0.53 ± 0.08	0.47 ± 0.08	ns	ns	ns
Yield Displacement (mm)	0.22 ± 0.03	0.24 ± 0.09	0.23 ± 0.02	0.21 ± 0.04	ns	ns	ns
Post-Yield Displacement (mm)	0.22 ± 0.11	0.19 ± 0.05	0.30 ± 0.08	0.27 ± 0.07	ns	ns	ns
Stiffness (N/mm)	89.67 ± 10.87	83.81 ± 5.68	76.52 ± 9.64	83.47 ± 7.99	ns	ns	ns
Total Work (N*mm)	3.48 ± 1.59	3.32 ± 0.59	3.87 ± 0.50	4.00 ± 0.93	ns	ns	ns
Yield Work (N*mm)	0.87 ± 0.18	1.06 ± 0.27	0.82 ± 0.10	0.88 ± 0.10	ns	ns	ns
Post-Yield Work (N*mm)	2.61 ± 1.50	2.25 ± 0.64	3.04 ± 0.56	3.13 ± 0.88	ns	ns	ns

Table 2-9: Mechanical testing parameters from the humerus of WT and KO mice fed either starch or 20% fructose with 10% sucrose, for 12 weeks; starting after weaning at 4 weeks of age (n=5-6 mice per group; mean ± SD). Significant differences between groups determined by ANOVA with Tukey Test correction ($p < 0.05$

Discussion

These two studies provide valuable insight into the relationship between fructose and genotype and calcium status. I was able to determine if the systemic metabolic effects had any bearing on bone quality. Study 1 evaluated the effects of sugars, glucose and fructose on whole body calcium metabolism. The low calcium diet (0.02%) was chosen to produce a calciotropic response and as an analogue for calcium need (i.e. pubertal growth, malnutrition and lactation). The sugar component (43%) was chosen to mimic the carbohydrate amount in standard chow and to emulate chronic exposure (>1yr) to fructose. This work confirms previous work performed in rats fed chronic loads of fructose during lactation and weaning (143). Study 2 evaluated the effects of fructose feeding on fructose concentrations and described a diet that would be safe for use with the KHK-KO mouse model. We found that fructose doses closer to 43% were not fit for an animal that could not metabolize the sugar, and that at most 25% was enough to alter fructose concentrations in KHK-KO mice.

Study 1 paints the picture of the calcium absorption being perturbed by the presence of fructose in the diet (118). Using the everted gut sac technique, it was determined that fructose reduced the transport of radiolabeled Ca^{2+} under low calcium conditions, with fructose-fed, calcium-restricted animals having a significantly lower response than glucose-fed, calcium-restricted animals. This was most likely due to reductions in intestinal calcium transporters TRPV6 and CaBP9k. Renal expression of Vitamin D metabolizing enzymes CYP24a1 and CYP27b1 were significantly increased by calcium-restriction, and the CYP27b1 response was muted in fructose-fed mice. Measurement of the 1,25-Vitamin

D3 revealed that calcium restriction significantly drove an increase in serum Vitamin D and significantly reduced serum FGF23 (118).

Despite a significant reduction in calcium-intake, our model was able to maintain plasma mineral levels exhibiting the robust methods used to conserve calcium. Fructose did not significantly cause any change in these parameters and neither calcium-availability or sugar-type were able to disrupt serum calcium or phosphate (118). I found that calcium has a significant effect on the maintenance of bone quality, resulting in weaker, but less rigid bone. I observed diminution of morphometry, mineral content and strength in long bones. The bone effects, coupled with increased luminal calcium absorption through the gut, helped to maintain plasma mineral levels. The bulk of these actions are carried out by 1,25VitD3 mediated processes.

Calcium is an important nutrient and calcium restriction results in impaired weight gain and bone development in rodents (144). Normal calcium in rodent models is provided by lab diets, with calcium composing 0.5-1.25% calcium (145). Calcium compositions of 0.01-0.02% are detrimental to bone growth and are used to illicit the Vitamin D calcium response (145). Calcium restriction has differential effects on bone in different strains of mice, which highlight the variability in calcium intake in human interventional studies (146). In our B6 model, 50% reduction of calcium (0.5% - 0.25%) causes an adaptive response to bone morphology, with minimal effect on BMD (146). Calcium restriction in B6 mice during pubertal growth reduced BMD accretion by 5-fold (147). Experimental

calcium-restriction diets do not represent calcium consumption in human but provide valuable insights into calcium metabolism.

Reduced calcium diet did not stunt the growth of the model and animals did not develop spontaneous fractures, despite reduced BMC. The long bones saw an increase in post-yield deflection, a phenomenon that would make bone more pliable before failure. This serves a temporary solution until adequate calcium becomes available and is utilized by osteoblasts to fortify the under-mineralized bone. However, this can have long term implications, potentially in larger models where age related bone-loss is a risk factor for fracture later in life.

Fructose affects the calcium related changes to bone by disrupting 1,25VitD3 activity. With the addition of fructose to the diet, the ability for the body to respond to low calcium fluxes is impeded. Though differences were seen in bone deposition and expression of calcium transporters in the intestine; the quality of bone from calcium-sufficient fructose fed mice was not significantly affected, compared to their glucose fed counterparts. These differences only appeared when calciotropic signaling is being carried out and leads to the presumption that fructose affects bone through 1,25VitD3 activity. Our mouse model has shown that it is very good at conserving mineral balance and maintain relatively good health when challenged with a low calcium diet. The substitution of fructose with glucose has shown to affect bone in part by disrupting 1,25VitD3. Also, independent of 1,25VitD3, disrupts adaptive intrinsic material responses to prevent fracture.

Study 2 further shows the usefulness of the KHK-KO model in determining the effects of fructose on the mouse insulin response. There has not been a published characterization of the KHK-KO bone phenotype and access to these bones was valuable in determining the use of this model for future work. I was able to infer a fructose diet that would be tolerable by mice when being fed. The difference between the work done in this study 2 and subsequent work, in the following chapters is the difference in age. These mice were sacrificed after skeletal maturity (~5-months-old), compared to the growing mouse model (~1 – 3-month-old) used in my feeding and pump experiments. Also, the addition of sucrose to the fructose diet provides a small amount of glucose that has been reported to be synergistic in their absorption from the gut. From 3-point-bending analysis I was able to determine that fructose increased ultimate load in a mouse that had significantly elevated fructose concentrations.

Much like the other fructose-rodent work, my collaborative work is different in design from the work described within but gives an insight into how different fructose doses, in different genetic models, at different ages, for different durations will have differential effects on bone effects. Study 1 evaluates the effect of fructose on calcium status on growing mice. I decided on using the fructose concentration closer to Study 2 to accommodate the KHK-KO mouse. These collaborative studies establish the framework for the work presented hereafter.

Chapter 3 : Bone Growth is Influenced by Fructose in Adolescent Male Mice Lacking Ketohexokinase (KHK)

Abstract

Fructose is metabolized in the cytoplasm by the enzyme ketohexokinase (KHK), and excessive consumption may affect bone health. Previous work in calcium-restricted, growing mice demonstrated that fructose disrupted intestinal calcium transport. Thus. we hypothesized that the observed effects on bone were KHK-dependent and examined the effects of fructose feeding on the long bones of growing mice. Four groups (n=12) of 4-week-old, male, C57BI/6 background, congenic mice with intact KHK (wild-type, WT) or global knockout of both isoforms of KHK A/C (KHK-KO), were fed 20% glucose (control diet) or fructose for 8 weeks. Dietary fructose increased by 40-fold plasma fructose in KHK-KO compared to the other three groups ($p < 0.05$). Obesity (no differences in epididymal fat or body weight) or altered insulin, was not observed in either genotype. Longitudinal growth was inhibited in the KHK-KO mice fed fructose whose femurs were reduced in length by 2%. Fructose feeding resulted in greater bone mineral density, percent volume and number of trabeculae as measured by μCT in the distal femur of KHK-KO. Moreover, higher plasma fructose concentrations correlated with greater trabecular bone volume, greater work-to-fracture in three-point bending of the femur mid-shaft, and greater plasma sclerostin. Since the metabolism of fructose is severely inhibited in the KHK-KO condition, our data suggest mechanism(s) that disrupt(s) bone growth may be related to the plasma concentration of fructose.

Introduction

During growth, adequate nutrition can ensure proper bone mass acquisition to reduce osteoporotic fracture risk later in life (43). Fructose, a nutritive carbohydrate, has increasingly been consumed, as an element of the western diet, by children in developed countries. Once consumed, most fructose absorption occurs in the lumen of the small intestine via transmembrane sugar transporters (GLUT2 and GLUT5), with adaptive expression of GLUT5 dependent on fructose consumption. Fructose travels to the liver via the portal vein and is metabolized by ketohexokinase (KHK). First-pass metabolism through the liver rapidly breaks down 50-75% of the load, reducing peripheral plasma fructose concentrations (23). For an increasing number of adolescents, excessive fructose consumption leads to non-alcoholic fatty liver disease, metabolic syndrome, obesity, insulin resistance, hypertension, atherosclerosis and dyslipidemia and eventually, Type 2 Diabetes Mellitus (148). Although these disorders have been associated with changes in bone growth and adaptation, the independent mechanism(s) by which fructose acts on bone is not fully understood.

Fructose may affect bone metabolism by disturbing the absorption, reabsorption and excretion of essential vitamins and minerals necessary for healthy bone growth (43, 118). In children and adolescents, fructose intake has been associated with increased fractures (149, 150). While no studies have demonstrated a direct causal link, the literature on rodent models has suggested possible effects on bone cells and their precursors. For example, Felice *et at.* reported decreased number of active bone cells *in vivo* via histology, and after *in vitro* osteogenic cell culture of marrow from rats that drank 10% fructose water ad

libitum, a level that induces the metabolic syndrome within weeks (41, 118, 143, 151-154) While likely that high levels of ingestion are required to raise plasma fructose in normal individuals, people with mutations in the KHK gene are unable to break down fructose and have elevated plasma concentrations (155). Some of these people are diagnosed, most as adults, with the inborn metabolic disorder, Essential Benign Fructosuria (EBF) (156). The KHK gene is mutually exclusively spliced into mRNA that result in isoforms A and C (21, 26). KHK-C is primarily found in hepatocytes, enterocytes, renal proximal tubule cells and white adipose tissue (WAT) cells and has the highest affinity for fructose of any hexokinase (157). Fructolytic activity is accomplished peripherally without KHK-C by way of KHK-A or other hexokinases (27, 158).

In normal rodents, fructose affects vitamin D metabolism during periods of increased calcium demand (i.e., pregnancy, lactation, growth and calcium restriction). We have previously demonstrated that fructose reduced Vitamin-D dependent calcium transport in the gut during growth due to disruption of renal Vitamin D metabolism (118). Vitamin D is activated into 1,25(OH) Vitamin D3 (1,25VitD3) by enzymes synthesized in the renal proximal tubule. Vitamin D is a steroid hormone integral to the signa ling of bone cells that regulate 99% of systemic calcium (97). As systemic calcium is tightly regulated, disruptions in calcium metabolism are detriments to bone. Therefore, we hypothesized that in the absence of KHK, fructose feeding raises plasma levels and affects the ability of growing mice to build bone. WT and KHK-KO mice were fed fructose to test effects on bone growth. We found that normal growth processes were disrupted when plasma fructose concentrations rose to high levels.

Materials and methods

Genotyping. KHK-KO (background: C57BL6) mice were donated by R. J. Johnson, University of Colorado, and the generation of the model was previously described (27). Both isoforms of KHK (KHK-A, KHK-C) were deleted, effectively abolishing fructose breakdown. Heterozygous progeny of KHK-KO male and WT females yielded the parents of experimental homozygotes. Pups were genotyped at 3 weeks old, with PCR on DNA extracted from 2-mm ear punches (PCRBio, London) and weaned at 3.5 weeks. Mice were then introduced to diets at the commencement of the experiment at 4 weeks old.

Dietary and experimental design. The effects of fructose were examined in growing (4-12-week-old) male WT or KHK KO mice. Protocols were approved by the Institutional Animal Care and Use Committee (New Jersey Medical School, Rutgers). Same-genotype mice were housed in groups of 3-5 per cage on a 12-hour day/ night cycle. The schematic of experimental design and timeline is found in the appendix (Figure A5-2). Two iso-caloric (equivalent kcal by weight), synthetic diets were designed, based on the standard American Institute of Nutrition (AIN)-93G formula containing other carbohydrates (Research Diets, New Brunswick, NJ; Table A6-1). Mouse and food weights were recorded twice a week. After 8 weeks of feeding, mice were euthanized. Specimen identities were blinded to all researchers while making measurements.

Tissue and cell collection. After sedation, blood was collected via cardiac puncture in tubes containing EDTA, and the inhibitors, protease (Pefabloc, Sigma) and DPP-IV (Millipore), at final concentrations of 2 µg/mL and 0.02 µL/mL, respectively. Centrifugation was at 1300g for 15 minutes and storage was at -80°C. The small intestine was removed and flushed with cold PBS. The first 10 cm distal to the stomach were considered as the duodenum. The subsequent 5 cm was disposed, and the following section was defined as the jejunum. Sections of duodenum and jejunum, 1 cm each, were sampled and stored at -80°C in RNALater (Invitrogen, Thermo Fisher Scientific, Waltham, MA) for subsequent RNA extraction and gene expression analysis. The intact caecum was weighed. Bilateral kidneys and liver were resected, weighed and flash frozen in liquid nitrogen. Tibias and femurs were dissected, and length recorded (0.01 mm caliper resolution). The right tibia was fixed in 10% neutral-buffered formalin for histomorphometry. The left femur was resected of muscle and placed in sterile ice-cold saline for flushing and cell culture and the right was wrapped in saline-soaked gauze and frozen for mechanical testing.

Plasma analysis. Plasma fructose was determined by high-performance liquid chromatography (HPLC) of terminal blood draw as previously described (159). Samples were diluted with acetyl-nitrile and stored (-80°C). Samples were filtered through a 0.45-µm membrane before being analyzed in triplicate and HPLC was performed using a GL-7400 series system (GL Sciences, Tokyo, Japan) equipped with an amino column Shodex Asahipak NH2P-50 4E (4.6 mm ID x 250 mm; Showa Denko, Tokyo, Japan) with a guard column at an injection volume of 5µL. Samples <50µM were reanalyzed at an injection volume of 20 µL. The separation of fructose was performed with a linear gradient in

hydrophilic interaction chromatography mode, as previously described (159). Flow rate and temperature were 1.0 mL/ minute and *40°C,* respectively. Post-column labeling of fructose with phenyl hydrazine was taken at *150°C* in a reactor 522 (Flom, Tokyo, Japan), and the flow rate of reaction reagent (mixture with 180 mL of acetic acid, 6 mL of phenyl hydrazine, and 220 mL of phosphoric acid) was 0.4 mL/ minute. Fluorescence was detected with GL-7453 (GL Sciences) set at an excitation and emission wavelength of 330 and 470 nm, respectively. Data was analyzed using EZChrom Elite version 3.1.5J (Agilent Technologies).

Plasma, bone and gut markers were measured using the Milliplex multi-analyte profiling (MAP) kits MBNMAG-41K and MGTMAG-78K (EMDMillipore, Billerica, MA). Analytes measured by the bone kit included: interleukin 6 (IL- 6), osteoprogerin (OPG), Dickkopf-related protein 1 (DKK1), sclerostin (SOST), tumor necrosis factor alpha (TNF-a) and fibroblast growth factor 23 (FGF23). Analytes measured by the gut kit included: gastric inhibitory protein (GIP), glucagon-like protein 1 (GLP-1), insulin, leptin and peptide YY (PYY). Bone kits were diluted 1:2 with assay buffer. Reaction plates were coated with assay buffer and decanted. Samples were incubated with antibody-coated magnetic beads overnight and then incubated with detection antibody and streptavidin-phycoerythrin 30 minutes for each subsequent incubation. Analysis was performed using MAGPIX® with xPONENT software.

Osteoblast colony forming assay. Left femurs were grouped by cage and trimmed of soft tissue and placed in ice-cold saline. The epiphyses were clipped, and the marrow flushed.

2 x 10^6 cells were plated in 55-cm^2 petri dishes and pooled cell populations were grown in culture for 14 days. Cells were pooled by cage and were cultured, in triplicate, with osteogenic media: alpha-MEM, supplemented with 10% fetal bovine plasma, 1% penicillin and 0.1% Amphotericin B, 50µg/mL ascorbic acid and 8mM beta glycerol phosphate. On day 5, media was changed, and non-adherent cells were removed. The remaining adherent cells were determined to be osteogenic cells by their appearance under light microscope (CKX41, Olympus, Tokyo, Japan). Osteoblast differentiation and activity were confirmed on day 14, when cells were fixed in methanol and stained for alkaline phosphatase (ALP) activity with a 2:1 NBT / BCIP (Sigma) dye buffered with 100 mM Tris, 100 mM NaCl and 5 mM $MgCl_2$.

Histomorphometry. Bones for histomorphometry were embedded in polymethyl-methacrylate (Sigma), trimmed, sectioned transversely at 25% of the length from proximal end (diaphysis) with a diamond saw (Isomet 5000, Buehler) and fine polished with silicon carbide abrasive paper and alumina slurries (successive particle diameters of 1.0 and 0.05 µm). Bone formation during the last week of feeding was assessed with dynamic histomorphometric measures using calcein labels that had been injected (i.p., 20 mg/kg of body weight, Invitrogen C-481) at 9 and 2 days prior to death to label bone-forming surfaces (osteoblast activity). Blocks were imaged with a reflective confocal microscope (AI, Nikon, Tokyo, Japan) at 20x and 60x magnification. Standardized bone parameter measurements were made on an interactive pen/ tablet desktop workstation (Wacom Cintiq 21 UX) using ImageJ software (160). Mineralizing surface (MS) and mineral apposition rate (MAR) were measured on 20x images, and bone formation rate (BFR) calculated for

both periosteal (Ps) and endosteal (Es) cortical surfaces. Mineralizing surface estimated the extent of actively mineralizing surface at the time of label administration and was the total extent of double label plus one half the extent of single label. Mineralizing surface was expressed as a ratio with bone surface (BS) as referent. MAR rate was the average distance between midpoints of the two consecutive labels, divided by the time between label injections. Bone formation rate was calculated as the product of MAR and MS/BS (142). Osteocyte lacunae between the calcein labels were point counted on 60x images.

μCT. Femurs were evaluated by μ-computed tomography (Bruker Skyscan 1172 120 μA, 80 keV, 0.5 mm aluminum filter) for density and morphology. Femurs were submerged in saline and scanned, four at a time in a custom holder, at an isotropic Voxel size of 8 μm. Density calibration phantoms (0.25 and 0.75 g/cm^3)) were included with each scan for calculation of bone mineral density (BMD). Bones were then returned to saline-soaked gauze and stored frozen (-20°C) prior to mechanical testing. Trabecular (Tb) and cortical (Ct) traits were measured at set distances from the distal growth plate. Two contiguous Tb regions of interest (ROIs) were hand drawn at the marrow / endosteal border. Starting 0.25 mm below the growth plate the distal ROI extended 1.75 mm and the distal ROI another 1.15 mm along the femur length. Ct ROI began 2.15 mm distal to the growth plate and were 0.43 mm in depth along the femur. Traits measured were: Trabecular: thickness (Tb.Th), spacing (Tb.Sp), number (Tb.N) , pattern factor (Tb.Pf), connectivity (Conn.Dn) and BMD; and Cortical: thickness (Ct.Th), area (Ct.Ar), and moments of inertia (Ct.MMI), and medullary area (or marrow, Ma.Ar). Cortical area fractions (Ct,Ar/Tt,Ar and Ma,Ar/Tt,Ar), were calculated, where Tt, or total, equals Ma.Ar + Ct.Ar

Whole-bone mechanical testing. The mechanical properties of mid-diaphyseal femurs were quantified by loading to failure in 3-point bending at 0.05 mm/sec until failure with an electro-mechanical actuator (Bose, Testbench, TA Instruments). All tests were conducted at room temperature in a controlled lab environment. Each femur was kept moist with saline and placed with the caudal surface down onto two lower supports, spaced 6 mm apart. Load and displacement signals were bridge amplified, with the same gain in each test. These signals, comprising the load-deflection curves, were digitally sampled with the Bose WinTest software (Version X). Load-deflection curves were analyzed in MATLAB (Version R2016b, MathWorks, Natick MA) for stiffness (the slope of the initial linear portion of the curve), strength (maximum load), post-yield deflection (deflection at failure minus deflection at yield, PYD) and work-to-failure (area under the curve prior to failure). Yield was defined as a 10% reduction of secant stiffness (load range normalized for deflection range) relative to the initial (tangent) stiffness.

Real-time RT-PCR. In intestinal tissues: Total RNA was isolated from each 0.5 cm section of duodenum and jejunum using mirVana® miRNA isolation kit according to the manufacturer's instructions (Ambion, France). After RNA quantification, reverse transcription was performed with 2 µg total RNA using High Capacity cDNA Reverse Transcription kit (Applied Biosystems, Foster City, CA) in a final volume of 25 µl. Real-time PCR was performed in the ABI Prism StepOnePlus™ Real Time PCR system using a 1:10 dilution of the cDNA and the SYBER-Green PCR Master Mix (Stratagene, La Jolla, CA according to the manufacturer's instructions. In kidney: Total RNA was isolated from

~20 mg kidney sections. Samples were homogenized using a stainless-steel bead within 1 mL of Qiazol (Qiagen, Hilden, Germany). RNA extraction was performed with the RNEasy Lipid Tissue Mini Kit (Qiagen, Hilden, Germany) according to the manufacturer's instructions. cDNA was synthesized with 1 µg total RNA using iScript™ RT Supermix (Bio-Rad, Hercules, CA) in a final volume of 20ng/ul. The MiniOpticon Real-Time PCR Detection System utilized SsoFAST EvaGreen® Supermix (Bio-Rad, Hercules, CA). For both tissues, expression values of target genes were calculated based on the comparative threshold cycle (Ct) method to generate ΔCt values (difference of Ct) between each target gene and tissue specific housekeeping gene. Housekeeping genes EFlα and β-actin were used for the kidney and intestine, respectively. The primers list is detailed in Table A7-1. The relative abundance of each mRNA in each sample was then normalized according to the equation: Relative Quantity $RQ = 2^{-\Delta\Delta Ct}$ (161). Ct values larger than 35 were removed (cut-off value> 35).

Analysis of Data. Researchers were blinded, whenever possible, to specimen identity during handling and analysis. Samples were analyzed in randomized order to restrict biases. During feeding and weighing the researchers were not blinded to groups or mouse IDs. A single observer made measurements within each organ system. Data is presented as mean values and standard deviations. Comparisons were analyzed with a two-way ANOVA and significant interactions and differences were determined by Tukey post-hoc method. Statistical significance is reported at $p< 0.05$, unless otherwise noted.

Results

Elevated plasma fructose with feeding. After 8 weeks of feeding, plasma fructose was elevated in KHK-KO mice fed fructose (Fig. 3-1a). Plasma fructose concentrations were approximately 40-fold greater in KHK-KO mice fed 20% fructose compared with those fed the control diet of glucose. There were no genotype-dependent effects on plasma concentration in mice fed control diet. The fructose diet increased plasma fructose concentration in KO mice only compared to WT fed glucose. KHK expression was increased in the duodenum and jejunum with fructose feeding in WT mice and, as expected, there was no measurable expression of KHK in KHK-KO (Fig. 3-1b). No differences were detected between groups in plasma concentrations of bone- and gut- derived cytokines after 8 weeks of feeding (Table 3-1).

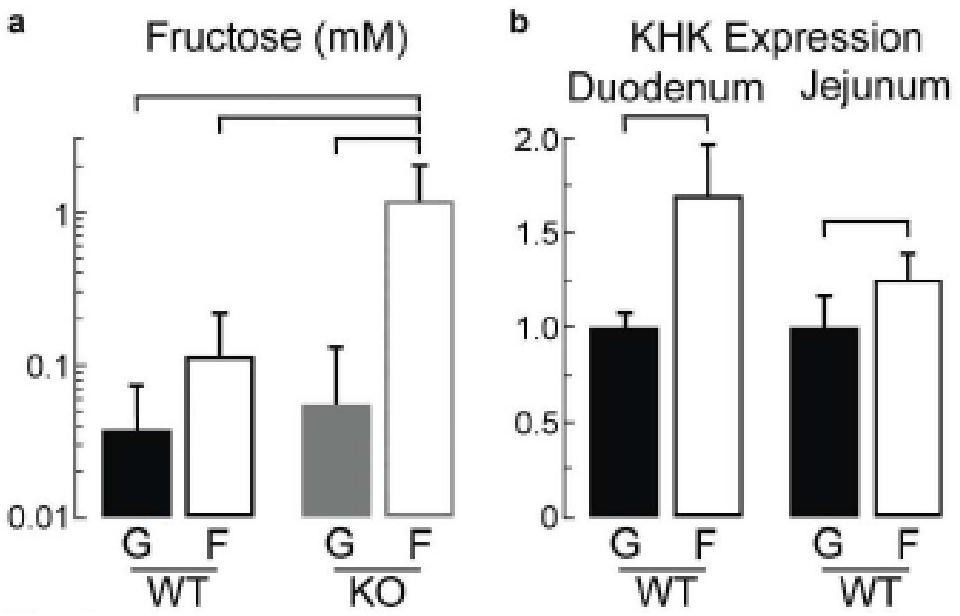

Figure 3-1: (a) Plasma fructose concentration and (b) KHK expression (fold difference) in duodenum and jejunum for WT and KO (KHK not detectable in KO) mice fed for 8 weeks on a 20% glucose (G, control) or 20% fructose (F) diet started after weaning at 4 weeks of age (n= 6-8 mice per group; means ± SD). Bars indicate significant differences between groups determined by ANOVA and Tukey post-hoc ($p < 0.05$).

	WT		KHK-KO	
	Glucose	**Fructose**	**Glucose**	**Fructose**
Plasma Bone Panel				
TNFα (pg/mL)	7.98 ± 4.09	18.77 ± 26.83	7.87± 3.29	7.14± 2.19
IL6 (pg/mL)	29.22 ± 12.21	28.65 ± 13.13	26.76 ± 18.69	18.19 ± 5.60
OPG (pg/mL)	4553.42 ± 1688.11	4387.82 ± 1231.64	4039.71 ± 566.43	4484.33 ± 1697.05
DKK1 (pg/mL)	4896.97 ± 7005.27	6637.47 ± 8464.22	5291.43 ± 5281.76	2815.89 ± 4141.24
SOST (pg/mL)	100.83 ± 63.60	110.28 ± 73.47	97.99 ± 43.54	152.23 ± 182.26
FGF23 (pg/mL)	496.64 ± 218.62	659.82 ± 451.42	777.86 ± 465.18	1004.13 ± 763.93
Plasma Gut Panel				
GIP (pg/mL)	8.62 ± 10.62	9.48 ± 15.73	13.12 ± 15.70	6.09 ± 9.82
GLP1 (pg/mL)	10.19 ± 3.63	28.18 ± 42.00	20.98 ± 22.26	33.64 ± 60.95
Insulin (pg/mL)	79.63 ± 89.47	52.62 ± 31.23	76.77 ± 121.24	48.05 ± 22.88
Leptin (pg/mL)	5231.40 ± 3409.62	3928.90 ± 2943.13	5367.78 ± 4175.53	5485.11 ± 3828.08
PYY (pg/mL)	44.85 ± 39.86	51.58 ± 58.21	83.66 ± 103.099	62.43 ± 59.96

Table 3-1: Plasma concentrations of bone and gut markers (n=10-12 mice per group). Values, presented as means ± SD, exhibited no significant differences by two-way ANOVA, $p < 0.05$.

Body weights were not different between any of the groups at weaning, and, as expected, body weight increased rapidly after weaning, during the 8 weeks of feeding (Fig. 3-2). Almost immediately after the onset of fructose feeding, a small but significant ($p < 0.05$) body weight reduction of 5-8% occurred in the KHK-KO mice. The reduced body weight persisted until 9 weeks of age (5 weeks of fructose feeding) at which point body weights equilibrated. At the end of the experiment, weights of individual organs were similar, except for the caecum which was enlarged in KHK-KO mice fed fructose (+ 200%, $p < 0.01$; Table 3-2).

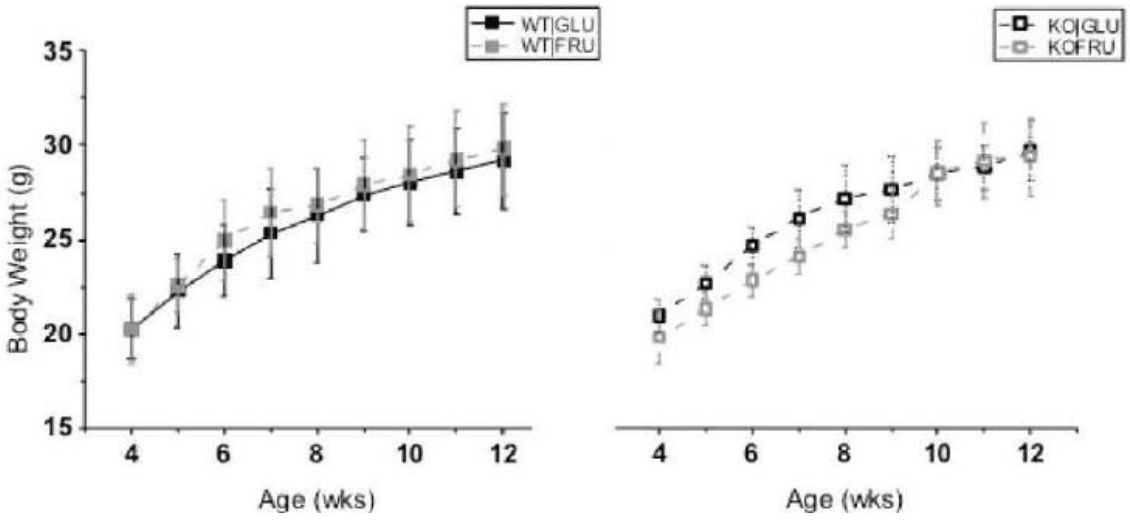

Figure 3-2: Body weight for WT and KO mice fed for 8 weeks on a 20% glucose (G, control) or 20% fructose (F) diet started after weaning at 4 weeks of age (n= 10-12 mice per group; means ± SD). KO mice had lower body weight after the first week of feeding with fructose and recovered to the WT glucose level after the fifth week of feeding ($p < 0.05$, KO fructose vs. all other groups).

	WT		KHK-KO		Statistics		
	Glucose	**Fructose**	**Glucose**	**Fructose**	**Diet**	**Genotype**	**Interaction**
Organ Weights							
Kidney (g)	0.173 ± 0.031	0.181 ± 0.034	0.173 ± 0.030	0.169 ± 0.014	ns	ns	ns
Liver (g)	1.152 ± 0.104	1.287 ± 0.152	1.197 ± 0.187	1.126 ± 0.150	ns	ns	0.029
Caecum (g)	0.202 ± 0.042[a]	0.197 ± 0.045[a]	0.216 ± 0.018[a]	0.628 ± 0.122[b]	< 0.001	< 0.001	< 0.001
Spleen (g)	0.098 ± 0.018	0.111 ± 0.033	0.098 ± 0.020	0.093 ± 0.019	ns	ns	ns
Epidemial Fat (g)	0.796 ± 0.24	0.871 ± 0.33	0.896 ± 0.293	1.022 ± 0.505	ns	ns	ns

Table 3-2 Organ weights. Values are mean ± SD (n=10-12 mice per group). Means were compared with two-way ANOVA. Similar superscripts indicate values that are not significantly different from each other at $p < 0.05$ by post-hoc Tukey test.

Effects of fructose on osteogenic bone cells. Osteogenic colonies detected by the presence of alkaline phosphatase demonstrated that cells from WT and KHK-KO mice fed fructose had significantly reduced OB-like colony counts compared to glucose-fed WT mice (Table 3-3). In contrast, the average colony size was similar between the 4 groups. Osteocyte lacunar density (#/mm^2) between double calcein labels was similar among groups (WT / Glucose: 991 ± 119; WT /Fructose: 968 ± 228; KO / Glucose: 978 ± 162; KO/ Fructose: 1077 ± 295).

	WT		KHK-KO		Statistics		
	Glucose	**Fructose**	**Glucose**	**Fructose**	**Diet**	**Genotype**	**Interaction**
Ob-CFU							
Count	1.00 ± 0.25[a]	0.54 ± 0.35[b]	0.87 ± 0.37[a,b]	0.64 ± 0.35[a,b]	0.002	ns	ns
Average Size	1.00 ± 0.43	0.92 ± 0.43	1.13 ± 0.11	0.75 ± 0.12	ns	ns	ns
Total Area	1.00 ± 0.57	0.48 ± 0.61	0.94± 0.30	0.46 ± 0.27	0.004	ns	ns

Table 3-3: Osteogenic potential of bone marrow cells measured by osteoblast colony formation unit (Ob-CFU) cultures. Primary bone marrow cells were cultured in osteogenic media for 14 days. Stained areas were normalized to WT-glucose control and are represented as means ± SD. Comparisons by two-way ANOVA. Similar superscripts indicate values that are not significantly different from each other by Tukey post-hoc test.

Reduced femur length in KHK-KO with fructose. Longitudinal growth of the long bones was inhibited in KHK-KO mice by fructose feeding such that the lengths of femurs were reduced by 2.4% when compared to glucose-fed KHK-KO and by 2.9% when compared to WT fed fructose ($p < 0.05$; Fig. 3-3a). Despite these growth differences, food intake relative to body weight over the early period of feeding was slightly increased in the fructose-fed mice, regardless of genotype (Fig. 3-3b), though there were no differences at the conclusion of the study.

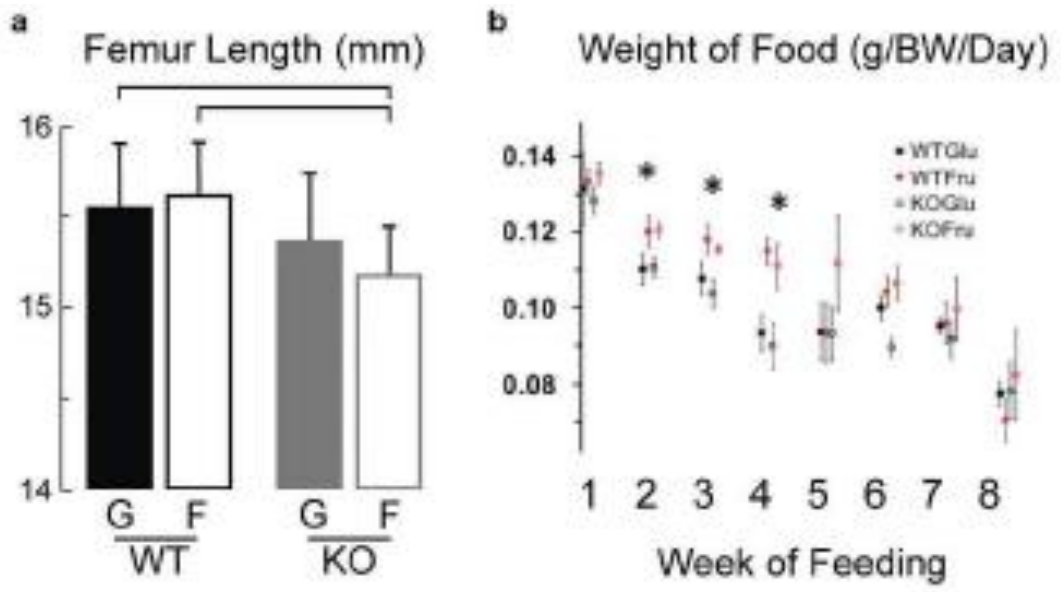

Figure 3-3: (a) Femur lengths and (b) food consumption of WT and KO mice fed for 8 weeks on a 20% glucose (G, control) or 20% fructose (F) diet started after weaning at 4 weeks of age (panel a. n= 10-12 mice per group; panel b, n= 3-4 cages per group. means ± SD). Weight of daily food provided was normalized to the body weight (BW) of all mice in a cage. Fructose-fed mice ate more than glucose-fed mice in weeks 2-4 only. Significant differences between groups determined by ANOVA with Tukey post-hoc test ($p < 0.05$).

Effects of fructose on metaphysis. Fructose had its greatest impact on the morphology of cancellous bone (Fig. 3-4). Fructose feeding affected the bone mineral density (BMD) and BV /TV of cancellous bone, more so in the KO than WT mice, and in the distal versus proximal ROIs. For example, cancellous BV /TV was greater with fructose feeding ($p < 0.05$) in KHK-KO by 91% and 61% in the distal and proximal ROIs, respectively. The increased volume was driven mainly by the increased Tb.N. The connectedness of the trabeculae was significantly increased by fructose with KHK-KO mice having higher

connectivity in the distal trabecular ROI. This is reflected by the reduced pattern factor between the fructose-fed KHK-KO versus all other groups.

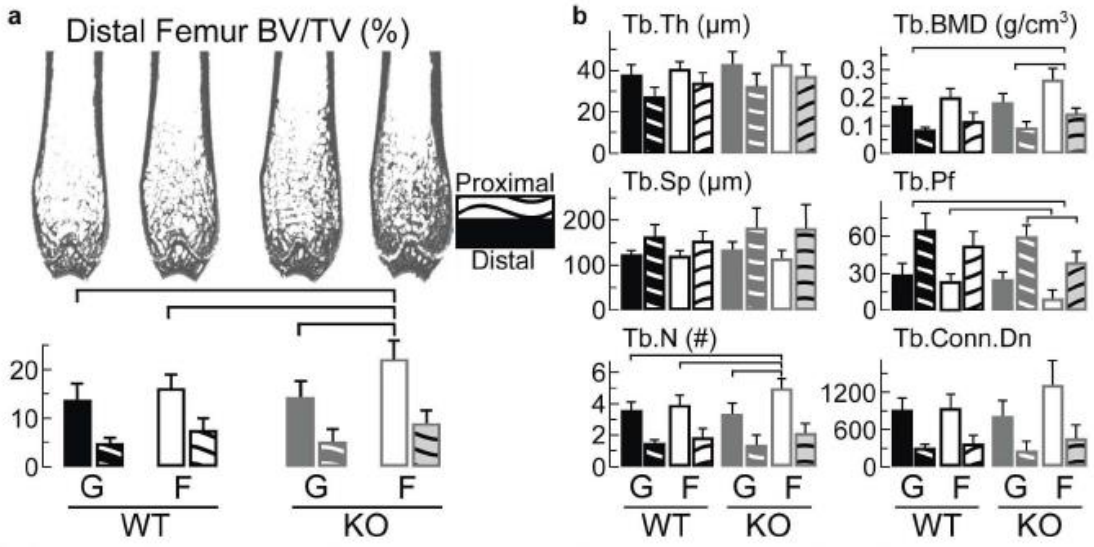

Figure 3-4: (a) 3D coronal reconstructions of 100 µm thick sections imaged with µCT from distal femurs of WT and KO mice fed for 8 weeks on a 20% glucose (G, control) or 20% fructose (F) diet started after weaning at 4 weeks of age. Plotted are trabecular bone volume fraction (BV/TV) of distal (solid box plots) and proximal ROIs. (b) Distal and proximal trabecular (Tb) morphology (Th, Sp, N), composition (BMD) and connectivity (Pf, Conn.Dn). Significant differences between groups determined by ANOVA with Tukey post-hoc test ($p < 0.05$; n= 10-12 mice per group; means ± SD).

Effects of fructose on diaphysis. The endosteal perimeter of fructose-fed mice, both WT and KHK-KO, were significantly smaller (-11%, $p < 0.05$) versus glucose-fed controls (Table 3-4). Consistent with the effect of fructose feeding on this histomorphometry parameter, fructose feeding influenced ($p < 0.05$) the fraction of cross-sectional cortical bone area to total area (%Ct.Ar) measured by µCT without affecting total area in KHK-

KO mice (13%, $p < 0.01$). Since there were no differences in total area or periosteal perimeter, the polar moment of inertia was unaffected. Three-point bending of femurs of WT and KHK-KO fed either glucose or fructose demonstrated similar structural mechanical properties. There were no significant differences in the load to failure, stiffness, and elastic or plastic displacement, regardless of diet or genotype (Table 3-5).

	WT		KHK-KO		Statistics		
	Glucose	**Fructose**	**Glucose**	**Fructose**	**Diet**	**Genotype**	**Interaction**
Femoral Cortical MicroCT							
Ct.BMD (g/cm^3)	0.98 ± 0.07	0.98 ± 0.06	0.99 ± 0.03	0.98 ± 0.09	ns	ns	ns
Ct.B.Ar (mm^2)	0.87 ± 0.06	0.96 ± 0.10	0.96 ± 0.12	1.03 ± 0.08	0.044	0.035	ns
Ct.M.Ar (mm^2)	1.82 ± 0.29	2.08 ± 0.28	2.21 ± 0.37	1.92 ± 0.24	ns	ns	0.023
Ct.Tt.Ar (mm^2)	2.69 ± 0.34	3.03 ± 0.38	3.17 ± 0.49	2.94 ± 0.29	ns	ns	0.048
%Ct.Ar (%)	32.56 ± 2.14^{a,b}	31.61 ± 1.37^{a,b}	30.40 ± 1.47^{a}	34.19 ± 1.49^{b}	0.036	ns	0.001
Ct.MMI (mm^4)	0.66 ± 0.13	0.83 ± 0.20	0.87 ± 0.23	0.83 ± 0.12	ns	ns	ns
Ct.Th (μm)	97.04 ± 3.84	95.17 ± 2.79	101.73 ± 7.83	101.16 ± 11.28	ns	ns	ns
Tibial Endosteal Histomorphometry							
Perimeter (mm)	4.51 ± 0.37^{a,b}	4.31 ± 0.45^{a}	5.01 ± 0.69^{b}	4.48 ± 0.24^{a,b}	0.047	ns	ns
Mineralizing Surface (%)	0.69 ± 0.22	0.74 ± 0.11	0.68 ± 0.17	0.67 ± 0.16	ns	ns	ns
Mineral Apposition Rate (μm/day)	1.46 ± 0.34	1.62 ± 0.38	1.25 ± 0.40	1.71 ± 0.49	ns	ns	ns
Bone Formation Rate (μm^3/μm^2/day)	1.04 ± 0.47	1.19 ± 0.33	0.91 ± 0.45	1.18 ± 0.48	ns	ns	ns
Tibial Periosteal Histomorphometry							
Perimeter (mm)	7.03 ± 0.56	7.17 ± 0.46	7.28 ± 0.63	7.27 ± 0.41	ns	ns	ns
Mineralizing Surface (%)	0.22 ± 0.05	0.21 ± 0.04	0.27 ± 0.05	0.20 ± 0.08	ns	ns	ns
Mineral Apposition Rate (μm/day)	1.27 ± 0.29	1.37 ± 0.44	1.12 ± 0.36	1.59 ± 0.31	ns	ns	ns
Bone Formation Rate (μm^3/μm^2/day)	0.30 ± 0.09	0.29 ± 0.10	0.30 ± 0.12	0.37 ± 0.13	ns	ns	ns

Table 3-4: Femoral and tibial cortical measurements made by µCT, and histomorphometry (n=10-12 mice per group; means ± SD). Means were compared with two-way ANOVA. Similar superscripts indicate values that are not significantly different from each other at $p < 0.05$ by post-hoc Tukey test.

	WT		KO	
	Glucose	**Fructose**	**Glucose**	**Fructose**
3-Point Bending Parameter				
Ultimate Load (N)	17.88 ± 3.55	19.08 ± 2.59	17.45 ± 1.46	19.06 ± 2.72
Yield Load (N)	13.68 ± 3.11	14.61 ± 3.76	13.59 ± 1.38	13.53 ± 3.95
Maximum Displacement (mm)	0.85 ± 0.15	0.86 ± 0.29	0.89 ± 0.37	0.80 ± 0.17
Yield Displacement (mm)	0.24 ± 0.08	0.22 ± 0.06	0.21 ± 0.10	0.21 ± 0.12
Post-Yield Displacement (mm)	0.61 ± 0.12	0.64 ± 0.28	0.67 ± 0.37	0.60 ± 0.20
Stiffness (N/mm)	103.97 ± 25.15	110.00 ± 24.13	110.89 ± 34.51	116.42 ± 22.21
Total Work (N*mm)	11.17 ± 3.11	11.73 ± 3.99	11.07 ± 3.79	11.22 ± 3.22

Yield Work (N*mm)	1.25 ± 0.56	1.31 ± 0.57	1.15 ± 0.43	1.27 ± 1.14
Post-Yield Work (N*mm)	9.91 ± 2.76	10.41 ± 3.81	9.91 ± 3.87	9.95 ± 3.59

Table 3-5: Mechanical testing parameters from femurs (n=10-12 mice per group). Values, presented as means ± SD, exhibited no significant differences by two-way ANOVA, $p < 0.05$.

Effects of fructose on expression of bone-relevant genes in kidney and gut. Expression of renal genes encoding for vitamin D metabolism was significantly different in KHK-KO fructose-fed mice, compared to all other groups (Figure 3-5). The expression of Cyp27b1 (catalyzing the conversion of 25-vitamin D to 1,25VitD3 D) was significantly lower (~80%) in KHK-KO fed fructose. The gene that encodes the Vitamin D degrader (Cyp24a1) was significantly increased (-300%) in the KHK-KO mice fed fructose. Renal expression for the calcium-binding protein Calbindin D9K (CaBP9k) was decreased (>50%) in fructose-fed KHK-KO compared to WT (Table 3-6). Expression of the apical calcium transporter, transient receptor potential vanilloid 5 (Trpv5), was significantly greater in KO mice compared to WT (-40%). Differences in renal gene expression were not associated with any variation in kidney weights (Table 3-7).

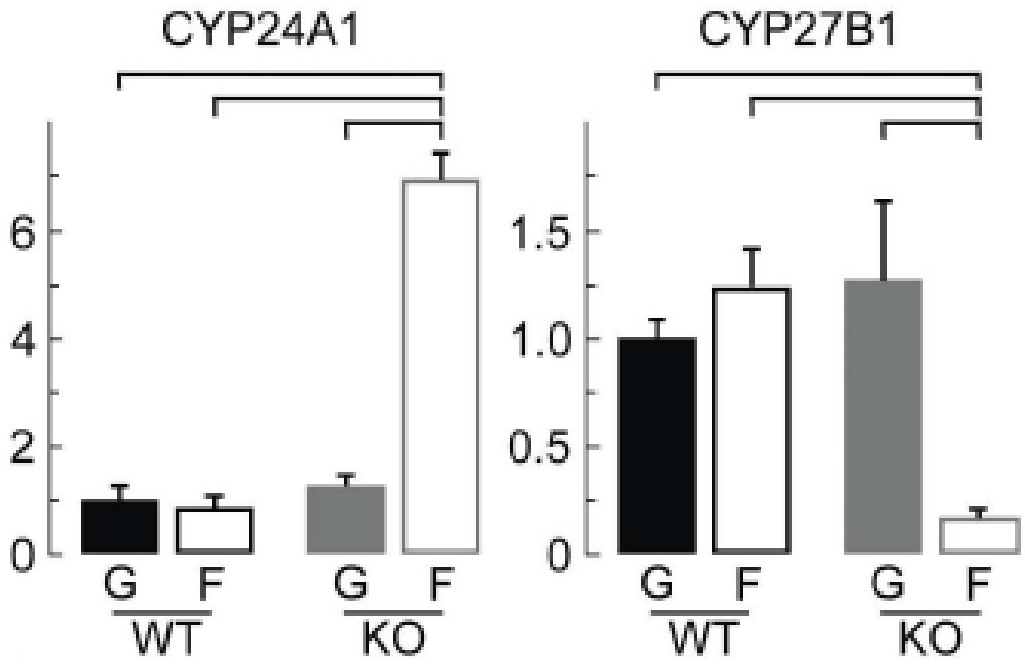

Figure 3-5: Renal gene expression of Vitamin D metabolizing enzymes from mice fed for 8 weeks on a 20% glucose (G, control) or 20% fructose (F) diet started after weaning at 4 weeks of age (n= 6-8 mice per group; means ± SD). Significant differences between groups determined by ANOVA with Tukey post-hoc test ($p < 0.05$).

	WT		KHK-KO		Statistics		
	Glucose	**Fructose**	**Glucose**	**Fructose**	**Diet**	**Genotype**	**Interaction**
Kidney							
KHK	1.00 ± 0.34	1.34 ± 0.68	nd	nd	ns	< 0.0001	ns
GLUT5	1.00 ± 0.28	1.19 ± 0.35	1.39 ± 0.49	1.20 ± 0.26	ns	ns	ns
CaBP9k	1.00 ± 0.23[a,b]	1.24 ± 0.40[a]	0.83 ± 0.51[a,b]	0.49 ± 0.14[b]	ns	0.003	0.043
TRPV5	1.00 ± 0.25[a]	1.19 ± 0.46[a]	1.67 ± 0.32[a,b]	1.85 ± 0.78[b]	ns	0.004	ns
Klotho	1.00 ± 0.29[a]	1.20 ± 0.21[a,b]	1.37 ± 0.13[b]	1.17 ± 0.21[a,b]	ns	ns	0.030
NaPi2a	1.00 ± 0.26[a]	1.02 ± 0.38[a]	1.89 ± 0.90[b]	1.28 ± 0.24[a,b]	ns	0.006	ns
GP6ASE	1.00 ± 0.12	1.01 ± 0.14	1.56 ± 0.50	1.29 ± 0.15	ns	ns	ns
Duodenum							
KHK	1.00 ± 0.08[a]	1.70 ± 0.26[b]	nd	nd	< 0.001	< 0.001	< 0.001
GLUT5	1.00 ± 0.36[a]	8.82 ± 5.75[b]	1.28 ± 0.50[a]	1.09 ± 0.35[a]	0.003	0.003	0.002
CaBP9k	1.00 ± 1.32	1.93 ± 2.01	2.09 ± 2.16	1.09 ± 1.59	ns	ns	ns
TRPV6	1.00 ± 0.94	1.13 ± 0.93	2.14 ± 1.09	1.36 ± 0.87	ns	ns	ns
Jejunum							
KHK	1.00 ± 0.17	1.25 ± 0.14	nd	nd	0.0081	< 0.001	0.0072
GLUT5	1.00 ± 0.38[a]	3.90 ± 0.94[b]	1.00 ± 0.53[a]	1.00 ± 0.35[a]	0.002	0.002	0.002
CaBP9k	1.00 ± 0.54	1.33 ± 1.52	1.57 ± 1.12	0.46 ± 0.24	ns	ns	0.025

TRPV6	1.00 ± 0.32	0.71 ± 0.26	1.83 ± 2.17	1.18 ± 1.02	ns	ns	ns
THP1	1.00 ± 0.09	0.96 ± 0.08	0.99 ± 0.12	1.04 ± 0.07	ns	ns	ns

Table 3-6: Fold differences (normalized to WT glucose) in renal and intestinal expression of genes involved in fructose and calcium metabolism (n=6-8 mice per group; means ± SD). Means were compared with two-way ANOVA. Similar superscripts indicate values that are not significantly different from each other ($p > 0.05$ by post-hoc Tukey test).

	WT		**KHK-KO**		**Statistics**		
	Glucose	**Fructose**	**Glucose**	**Fructose**	**Diet**	**Genotype**	**Interaction**
Organ Weights							
Kidney (g)	0.173 ± 0.031	0.181 ± 0.034	0.173 ± 0.030	0.169 ± 0.014	ns	ns	ns
Liver (g)	1.152 ± 0.104	1.287 ± 0.152	1.197 ± 0.187	1.126 ± 0.150	ns	ns	0.029
Caecum (g)	0.202 ± 0.042[a]	0.197 ± 0.045[a]	0.216 ± 0.018[a]	0.628 ± 0.122[b]	< 0.001	< 0.001	< 0.001
Spleen (g)	0.098 ± 0.018	0.111 ± 0.033	0.098 ± 0.020	0.093 ± 0.019	ns	ns	ns
Epidemial Fat (g)	0.796 ± 0.24	0.871 ± 0.33	0.896 ± 0.293	1.022 ± 0.505	ns	ns	ns

Table 3-7: Organ weights. Values are mean ± SD (n=10-12 mice per group). Means were compared with two-way ANOVA. Similar superscripts indicate values that are not significantly different from each other at $p < 0.05$ by post-hoc Tukey test.

As expected, Glut5 in the duodenum and jejunum was significantly increased with fructose feeding in WT and not in KO. Intestinal expression of the calcium transporters Trpv6 and CaBP9k were unaffected by sugar type regardless of genotype. Jejunal expression of tryptophan hydroxylase 1 (Tph1), the rate-limiting enzyme for serotonin synthesis, was also not affected.

Relationships between plasma fructose and bone parameters. To explore the large variation in plasma fructose levels in KHK-KO mice fed either glucose or fructose, we examined relationships between plasma fructose and bone parameters (Figure 3-6, Table 3-8), including ultimate load ($R^2 = 0.48$, $p < 0.02$), post-yield displacement ($R^2 = 0.49$, $p < 0.02$), and post-yield and total work to failure ($R^2 = 0.55$, $R^2 = 0.57$, $p < 0.01$). Sclerostin (SOST), an inhibitor of bone formation produced by osteocytes and involved in the FGF23/1,25VitD3 kidney to bone cytokine signaling axis, also demonstrated a strong positive relationship with plasma fructose levels ($R^2 = 0.58$, $p < 0.01$). Significant, strong relationships between plasma fructose and trabecular bone μCT measurements were also observed (Tb.BMD: $R^2 = 0.71$, $p < 0.001$, Distal Tb.BV/TV: $R2 = 0.62$, $P < 0.01$).

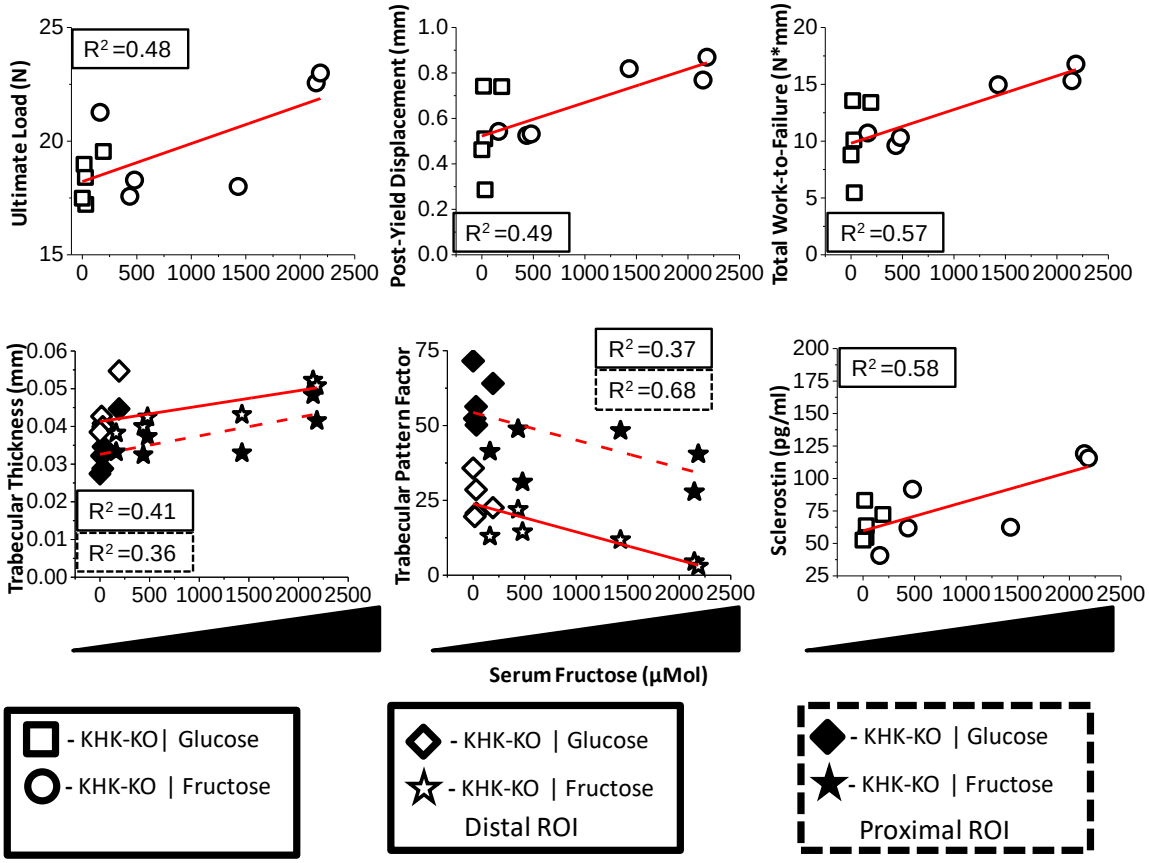

Figure 3-6: Relationships ($p < 0.05$) between bone parameters and plasma fructose in KHK-KO mice. For trabecular thickness and pattern factor, open and closed shapes refer to the distal and proximal ROIs, respectively (see Figure 3-4)

	r^2			p-values		
	all	WT	KO	all	WT	KO
Mechanical Testing						
Ultimate Load	+ **0.20**	+ 0.10	+ **0.48**	0.037	0.354	0.018
Max. Displacement	+ **0.20**	+ 0.14	+ **0.53**	0.043	0.279	0.012
PY Displacement	+ 0.09	- 0.06	+ **0.49**	0.245	0.485	0.016
PY Work	+ **0.19**	- 0.05	+ **0.55**	0.040	0.509	0.009
Total Work	+ 0.17	- 0.06	+ **0.57**	0.059	0.475	0.007
µCT						
Ct.B.Ar	+ **0.18**	+ 0.19	+ 0.16	0.046	0.162	0.217
Ct.Th	+ **0.18**	- 0.01	+ 0.12	0.042	0.709	0.290
Distal.Tb.BMD	+ **0.60**	+ **0.42**	+ **0.71**	0.001	0.023	0.001
Distal.Tb.BV/TV	+ **0.52**	+ 0.32	+ **0.62**	0.001	0.053	0.004
Distal.Tb.Th	+ **0.38**	+ 0.10	+ **0.36**	0.002	0.316	0.050
Distal.Tb.Sp	+ 0.01	- **0.45**	- 0.01	0.943	0.017	0.895
Distal.Tb.N	+ **0.27**	+ **0.38**	+ 0.31	0.011	0.034	0.073
Distal.Tb.Pf	- **0.47**	- 0.19	- **0.68**	0.001	0.159	0.002
Proximal.Tb.BMD	+ **0.23**	+ **0.64**	+ 0.27	0.021	0.002	0.101
Proximal.Tb.Th	+ **0.32**	+ 0.16	+ **0.41**	0.005	0.192	0.035
Proximal.Tb.N	+ 0.01	+ **0.84**	+ 0.01	0.595	0.001	0.759
Proximal.Tb.Conn.Dn	- 0.01	+ **0.78**	- 0.01	0.881	0.001	0.742
Proximal.Tb.Pf	- **0.26**	- 0.29	- **0.37**	0.013	0.070	0.048
Histomorphometry						
Oc.Lc.Dn/Avg.BFR	+ **0.35**	- 0.01	+ **0.60**	0.020	0.959	0.025
Bone Markers						
SOST	+ **0.54**	+ 0.19	+ **0.58**	0.001	0.185	0.007
FGF23	+ 0.06	+ **0.40**	+ 0.04	0.300	0.037	0.598
Weights						
Kidney	- 0.01	+ **0.45**	- 0.03	0.882	0.023	0.607
Liver	- 0.01	+ **0.35**	- 0.03	0.578	0.041	0.598
Caecum	+ **0.65**	+ 0.19	+ **0.58**	0.001	0.151	0.007
Gene Expression						
Renal Cyp24a1	+ **0.41**	+ **0.67**	+ 0.25	0.002	0.004	0.145
Renal Trpv5	+ **0.21**	+ 0.14	+ 0.08	0.041	0.279	0.419
Douadenal Trpv6	- 0.04	+ **0.41**	- **0.49**	0.349	0.024	0.017
Jujunal Khk	+ **0.47**	+ **0.47**	nd	0.014	0.014	-
Jujunal CaBP9k	- **0.17**	- 0.12	- 0.23	0.049	0.276	0.140

Table 3-8: Significant ($p < 0.05$) relationships between plasma fructose and other measured study parameters.

Discussion

Increased fructose in the KHK-KO impaired the attainment of peak bone length and mineral content during growth. In humans, the attainment of these peaks contributes to osteoporosis prevention and a healthy lifespan (83, 87). Importantly, our mouse study utilized a calorie-matched, 20% fructose-in-food diet, presenting a fructose level attained with some current western diets, and a lower level than often studied, probably due to a lack of association with obesity, early onset metabolic syndrome, non-alcoholic fatty liver disease or diabetes. Thus, as opposed to work with higher fructose concentration (154), we did not observe effects on plasma insulin, or the weights of the epididymal WAT pad, or liver (Table 3-1and Table 3-2).

The data (Figs. 1 and 3) also do not support our original hypothesis, that consumption of 20% dietary fructose by WT mice for 8 weeks would raise plasma levels and affect normal bone growth. However, the data unveiled a previously unrecognized, possibly direct effect that may not require fructose metabolism in central (intestine and liver) or peripheral tissues to affect bone growth. The KHK-KO (both isoforms) does not possess the primary mechanisms for central metabolism and control of circulating fructose, and peripheral fructolytic activity is also substantially inhibited. Peripheral plasma fructose concentrations rose over 40-fold, to the mM range in this current study (Fig. 1a). These data confirm the recent demonstration that as intestinal capacity to cope with fructose is overwhelmed, fructose plasma concentration rises (162). Similar to our findings in KHK-KO mice, the plasma fructose concentrations are elevated in individuals diagnosed with EBF (22, 163). Increased plasma fructose in the mice may be responsible for the significant bone growth

disruption, including decreased long-bone length, and increased trabecular volume fraction with altered pattern factor after 8 weeks of feeding (Figs. 3 and 4).

Plasma fructose concentrations are rarely accurately measured in rodents or humans and, based on this study and one previous, may be highly variable despite utilization of controlled-content diets (140). We utilized HPLC to isolate fructose from other sugars and metabolites found in plasma. Though more labor intensive and costly than enzymatic assays that measure fructose by direct metabolism of fructokinase or indirect sugar conversion (159), the high sensitivity of HPLC is required to measure concentrations that do not normally exceed 100 μM. Additionally, in the current study this high sensitivity allowed possible relationships between fructose and bone to emerge (Fig. 6 and Table 3-8). Feeding fructose at a supra-physiological level, 60% or greater to WT rats for 4-6 weeks also elevates plasma fructose to the mM range (116, 143). Supporting the hypothesis that an elevated plasma fructose level contributes to inhibiting long bone growth, our group reported that a high, chronic diet (63%, 4 weeks) reduced femur length by - 5% in rapidly growing male rats (115).

In the present study, there were no differences in gene expression for the calcium transport genes Trpv6 in the jejunum or CaBP9K and Trpv6 in the duodenum, confirming our previous findings (118, 143). However, in the kidney, Trpv5 was greater and CaBP9K lower by half in the fructose-fed KO compared to the age-matched, WT fed glucose (Table 3-6). CaBP9K and Trpv5 are Vitamin D dependent calcium transporters. Previously, we

also found fructose-dependent reductions in Vitamin D receptor binding to the promoter of CaBP9K (116).

Fructose consumption in KHK-KO also resulted in reduced and increased renal expression of Cyp27b1 and Cyp24a1 genes, respectively, confirming the effects we observed previously and associated with reduced systemic levels of 1,25(OH)Vitamin D3 (1,25VitD3) (115, 116, 118, 140, 143). There are strong relationships between these Cyps and the bone morphological parameters (Table 3-8). The Cyp27b1 gene encodes for a mitochondrial cytochrome P450 enzyme, *1α*-hydroxylase, which hydroxylates 25-hydroxyvitamin D3 at the 1α position to its active form of 1,25VitD3. 1α-hydroxylase-KO mice have shortened long bones and increased trabecular BV/TV (164-166). Osteogenic expansion of their marrow in the obCFU assay also leads to fewer number of ALP-stained colonies (165). The poor growth associated with Cyp27b1 deficiency could account for decreased long bone length in our work (168). Cyp24a1 is the gene responsible for degrading active 1,25VitD3 to its inactive form 24,25VitD and a regulator is FGF23, an endocrine cytokine produced by osteocytes that binds with a renal co-factor Klotho produced in the kidney, to reduce systemic 1,25VitD3 and to increase phosphate clearing (169). No differences in systemic FGF23 (Table 3-1) or Klotho (Table 3-6) expression were detected. Thus, overall, our data raise the important question of how circulating fructose with a limited ability for metabolism, can mediate regulators of Vitamin D with the possible effect of lowering calcium reabsorption in the kidney. To help answer this question in future work will require accurate measurement of not only Vitamin D (25VitD and 1,25VitD3), but also calcium and phosphate in plasma.

Generally, studies that found detrimental effects on growing bone in other rodent models, included increased fat and calories by introducing sugars in ad-libitum drinking water (41, 151-153, 170). Bass *et al.* fed two-month old rats for 12 weeks into skeletal maturity and found that a 40% fructose diet (with 10% glucose) increased distal femur BV/TV (+14%) and trabecular thickness (+16%) with no differences demonstrated by dynamic histomorphometry (154). Our group found that this level of fructose would not be tolerated by the KHK KO for more than a few days (157). To our knowledge, no other groups have specifically examined the effects of fructose alone on bone growth.

Fructose feeding reduced the number of potential osteogenic progenitor cells in an Ob-CFU assay of bone marrow cells (Table 3-3). Felice *et al.* made similar findings with a high-fructose diet that was not matched for calories (41, 151). This potential reduction of *in vitro* primary osteoblasts did not manifest in any *in vivo* mineral apposition or bone formation rate differences in either study. While interesting, the differences may simply reflect a loss of progenitor cell plasticity after removal from their niche. Though we did not detect overall significant differences in plasma sclerostin (SOST; Table 3-1), there is a relationship between elevated plasma fructose and elevated plasma sclerostin (Fig. 6). Sclerostin is an inhibitor of osteoblast activation and knocking out the gene in mice leads to increased cortical bone mass (69). The elevation of systemic sclerostin in fructose-fed mice could reduce the potential of bone marrow cells to commit to the osteogenic lineage. These studies should be repeated with pooling of marrow from multiple bones of individual

mice to examine whether the variability between individual mice in blood fructose levels might explain differences in progenitor cell populations in the bone marrow.

Several other limitations exist in this study. Plasma collection from each mouse was limited to 100-300 µL. Thus, we utilized the most economical assays of HPLC and magnetic enzyme-linked analysis. Our bone plasma parameters were limited in that we were unable to measure osteocalcin and RANKL, due to conflict arising from dilution and cross reactivity, and active 1,25VitD3 and tartrate-resistant acid phosphatase 5b, due to volume limitations. The possibility exists that KHK-KO did not adjust as quickly to the fructose diet as indicated by smaller body weights early on in feeding. All other measurements were completed at the end of the 8 weeks of feeding and after body weights had quickly equilibrated so that all groups had equivalent weights (Fig. 2). Experiments in male mice thus far should be repeated in females and results verified at younger ages to determine whether the effects on jejunum, kidney and bone are cumulative as plasma fructose levels rise or could be reversed.

In conclusion, fructose affected bone independent of fructose metabolism in mice. In KHK-KO, dysregulated fructose metabolism raised the concentration of the sugar ~40-fold with fructose diet (Fig. 1a). Like observations after chronic fructose feeding of rats, our KHK-KO mice demonstrated reduced bone length and perturbation of Vitamin D metabolism, possibly indicating a direct interaction between fructose and the proximal tubule cells (Figs. 2a and 5; Table 3-6). The bones of KHK-KO mice with the highest levels of fructose were shorter in stature, like mice with Cyp27bl gene deletion. The mechanism by which

fructose directly interacts with the kidney-bone axis requires further study. In humans, EBF is rarely diagnosed in childhood. As the diets of industrialized nations incorporate more fructose, non-benign effects in those with EBF and others with inhibited fructose metabolism may include reduced stature and vitamin D metabolism.

Acknowledgments

Publication was supported by the National Institute of Arthritis and Musculoskeletal and Skin Diseases of the NIH (AR063351) and Rutgers University. We thank Drs. Joseph Geissler, George Pellegrino, Stephen Flowers and Chirag Patel, as well as Brian Canter, Mayuri Kinkhabwala, Juby Roy, David Sadegh, Timothy Ngoge, Alexander Kheshvadjian, Joe Lumuti and Luke Fritzky for technical assistance. As this dissertation was being submitted the manuscript based on this chapter was undergoing peer review and will be published with the following author list: Edek A.J. Williams[1], Veronique Douard[2], Keiichiro Sugimoto[3,4], Fabienne Devime[2], Xufei Zhang[2], Kunihiro Kishida[5], Ronaldo P. Ferraris[6], J. Christopher Fritton[1], 1) Department of Biomedical Engineering, Graduate School, Rutgers University, New Brunswick & Department of Orthopaedics, New Jersey Medical School, Rutgers University, Newark, NJ, USA, 2) MICALIS Institute, INRA, AgroParisTech, Université Paris-Saclay, Jouy-en-Josas, France, 3) Research and Development Center, Nagaoka Co. Ltd., Ibaraki, Osaka, Japan, 4) Center for Research and Development of Bioresources & Department of Clinical Nutrition, College of Health and Human Sciences, Osaka Prefecture University, Habikino, Osaka, Japan, 5) Department of Science and Technology on Food Safety, Kindai University, Wakayama, Japan; 6) Department of Pharmacology and Physiology, New Jersey Medical School, Rutgers

University, Newark, NJ, USA. All authors contributions are gratefully acknowledged. Specifically, the contributions of authors were to study design (EW, VD, RF, JF), data collection (EW, KS, FD, XZ, KK), data analysis and interpretation (EW, VD, RF, JF), writing of first draft (EW), and critical editing of the final version of the manuscript (VD, RF, JF).

Chapter 4 : Elevation of Serum Fructose in both ketohexokinase sufficient and deficient mice with the use of osmotic pumps

Abstract

Fructose is a simple sugar metabolized by cells through the enzyme ketohexokinase (KHK). Studies in humans and rodents have demonstrated that fructose affects bone, though few have measured plasma fructose to determine if the sugar has a direct effect. We previously found that serum fructose correlates with several mechanical factors. We hypothesize that fructose effects could be elicited by raising and maintaining postprandial plasma fructose levels with the use of osmotic pumps. We utilized male mice: 8 groups (n=12) of 4-week-old, wild-type C57Bl/6 and KHK-null; implanted with an osmotic pump containing either fructose or saline. Implant groups were further divided into normal or low calcium diets for the duration of implantation (8 weeks). As expected, calcium status elicited differences in bone formation rate and the number of osteocytes as measured by histology, and bone morphometry by microCT. Fructose was elevated > 100% in fructose implanted animals, but this did not reach postprandial levels. Fructose administration, increased tibia length, but did not affect circumferential bone formation. This work serves as a proof of concept that fructose levels can be elevated with the use of an osmotic pump and that peripheral tissues are sensitive to the direct fructose interaction.

Introduction

Fructose intake has increased greatly over the past 50 years and its effects have been studied extensively in humans and rodents. Feeding experiments in rodents use high dosages of fructose to illicit a metabolic response. Fructose is catabolized, in an unregulated manner by two isoforms of ketohexokinase (KHK), A and C (21, 26). KHK-C has the highest affinity for fructose and is primarily found in hepatocytes, enterocytes, renal proximal tubule cells and white adipose tissue (WAT) cells (157). In peripheral tissues, KHK-C is not expressed and fructolysis is facilitated by way of KHK-A or hexokinases other than KHK, with a lower affinity for fructose (27). Fructose is transported from the intestinal lumen to the liver via the portal vein, where 50-75% of the fructose load is metabolized before reaching the systemic blood supply (23, 24). In humans, ingestion of a fructose sweetened drink, fructose levels rapidly spike from 5µM to 300µM, and remain elevated for up to 3 hours (32).

Though fructose is minimally used by extra-hepatic tissues, metabolism still occurs (8, 19). There may be a direct interaction between fructose on extra-hepatic tissues, either by local metabolism or changes to the extracellular matrix. These direct interactions may be confounded by systemic metabolism. Fructose is known to disrupt normal energy metabolism and is linked to the development of non-alcoholic fatty liver disease, glucose intolerance, hyperlipidemia, obesity, insulin resistance (IR), metabolic syndrome (MS), hypertension, gout, atherosclerosis, dyslipidemia and eventually, Type-2 Diabetes Mellitus (T2DM) (21, 23, 28, 172). These pathologies all have negative effects on bone. When fructose is studied in bone, confounding effects may mask potential mechanism(s).

Rodent models where fructose is given by food or drink have not been able to elucidate a mechanism or a direct effect of the sugar on bone. When given free access to 10%v/v fructose water rat bones saw decreased number of active bone cells (osteoblasts, osteoclasts and osteocytes) via histology and osteogenic marrow cell culture, (41, 151). There is currently no consensus in the field of fructose and bone on: fructose administration by D-fructose, HFCS or sucrose; choice of animal model; administration via chow or addition to water; fructose concentrations; animal age (41, 118, 143, 151-154), making comparison between studies difficult.

The rise and fall of plasma fructose concentrations resemble drug kinetics and maintaining elevated plasma fructose concentrations is difficult experimentally. It would be advantageous in determining direct mechanisms of fructose *in vivo* if fructose concentrations were controlled. Osmotic pumps are rate-controlled systems that continuously deliver a target drug for the duration of a study. Fructose and saline, with similar osmotic pressures, are both used as vehicles for drug delivery (173). Using an osmotic pump filled with fructose, we will elevate plasma fructose concentrations to a constant level, independent of consumption or ability to metabolize the sugar. These increases in serum plasma will lessen the adaptive response of bone to calcium restriction.

Previously, we demonstrated that fructose reduced Vitamin-D dependent calcium transport in the gut, during growth (118) due to disruption of renal Vitamin D metabolism. Calcium restriction thru diet, elicits the Vitamin D cascade, which includes increased calcium

transport at the gut, increased calcium reabsorption and excavation of calcium from the skeleton. Fructose disrupts this cascade at the 1,25 Vitamin D hydroxylation. As systemic calcium is tightly regulated, disruptions in calcium metabolism are detriments to bone, with increased fracture risk. Therefore, we hypothesize plasma fructose levels, elevated by osmotic pumps will affect the adaptive responses of bone to calcium restricted diet.

Materials and Methods

The effects of fructose were examined in male mice with protocols approved by the Institutional Animal Care and Use Committee (New Jersey Medical School, Rutgers). Mice were housed in groups of 3 – 5 mice per cage in a barrier facility on a 12-hour day/night cycle. Schematics of experimental designs and timelines are found in supplementary material (Figure A5-3). To isolate the effects of plasma fructose versus that passing through the gut, fructose was provided either in the chow or via an osmotic pump (Alzet® Model 1004, DURECT Corporation, Cupertino, Ca). Experimental diets were modified from a standard American Institute of Nutrition (AIN)-93G formula by the manufacturer (Research Diets, New Brunswick, NJ) (Table A6-2).

Osmotic Pump Preparation and Implantation. An osmotic pump was utilized to raise plasma fructose levels. Saline and fructose diluted in saline were filtered through a 0.20µm syringe filter and injected into pump using filler tubes. Pumps were filled with 100µL of saline or a fructose concentration determined by body weight. Pump implantation was completed as per manufacturer instructions subcutaneously on the back. Sedation was induced and maintained with 5% and 3% isoflurane, respectively. The incision site was

cleaned with antiseptic and local anesthesia was accomplished with 2mg/kg of body weight Bupivacaine (Marcaine, Hospira, Inc, Lake Forest, IL) was injection. A 15 mm incision was made above the scapula from the midline, laterally. A hemostat was used to separate the skin from the fascia to create a 2-3 cm pocket. A pump was then placed flow regulator first into the pocket and the incision closed with 1-2 7mm wound clips (Reflex7, CellPoint Scientific Inc, Gaithersburg MD). Pumps were replaced after 4 weeks. Implantation and re-implantation were performed within 20 minutes of initial isoflurane exposure.

Genotyping. KHK-KO (background: C57BL6) mice were donated by R. J. Johnson, University of Colorado, and the generation of the model was previously described (27). Both isoforms of KHK (KHK-A, KHK-C) were deleted, effectively abolishing fructose breakdown. Heterozygous progeny of KHK-KO male and WT females yielded the parents of experimental homozygotes. Pups were genotyped at 3 weeks old, with PCR on DNA extracted from 2-mm ear punches (PCRBio, London).

Tissue and Cell Collection. After sedation, blood was collected via cardiac puncture in tubes containing EDTA, and inhibitors, protease (Pefabloc, Sigma) and DPP-IV (Millipore), at final concentrations of 2 µg/mL and 0.02 µL/mL, respectively. Centrifugation was at 1300g for 15 minutes and storage was at -80°C. Bilateral kidneys and liver were resected, weighed and flash frozen in liquid nitrogen. Tibias and femurs were dissected, and length recorded (0.01 mm caliper resolution). The right tibia was fixed in 10% neutral-buffered formalin for histomorphometry. The left femur was resected of

muscle and placed in sterile ice-cold saline for flushing and cell culture and the right was wrapped in saline-soaked gauze and frozen for mechanical testing.

Plasma Analysis. Plasma fructose was determined by high-performance liquid chromatography (HPLC) of terminal blood draw as previously described (159). Samples were diluted with acetyl-nitrile and stored (-80C). Samples were filtered through a 0.45-µm membrane before being analyzed in triplicate and HPLC was performed using a GL-7400 series system (GL Sciences, Tokyo, Japan) equipped with an amino column Shodex Asahipak NH2P-50 4E (4.6 mm ID x 250 mm; Showa Denko, Tokyo, Japan) with a guard column at an injection volume of 5 µL. Samples <50 µM were reanalyzed at an injection volume of 20 µL. The separation of fructose was performed with a linear gradient in hydrophilic interaction chromatography mode, as previously described (159). Flow rate and temperature were 1.0 mL/minute and 40° C, respectively. Post-column labeling of fructose with phenylhydrazine was taken at 150° C in a reactor 522 (Flom, Tokyo, Japan), and the flow rate of reaction reagent (mixture with 180 mL of acetic acid, 6 mL of phenyl hydrazine, and 220 mL of phosphoric acids) was 0.4 mL/minute. Fluorescence was detected with GL-7453 (GL Sciences) set at an excitation and emission wavelength of 330 and 470 nm, respectively. Data was analyzed using EZChrom Elite version 3.1.5J (Agilent Technologies)

Plasma bone and gut makers were measured using the Milliplex multi-analyte profiling (MAP) kits MBNMAG-41K and MGTMAG-78K (EMDMillipore, Billerica, MA). Analytes measured by the bone kit included: interleukin 6 (IL-6), osteoprogerin (OPG),

Dickkopf-related protein 1 (DKK1), sclerostin (SOST), tumor necrosis factor alpha (TNF-α) and fibroblast growth factor 23 (FGF23). Analytes measured by the gut kit included: gastric inhibitory protein (GIP), glucagon-like protein 1 (GLP-1), insulin, leptin and peptide YY (PYY). Bone kits were diluted 1:2 with assay buffer. Reaction plates were coated with assay buffer and decanted. Samples were incubated with antibody coated magnetic beads overnight and then incubated with detection antibody and streptavidin-phycoerythrin 30 minutes for each subsequent incubation. Analysis was performed using MAGPIX® with xPONENT software.

Histomorphometry. Bones for histomorphometry were embedded in polymethyl-methacrylate (Sigma), trimmed, sectioned transversely at 25% of the length from proximal end (diaphysis) with a diamond saw (Isomet 5000, Buehler) and fine polished with silicon carbide abrasive paper and alumina slurries (successive particle diameters of 1.0 and 0.05 μm). Bone formation during the last week of feeding was assessed with dynamic histomorphometric measures using calcein labels that had been injected (i.p., 20 mg/kg of body weight, Invitrogen C-481) at 9 and 2 days prior to death to label bone-forming surfaces (osteoblast activity). Blocks were imaged with a reflective confocal microscope (A1, Nikon, Tokyo, Japan) at 20x and 60x magnification.

Standardized bone parameter measurements were made on an interactive pen/tablet desktop workstation (Wacom Cintiq 21UX) using ImageJ software (160). Mineralizing surface (MS) and mineral apposition rate (MAR) were measured on 20x images, and bone formation rate (BFR) calculated for both periosteal (Ps) and endosteal (Es) cortical

surfaces. Mineralizing surface estimated the extent of actively mineralizing surface at the time of label administration and was the total extent of double label plus one half the extent of single label. Mineralizing surface was expressed as a ratio with bone surface (BS) as referent. Marrow apposition rate was the average distance between midpoints of the two consecutive labels, divided by the time between label injections. Bone formation rate was calculated as the product of MAR and MS/BS (142). Osteocyte lacunae between the calcein labels were point counted on 60x images.

µCT. Femurs were evaluated by µ-computed tomography (Bruker Skyscan 1172 120uA, 80 keV, 0.5 mm aluminum filter) for density and morphology. Femurs were submerged in saline and scanned, four at a time in a custom holder, at an isotropic voxel resolution of 8 µm. Density calibration phantoms (0.25 and 0.75 g/cm^3) were included with each scan for calculation of bone mineral density (BMD). Bones were then returned to saline soaked gauze and stored frozen (-20° C) prior to mechanical testing.

Trabecular (Tb) and cortical (Ct) traits were measured at set distances from the distal growth plate. Tb regions of interest (ROIs) were hand drawn at the marrow / endosteal border, starting 0.25 mm below the growth plate and were 3.9 mm in depth along the femur length. Ct midshaft ROI began 2.15 mm distal to the growth plate and were 0.43 mm in depth along the femur. Traits measured were: Trabecular: thickness (Tb.Th), spacing (Tb.Sp) number (Tb.N), pattern factor (Tb.Pf) and BMD; and Cortical: thickness (Ct.Th), area (Ct.Ar), and moments of inertia (Ct.MMI), and medullary area (or marrow, Ma.Ar).

Cortical area fractions (Ct.Ar/Tt.Ar and Ma.Ar/Tt.Ar), were calculated, where Tt, or total, equals Ma.Ar + Ct.Ar.

Whole-bone Mechanical Testing. The mechanical properties of mid-diaphyseal femurs were quantified by loading to failure in 3-point bending at 0.05 mm/sec until failure with an electro-mechanical actuator (Bose, Testbench, TA Instruments). All tests were conducted at room temperature in a controlled lab environment. Each femur was kept moist with saline and placed with the caudal surface down onto two lower supports, spaced 6 mm apart. Load and displacement signals were bridge amplified, with the same gain in each test. These signals, comprising the load-deflection curves, were digitally sampled with the Bose WinTest software (Version X).

Load-deflection curves were analyzed in MATLAB (Version R2016b, MathWorks, Natick MA) for stiffness (the slope of the initial linear portion of the curve), strength (maximum load), post-yield deflection (deflection at failure minus deflection at yield, PYD) and work-to-failure (area under the curve prior to failure). Yield was defined as a 10% reduction of secant stiffness (load range normalized for deflection range) relative to the initial (tangent) stiffness.

Statistics. Researchers were blinded, whenever possible, to specimen identity during handling and analysis. Samples were analyzed in randomized order to restrict biases. During feeding and weighing the researchers were not blinded to groups or mouse IDs. A single observer made measurements within each organ system. Data is presented as mean

values and standard deviations. Comparisons were analyzed with a two-way ANOVA and significant interactions and differences were determined by Tukey method.

Results

Elevated Plasma Fructose with Osmotic Pump. After 8 weeks of osmotic pump infusion, plasma fructose was elevated in all fructose exposed groups (Figure 4-1). Fructose pumps increased plasma fructose at least 3-fold regardless of calcium status or genotype. Serum sclerostin (Table 4-1) and leptin (Table 4-2) were reduced due to calcium. When separated by calcium status, KHK-KO is shown to reduce plasma GIP and GLP-1 concentrations. Under normal calcium diet, KHK-KO mice had higher levels of PYY. KHK-KO with restricted calcium had lower insulin concentrations than wild-type mice with the same calcium status. Calcium status had the greatest effect on body weight, with calcium restricted mice weighing less (Figure 4-2). Calcium restriction increased kidney weight in all mice and increased caecum weight in WT mice (Table 4-3). Fructose pump implantation increased the weight of the spleen.

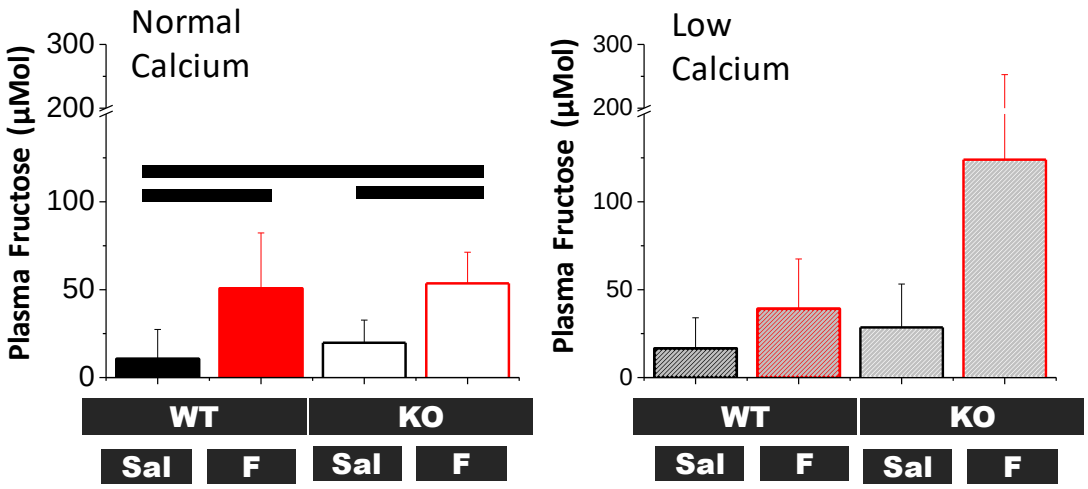

Figure 4-1: Plasma fructose concentration for WT and KO mice fed for 8 weeks on a Normal Calcium (solid, blank bars) or Low Calcium (shaded bars) diets, with either a saline (Sal) or fructose (F) filled pump, starting after weaning at 4 weeks of age (n=6-8 mice per group; mean ± SD). Bars indicate significant differences between groups determined by ANOVA with Tukey Test correction ($p < 0.05$).

		WT		KHK-KO		Statistics		
	Calcium	**Saline**	**Fructose**	**Saline**	**Fructose**	**Pump**	**Genotype**	**Interaction**
Serum Bone Panel								
OPG (pg/ml)	**Normal**	**10992.00 ± 2366.37**	**11358.50 ± 1972.03**	**10812.60 ± 1407.08**	**10348.25 ± 1921.37**	**ns**	**ns**	**ns**
	Low*	**9603.50 ± 2246.47**	**8843.80 ± 1825.16**	**10902.40 ± 797.48**	**10942.70 ± 2282.79**	**ns**	**ns**	**ns**
DKK1 (pg/ml)	**Normal**	**4187.60 ± 1455.79**	**2578.00 ± 887.70**	**2960.75 ± 615.47**	**3918.00± 447.53**	**ns**	**ns**	**0.029**
	Low	**2851.86 ± 2064.39**	**3468.20 ± 2868.92**	**2406.20 ± 968.38**	**4372.80 ± 2592.06**	**ns**	**ns**	**ns**
SOST (pg/ml)	**Normal**	**311.04 ± 23.69**	**246.93 ± 54.12**	**214.63 ± 90.233**	**157.76 ± 41.44**	**ns**	**0.022**	**ns**
	Low	**152.87 ± 110.89**	**132.21 ± 75.61**	**136.21 ± 50.07**	**174.07 ± 103.83**	**ns**	**ns**	**ns**
FGF23 (pg/ml)	**Normal**	**360.17 ± 147.42**	**502.42 ± 97.29**	**429.33 ± 208.00**	**562.45 ± 190.13**	**ns**	**ns**	**ns**
	Low	**421.31 ± 213.87**	**352.23 ± 108.31**	**439.41 ± 365.12**	**398.47 ± 171.89**	**ns**	**ns**	**ns**

Table 4-1: Serum concentrations of bone markers for WT and KO mice fed for 8 weeks on a Normal Calcium or Low Calcium diets, with either a saline or fructose filled pump, starting after weaning at 4 weeks of age (n=6-8 mice per group; mean ± SD). Asterisk (*) represent differences between normal calcium and low calcium group. Significant differences between groups determined by ANOVA with Tukey Test correction ($p < 0.05$).

		WT		KHK-KO		Statistics		
	Calcium	**Saline**	**Fructose**	**Saline**	**Fructose**	**Pump**	**Genotype**	**Interaction**
Serum Gut Panel								
GIP (pg/ml)	Normal	18.01 ± 8.82^{ab}	33.54 ± 13.80^{a}	12.48 ± 12.23^{ab}	1.67 ± 1.73^{b}	ns	0.005	0.036

	Low	62.97 ± 38.18[c]	29.13 ± 14.34[cd]	3.99 ± 4.29[d]	4.72 ± 3.39[d]	ns	0.001	ns
GLP1 (pg/ml)	Normal	12.72 ± 2.15[a]	12.54 ± 1.97[a]	8.70 ± 0.49[b]	8.42 ± 0.46[b]	ns	0.000	ns
	Low	12.10 ± 1.10[c]	12.42 ± 1.66[c]	12.15 ± 4.94[cd]	8.15 ± 0.34[d]	ns	0.040	0.036
Insulin (pg/ml)	Normal	72.94 ± 32.59	46.32 ± 18.73	67.44 ± 61.80	25.04 ± 10.60	ns	ns	ns
	Low	129.65 ± 83.18	101.80 ± 68.48	73.12 ± 71.30	40.82 ± 37.83	ns	0.050	ns
Leptin (pg/ml)	Normal	4189.40 ± 950.58	4420.83 ± 1738.21	3824.33 ± 1199.03	4354.40 ± 2145.44	ns	ns	ns
	Low*	2757.46 ± 1482.79	3171.99 ± 2251.92	2415.50 ± 1380.14	3100.40 ± 1799.13	ns	ns	ns
PYY (pg/ml)	Normal	27.23 ± 23.20	16.91 ± 10.12	63.06 ± 40.26	74.72 ± 22.61	ns	0.013	ns
	Low	31.42 ± 31.80	38.22 ± 22.37	13.86 ± 9.61	45.40 ± 36.20	ns	ns	ns

Table 4-2: Serum concentrations of gut markers for WT and KO mice fed for 8 weeks on a Normal Calcium or Low Calcium diets, with either a saline or fructose filled pump, starting after weaning at 4 weeks of age (n=6-8 mice per group; mean ± SD). Asterisk (*) represent differences between normal calcium and low calcium group. Similar superscript indicates values that are not significantly different from each other by Tukey post-hoc test. Significant differences between groups determined by ANOVA with Tukey Test correction ($p < 0.05$).

		WT		**KHK-KO**		**Statistics**		
	Calcium	**Saline**	**Fructose**	**Saline**	**Fructose**	**Pump**	**Gene**	**Interaction**
Organ Weights								

Kidney (g)	Normal	0.158 ± 0.011	0.166 ± 0.010	0.158 ± 0.013	0.165 ± 0.023	ns	ns	ns
	Low*	0.173 ± 0.023	0.176 ± 0.020	0.159 ± 0.018	0.177 ± 0.019	ns	ns	ns
Liver (g)	Normal	1.052 ± 0.086	1.127 ± 0.090	1.106 ± 0.098	1.162 ± 0.160	ns	ns	ns
	Low	1.190 ± 0.130	1.032 ± 0.167	0.968 ± 0.170	1.097 ± 0.172	ns	ns	0.040
Caecum (g)	Normal	0.173 ± 0.041	0.165 ± 0.042	0.175 ± 0.043	0.188 ± 0.044	ns	ns	ns
	Low*	0.216 ± 0.062	0.206 ± 0.041	0.172 ± 0.029	0.185 ± 0.020	ns	ns	ns
Spleen (g)	Normal	0.078 ± 0.011	0.085 ± 0.012	0.091 ± 0.028	0.094 ± 0.024	ns	ns	ns
	Low	0.125 ± 0.029	0.128 ± 0.021	0.076 ± 0.015	0.099 ± 0.047	ns	ns	ns

Table 4-3: Organ weights for WT and KO mice fed for 8 weeks on a Normal Calcium or Low Calcium diets, with either a saline or fructose filled pump, starting after weaning at 4 weeks of age (n=6-8 mice per group; mean ± SD). Asterisk (*) represent differences between normal calcium and low calcium group. Significant differences between groups determined by ANOVA with Tukey Test correction ($p < 0.05$).

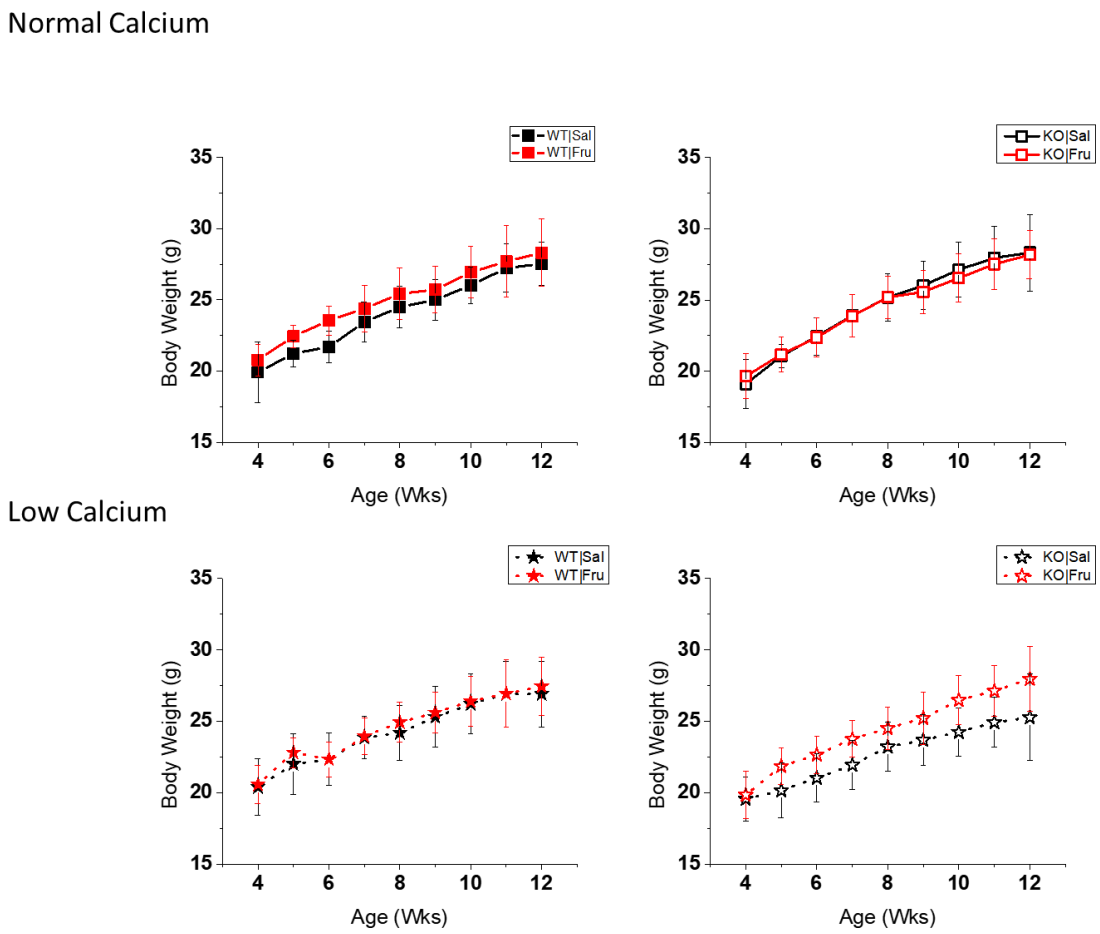

Figure 4-2: Plasma fructose concentration for WT and KO mice fed for 8 weeks on a Normal Calcium (solid, blank squares) or Low Calcium (solid, blank stars) diets, with either a saline (Sal) or fructose (Fru) filled pump, starting after weaning at 4 weeks of age (n=6-8 mice per group; mean ± SD). Significant differences between groups determined by ANOVA with Tukey Test correction ($p < 0.05$).

Effects of Fructose on In vitro Colony Formation (OB-CFU). The osteoblast colony forming assay revealed that WT and KHK-KO mice had differences in osteogenic potential (Table 4-4). Alkaline phosphatase activity was not affected by pump contents or calcium status.

		WT		KHK-KO		Statistics		
	Calcium	Saline	Fructose	Saline	Fructose	Pump	Gene	Interaction
Ob-CFU								
Count	**Normal**	**1.00 ± 0.70**	**0.97 ± 0.58**	**1.19 ± 0.91**	**1.06 ± 0.66**	**ns**	**ns**	**ns**
	Low	**1.21 ± 0.55**	**1.96 ± 1.04**	**1.18 ± 0.98**	**0.88 ± 0.39**	**ns**	**ns**	**ns**
Average Size	**Normal**	**1.00 ± 0.60**	**0.80 ± 0.23**	**2.74 ± 1.67**	**1.79 ± 0.83**	**ns**	**0.003**	**ns**
	Low	**0.88 ± 0.25**	**0.89 ± 0.24**	**2.03 ± 1.00**	**1.85 ± 0.74**	**ns**	**0.001**	**ns**
Total Area	**Normal**	**1.00 ± 1.18**	**0.63 ± 0.54**	**2.76 ± 2.24**	**1.66 ± 1.46**	**ns**	**0.033**	**ns**
	Low	**0.86 ± 0.27**	**1.33 ± 0.52**	**2.15 ± 1.98**	**1.43 ± 0.93**	**ns**	**ns**	**ns**

Table 4-4: Osteogenic potential of bone marrow cells measured by osteoblast colony formation unit (Ob-CFU) cultures. Primary bone marrow cells were cultured in osteogenic media for 14 days. Stained areas were normalized to WT-glucose control and are represented as means ± SD. Significant differences between groups determined by ANOVA with Tukey Test correction ($p < 0.05$). Significant differences between groups determined by ANOVA with Tukey Test correction ($p < 0.05$).

Fructose Pump Increased Long Bone Length. Tibial length was increased by ~2% in KHK-KO mice implanted with the fructose pump under normal calcium compared to WT mice with a sham pump with the same calcium status (Figure 4-3). KHK-KO mice already had significantly longer tibias; however, fructose pump significantly increased tibial length. The effects were not seen in femur lengths.

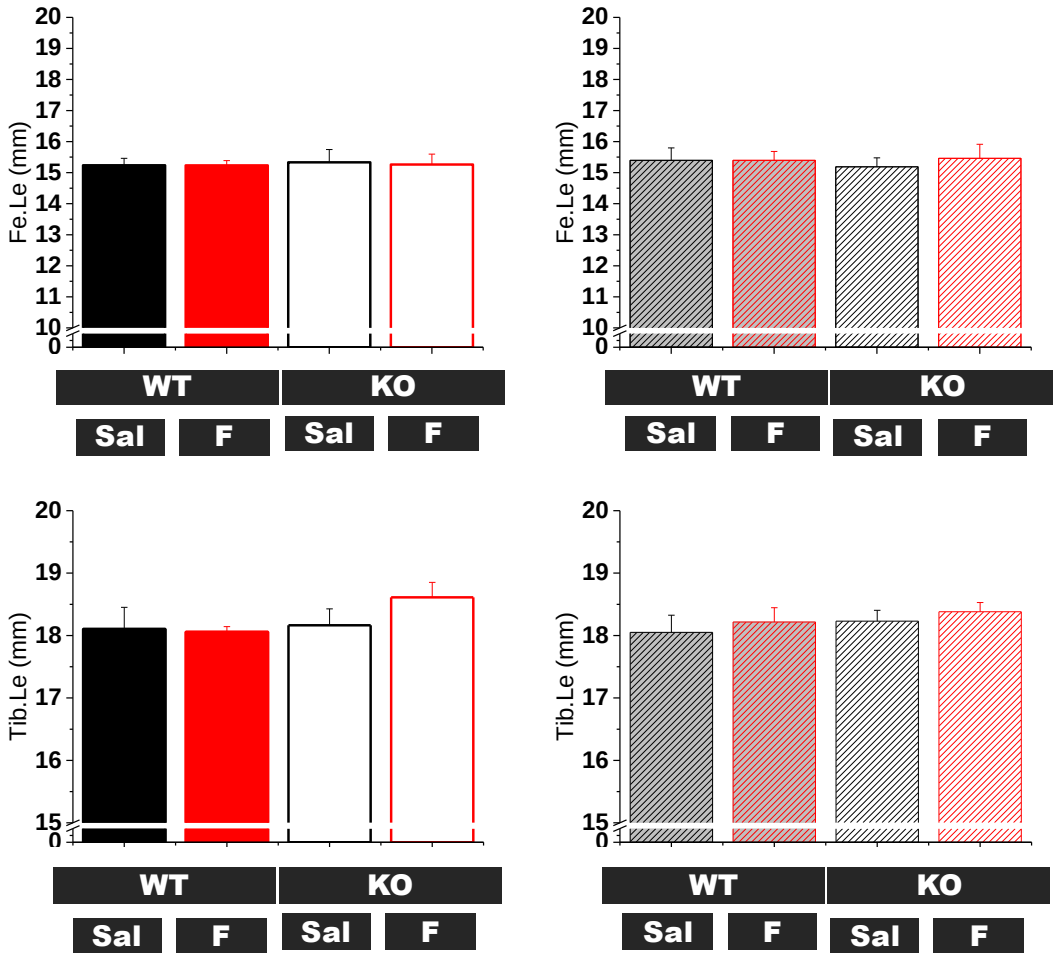

Figure 4-3: Femur and tibia length for WT and KO mice fed for 8 weeks on a Normal Calcium (solid, blank bars) or Low Calcium (shaded bars) diets, with either a saline (Sal) or fructose (F) filled pump, starting after weaning at 4 weeks of age (n=6-8 mice per group; mean ± SD). Significant differences between groups determined by ANOVA with Tukey Test correction ($p < 0.05$).

Calcium significantly affected bone morphology and histomorphometry. The strongest effector of bone histomorphometry parameters from this study was reduced calcium. Low calcium increased the activity of the bone forming cells in both genotypes with a diminished response in fructose fed wild-type mice (Table 4-5). On the periosteal surface,

low calcium increased the active mineralizing surface by >30% in WT saline pump and both KHK-KO groups; increases in bone formation rate were also detected the KHK-KO but not in the fructose infused WT mice. On the endosteal surface, bone formation rates did not show great significant differences between sugars; however, KHK-KO mice had a greater response to low calcium diets with increased bone formation. Calcium restriction significantly reduced osteocyte lacunar density, when adjusted for bone formation rate (Table 4-6).

		WT		KHK-KO		Statistics		
	Calcium	**Saline**	**Fructose**	**Saline**	**Fructose**	**Pump**	**Genotype**	**Interaction**
Tibial Endosteal Histomorphometry								
Perimeter (mm)	Normal	4.37 ± 0.59	4.24 ± 0.18	4.04 ± 0.37	4.43 ± 0.38	ns	ns	ns
	Low	4.31 ± 0.26	4.2.5 ± 0.51	4.23 ± 0.38	4.70 ± 0.26	ns	ns	ns
Mineralizing Surface (%)	Normal	0.77 ± 0.12	0.82 ± 0.10	0.80 ± 0.07	0.74 ± 0.11	ns	ns	ns
	Low*	0.82 ± 0.12	0.83± 0.08	0.88 ± 0.09	0.84 ± 0.08	ns	ns	ns
Mineral Apposition Rate (μm/day)	Normal	1.83 ± 0.36	1.67 ± 0.33	1.73 ± 0.38	1.88 ± 0.43	ns	ns	ns
	Low*	2.02 ± 0.26	1.75 ± 0.42	2.27 ± 0.34	2.41 ± 0.26	ns	0.005	ns
Bone Formation Rate ($\mu m^3/\mu m^2$/day)	Normal	1.41 ± 0.32	1.39 ± 0.38	1.37 ± 0.29	1.39 ± 0.42	ns	ns	ns
	Low*	2.02 ± 0.26	1.75 ± 0.42	2.27 ± 0.34	2.01 ± 0.29	ns	0.007	ns
Tibial Periosteal Histomorphometry								
Perimeter (mm)	Normal	6.88 ± 0.46	6.89 ± 0.07	6.57 ± 0.33	6.98 ± 0.17	ns	ns	ns
	Low	6.93 ± 0.40	6.64 ± 0.28	6.69 ± 0.25	6.92 ± 0.22	ns	ns	0.049
Mineralizing Surface (%)	Normal	0.18 ± 0.03	0.15 ± 0.09	0.13 ± 0.07	0.16 ± 0.09	ns	ns	ns
	Low*	0.31 ± 0.05	0.16 ± 0.07	0.28 ± 0.07	0.30 ± 0.04	0.022	0.048	0.004
Mineral Apposition Rate (μm/day)	Normal	1.31 ± 0.30	1.05 ± 0.48	0.78 ± 0.18	1.37 ± 0.57	ns	ns	0.040
	Low*	1.38 ± 0.36	1.23 ± 0.16	1.32 ± 0.30	1.65 ± 0.51	ns	ns	ns
Bone Formation Rate ($\mu m^3/\mu m^2$/day)	Normal	0.24 ± 0.07	0.20 ± 0.13	0.11 ± 0.07	0.28 ± 0.15	ns	ns	ns

Low*	0.43 ± 0.16	0.20 ± 0.11	0.37 ± 0.15	0.51 ± 0.21	ns	ns	0.025

Table 4-5: Dynamic histomorphometric parameters measured on the endosteal and periosteal surfaces of tibias from WT and KO mice fed for 8 weeks on a Normal Calcium or Low Calcium diet, with either a saline or fructose filled pump, starting after weaning at 4 weeks of age (n=6-8 mice per group; mean ± SD). Asterisk (*) represent differences between normal calcium and low calcium group. Significant differences between groups determined by ANOVA with Tukey Test correction ($p < 0.05$).

		WT		KHK-KO		Statistics	
	Calcium	**Saline**	**Fructose**	**Saline**	**Fructose**	**Pump**	**Genotyp**
Osteocyte							
Lacunar Density (mm-2)	Normal	804.22 ± 144.29	770.63 ± 90.18	757.10 ± 235.96	877.71 ± 196.07	ns	ns
	Low	670.16 ± 65.50	725.54 ± 109.93	790.47 ± 98.61	775.62 ± 156.10	ns	ns
Lacunar Density/Double Label Length (mm-2/mm-1)	Normal	126.72 ± 42.96	154.39 ± 7.50	186.02 ± 46.56	214.60 ± 88.36	ns	ns
	Low	139.50 ± 29.51	120.08 ± 12.44	282.08 ± 273.00	211.88 ± 137.37	ns	ns
Lacunar Density/Bone Formation Rate (mm-2/ µm3/µm2/day)	Normal	1029.82 ± 365.97	775.22 ± 142.15	919.37 ± 398.80	1048.66 ± 446.65	ns	ns
	Low*	667.63 ± 192.70	912.14 ± 371.58	688.58 ± 166.49	555.58 ± 170.53	ns	ns

Table 4-6: Osteocyte lacunar density between calcein double labels on endosteal and periosteal surfaces of tibias from WT and KO mice fed for 8 weeks on a Normal Calcium or Low Calcium diet, with either a saline or fructose filled pump, starting after weaning at 4 weeks of age (n=6-8 mice per group; mean ± SD). Asterisk (*) represent differences between normal calcium and low calcium group. Significant differences between groups determined by ANOVA with Tukey Test correction ($p < 0.05$).

Calcium restriction reduced cortical morphological parameters (Ct.B.Ar, Ct.Tt.Ar, Ct.Th, Ct.MMI, %Ct.Ar). Fructose only reduced Ct.Th with normal calcium diet (Table 4-7). Trabecular BMD and morphology were reduced due to low calcium with equal effect on both WT and KHK-KO genotypes. Under normal calcium diets, KHK-KO mice had a greater number of trabeculae per unit volume.

		WT		KHK-KO		Statistics		
	Calcium	**Saline**	**Fructose**	**Saline**	**Fructose**	**Pump**	**Gene**	**Interaction**
Femoral Cortical MicroCT								
Ct.BMD (g/cm^3)	Normal	1.06 ± 0.05	1.07 ± 0.03	1.08 ± 0.04	1.04 ± 0.01	ns	ns	ns
	Low*	1.03 ± 0.08	1.03 ± 0.06	1.04 ± 0.04	1.02 ± 0.04	ns	ns	ns
Ct.B.Ar (mm^2)	Normal	0.85 ± 0.06	0.86 ± 0.04	0.85 ± 0.04	0.84 ± 0.04	ns	ns	ns
	Low*	0.69 ± 0.05	0.67 ± 0.04	0.70 ± 0.03	0.69 ± 0.06	ns	ns	ns
Ct.M.Ar (mm^2)	Normal	1.74 ± 0.10	1.83 ± 0.17	1.82 ± 0.29	1.93 ± 0.28	ns	ns	ns
	Low	1.89 ± 0.49	1.80 ± 0.16	1.66 ± 0.18	1.84 ± 0.19	ns	ns	ns
Ct.Tt.Ar (mm^2)	Normal	2.59 ± 0.15	2.69 ± 0.20	2.68 ± 0.32	2.77 ± 0.31	ns	ns	ns
	Low*	2.59 ± 0.53	2.47 ± 0.17	2.36 ± 0.20	2.53 ± 0.21	ns	ns	ns
%Ct.Ar (%)	Normal	32.69 ± 0.70	32.09 ± 1.50	32.12 ± 2.78	30.64 ± 2.32	ns	ns	ns
	Low*	27.39 ± 3.68	27.06 ± 2.09	29.77 ± 1.78	27.16 ± 2.59	ns	ns	ns
Ct.MMI (mm^4)	Normal	0.63 ± 0.08	0.66 ± 0.08	0.65 ± 0.11	0.69 ± 0.12	ns	ns	ns
	Low*	0.53 ± 0.14	0.49 ± 0.05	0.49 ± 0.06	0.51 ± 0.07	ns	ns	ns
Ct.Th (μm)	Normal	113.60 ± 3.87^{ab}	110.12 ± 4.63^{ab}	116.63 ± 9.23^{a}	105.69 ± 5.92^{b}	0.011	ns	ns
	Low*	93.74 ± 13.04	90.56 ± 10.85	98.37 ± 10.37	94.80 ± 12.81	ns	ns	ns
Distal Femur Trabecular MicroCT								
Tb.BMD (g/cm^3)	Normal	0.17 ± 0.02	0.18 ± 0.02	0.17 ± 0.02	0.17 ± 0.03	ns	ns	ns
	Low*	0.13 ± 0.03	0.10 ± 0.02	0.11 ± 0.02	0.10 ± 0.04	ns	ns	ns

Tb.BV/TV (%)	Normal	9.99 ± 1.90	10.58 ± 2.05	9.03 ± 2.03	9.55 ± 2.57	ns	ns	ns
	Low*	6.69 ± 3.76	4.82 ± 1.60	4.57 ± 2.01	5.10 ± 2.34	ns	ns	ns
Tb.Th (mm)	Normal	4.00 ± 0.13	4.01 ± 0.33	4.26 ± 0.56	4.12 ± 0.37	ns	ns	ns
	Low	4.06 ± 0.63	3.85 ± 0.45	3.69 ± 0.34	3.94 ± 0.17	ns	ns	ns
Tb.N (#)	Normal	2.50 ± 0.45	2.63 ± 0.41	2.11 ± 0.25	2.29 ± 0.40	ns	0.030	ns
	Low*	1.58 ± 0.66	1.25 ± 0.38	1.22 ± 0.47	1.30 ± 0.57	ns	ns	ns
Tb.Sp (mm)	Normal	0.17 ± 0.02^{ab}	0.16 ± 0.01^{a}	0.19 ± 0.01^{b}	0.17 ± 0.00 ^{ab}	ns	0.010	ns
	Low	0.22 ± 0.02	0.22 ± 0.03	0.23 ± 0.02	0.20 ± 0.04	ns	ns	ns
Tb.Conn.Dn (mm^4)	Normal	332.01 ± 95.08	343.28 ± 102.14	257.18 ± 43.79	290.31 ± 70.33	ns	ns	ns
	Low*	203.20 ± 106.73	152.08 ± 78.91	161.96 ± 95.24	176.20 ± 137.89	ns	ns	ns
Proximal Femur Trabecular MicroCT								
Tb.BMD (g/cm^3)	Normal	0.10 ± 0.01	0.11 ± 0.01	0.09 ± 0.15	0.10 ± 0.02	ns	ns	ns
	Low*	0.07 ± 0.01	0.06 ± 0.02	0.07 ± 0.01	0.10 ± 0.02	ns	ns	ns
Tb.BV/TV (%)	Normal	2.59 ± 1.55	2.60 ± 0.84	1.23 ± 0.72	2.09 ± 1.24	ns	ns	ns
	Low*	1.17 ± 1.02	1.15 ± 0.72	0.97 ± 0.96	1.00 ± 0.71	ns	ns	ns
Tb.Th (mm)	Normal	3.32 ± 0.46	3.31 ± 0.36	3.31 ± 0.73	3.05 ± 0.81	ns	ns	ns
	Low	3.08 ± 1.17	3.17 ± 0.73	2.87 ± 1.34	3.23 ± 0.62	ns	ns	ns
Tb.N (#)	Normal	0.80 ± 0.47	0.79 ± 0.27	0.36 ± 0.18	0.66 ± 0.25	ns	0.038	ns
	Low*	0.34 ± 0.20	0.34 ± 0.17	0.28 ± 0.17	0.30 ± 0.17	ns	ns	ns
Tb.Sp (mm)	Normal	0.28 ± 0.10	0.28 ± 0.08	0.37 ± 0.09	0.27 ± 0.07	ns	ns	ns
	Low	0.30 ± 0.05	0.27 ± 0.04	0.33 ± 0.08	0.30 ± 0.13	ns	ns	ns

Tb.Conn.Dn (mm^4)	Normal	72.34 ± 55.55	77.09 ± 33.13	29.93 ± 17.22	69.15 ± 34.14	ns	ns	ns
	Low*	29.18 ± 23.59	25.06 ± 20.05	33.53 ± 33.15	28.40 ± 23.66	ns	ns	ns

Table 4-7: µCT measurements from (one) cortical location and (two) trabecular locations from WT and KO mice fed for 8 weeks on a Normal Calcium or Low Calcium diet, with either a saline or fructose filled pump, starting after weaning at 4 weeks of age (n=6-8 mice per group; mean ± SD). Asterisk (*) represent differences between normal calcium and low calcium group. Similar superscript indicates values that are not significantly different from each other by Tukey post-hoc test. Significant differences between groups determined by ANOVA with Tukey Test correction ($p < 0.05$).

Calcium restriction significantly reduced diaphyseal mechanical properties. Calcium had the greatest effect on bone mechanical properties, and reduced ultimate load, yield load and stiffness (Table 4-8). Calcium restriction increased the maximum displacement and post-yield deflection only in WT, but not KHK-KO mice. The femurs of KHK-KO mice were more elastic than WT mice when faced with restricted calcium. These bones were able to withstand greater loads, dissipate more energy and remain in the elastic range. There was an interaction between calcium and pump on post-yield deflection, with decreased PYD between sugars with normal calcium diet and increased PYD with calcium restriction.

		WT		KHK-KO		Statistics		
	Calcium	Saline	Fructose	Saline	Fructose	Pump	Gene	Interaction
3-Point Bending Parameter								
Ultimate Load (N)	**Normal**	**17.23 ± 1.24**	**17.35 ± 1.78**	**17.18 ± 2.28**	**16.70 ± 1.38**	**ns**	**ns**	**ns**
	Low*	**12.50 ± 1.94**	**11.95 ± 2.45**	**12.52 ± 1.00**	**12.67 ± 1.98**	**ns**	**ns**	**ns**
Yield Load (N)	**Normal**	**10.33 ± 2.94**	**11.54 ± 1.63**	**11.11 ± 3.11**	**10.68 ± 2.60**	**ns**	**ns**	**ns**
	Low*	**4.95 ± 2.60**	**5.27 ± 4.31**	**8.54 ± 2.62**	**8.86 ± 3.20**	**ns**	**0.006**	**ns**
Maximum Displacement (mm)	**Norma***	**0.63 ± 0.13**	**0.59 ± 0.05**	**0.73 ± 0.17**	**0.68 ± 0.15**	**ns**	**ns**	**ns**
	Low*	**0.84 ± 0.44**	**1.08 ± 0.50**	**0.76 ± 0.20**	**0.89 ± 0.10**	**ns**	**0.013**	**ns**
Yield Displacement (mm)	**Normal**	**0.11 ± 0.03**	**0.12 ± 0.02**	**0.14 ± 0.07**	**0.13 ± 0.07**	**ns**	**ns**	**ns**
	Low	**0.07 ± 0.04**	**0.07 ± 0.04**	**0.15 ± 0.10**	**0.12 ± 0.06**	**ns**	**ns**	**ns**
Post-Yield Displacement (mm)	**Normal**	**0.53± 0.15**	**0.47 ± 0.04**	**0.58 ± 0.16**	**0.55 ± 0.12**	**ns**	**ns**	**ns**
	Low*	**0.77 ± 0.44**	**1.02 ± 0.52**	**0.61 ± 0.13**	**0.76 ± 0.13**	**ns**	**ns**	**ns**
Stiffness (N/mm)	**Normal**	**104.78 ± 10.21**	**106.83 ± 10.88**	**111.45± 20.99**	**108.53 ± 26.61**	**ns**	**ns**	**ns**
	Low*	**79.99 ± 18.66**	**75.59 ± 18.66**	**84.51 ± 24.76**	**89.45 ± 18.69**	**ns**	**ns**	**ns**
Total Work (N*mm)	**Normal**	**8.57 ± 2.16**	**8.07 ± 1.03**	**9.44 ± 3.09**	**8.72 ± 2.30**	**ns**	**ns**	**ns**
	Low	**8.24 ± 4.91**	**8.85 ± 2.80**	**7.25 ± 1.64**	**8.85 ± 1.51**	**ns**	**ns**	**ns**
Yield Work (N*mm)	**Normal**	**0.60 ± 0.32**	**0.72 ± 0.19**	**0.76 ± 0.47**	**0.73 ± 0.54**	**ns**	**ns**	**ns**
	Low	**0.21 ± 0.21**	**0.25 ± 0.35**	**0.66 ± 0.54**	**0.56 ± 0.35**	**ns**	**0.019**	**ns**
Post-Yield Work (N*mm)	**Normal**	**7.97 ± 2.23**	**7.35 ± 0.88**	**8.68 ± 2.91**	**7.99 ± 2.01**	**ns**	**ns**	**ns**
	Low	**8.02 ± 4.90**	**8.60 ± 2.84**	**6.59 ± 1.34**	**8.28 ± 1.34**	**ns**	**ns**	**ns**

Table 4-8: Mechanical testing parameters from the femurs of WT and KO mice fed for 8 weeks on a Normal Calcium or Low Calcium diets, with either a saline or fructose filled pump, starting after weaning at 4 weeks of age (n=6-8 mice per group; mean ± SD). Asterisk (*) represent differences between normal calcium and low calcium group. Significant differences between groups determined by ANOVA with Tukey Test correction ($p < 0.05$).

Discussion

The work presented in this study addresses mechanical, structural, cellular and biochemical changes caused by fructose consumption. Direct fructose infusion into the bloodstream maintains a plasma concentration of fructose that does not see post-prandial declines. Fructose infusion bypasses the gut and liver, limiting the metabolites formed by incomplete digestion of sugar; eliminating confounding effects of those metabolites on bone cells. We have greater control on fructose dosage by limiting the sugar to food or by directly infusing the sugar into the bloodstream.

Calcium status had the greatest effect on bone parameters. Calcium is an essential mineral that is stored in bone as hydroxyapatite (HA). Low calcium triggers a cascade of hormones that regulate calcium by increasing its absorption at the gut, reabsorption at the kidney and resorption of bone matrix to release calcium into the bloodstream. This concerted effort keeps serum calcium levels stable, despite restriction in the diet. We are limited by the absence of 1,25-Vitamin D3, Ca^{2+}, PTH and Pi plasma measurements. However previous work in WT mice has shown that PTH and 1,25-Vitamin D3 are elevated with calcium restriction and that Ca^{2+} and Pi would be minimally perturbed (118).

Viguet-Carrin et al evaluated the effects of calcium status on growing male Sprague-Dawley rats, by feeding diets containing restricted, adequate and excessive calcium (145). Contrary to our findings, low calcium feeding in growing rats reduced both femur length and femur diameter. This reduction in bone geometry was due to reductions in bone formation, measured by dynamic histomorphometry on the tibia (145). We found that low calcium did not affect the longitudinal growth and that bone formation was increased. The

contradictory findings could be attributed to the difference in animal model and the duration of feeding.

Mechanically, bones from calcium-restricted mice were significantly weaker than the calcium-replete group. Work in rats have shown that low calcium reduces mechanical properties of bone (145). Our findings show that KHK-KO mice are protected from some of the detrimental effects of calcium-restriction. The stiffness of the bones was unaffected, yet KHK-KO mice with calcium-restriction had a greater yield load, lower max displacement and work before the yield point is reached. Indicating that under calcium restriction KHK-KO mice can withstand greater loads and remain in the elastic range.

Glucose consumption and metabolism, unlike fructose, is regulated by metabolic hormones produced by the gut and pancreas. Moreover, direct infusion of fructose into the bloodstream should have even less change of the metabolic markers. Regardless of calcium status or pump contents KHK-KO mice had different levels of plasma cytokines than WT mice. KHK-KO mice had lower levels of GIP, GLP and insulin.

The aim of this work was to create a pervasive elevation in plasma fructose that matched post-prandial levels. Plasma fructose was significantly increased. However, the increase was an order of magnitude lower than that due to fructose feeding in previous work. Unlike KHK-KO animals where the sugar builds up, feeding fructose to WT mice elevated plasma fructose to about 0.1 mMol, due to the systemic breakdown and clearance of the sugar. Fructose concentrations, in mice implanted with a fructose pump, were about 0.05 mMol

and did not exceed 0.5mMol. Post-prandial fructose concentrations were not reached with osmotic pump; however, the pump was able to elevate fructose in both genotypes. . This level of fructose is also difficult to measure using enzymatic fructose kits, and high-quality methods like HPLC were necessary to resolve discreet fructose differences.

The amount of fructose added to each pump was calculated such that each mouse would have the same amount of fructose. Jackson Laboratory mouse data revealed C57BL/6 mouse blood volume to be ~5.5mL/100g body weight (BW) or 55µL/g BW (174). To create a 0.5 mM solution in a mouse, 4.9544µg of fructose must be present in plasma for every g BW. We did not establish the clearance of fructose for WT or KHK-/- mice so we desired that 4.9544µg x BW of fructose be released hourly. At an infusion rate of 0.11µL/hr; the reservoir solution was filled with 250 mM fructose per g BW. Future work will need to determine the clearance of fructose and the efficacy of raising plasma fructose needs to be calibrated to the animals used.

Though fructose is metabolized primarily by the two iso-forms of KHK, which we deleted in our KO animals, the sugar is still able to be metabolized by other hexokinases (27). KHK-KO mice, on calcium-restricted diet, with a fructose pump, had the greatest amount of fructose in plasma at the time of sacrifice. Future work should measure fructose concentrations in urine and feces to account for fructose losses.

The work presented is novel, in that we are the first to report the use of an osmotic pump to elevate plasma fructose. By maintaining fructose concentrations at what would be post-

prandial levels we would be able to directly compare how elevated fructose level affects WT animals versus KHK-KO animals. We previously found that this elevation in fructose concentration has a hand in disrupting Vitamin D metabolism. Serum 1,25-Vitamin D3 or renal gene expression of CYP24b1 and CYP27a1 were not measured, and the fructose levels reported here would likely not be enough to perturb Vitamin D, at least with normal calcium diet. The large impact of calcium restriction was much greater than that elicited by the fructose pumps. By increasing the amount of fructose inside of the pump, this model may mimic the fructose concentrations observed in feeding models and will be able to overcome the limitations of comparing animals that are able to metabolize fructose and those who are not.

Acknowledgments

Publication was supported by the National Institute of Arthritis and Musculoskeletal and Skin Diseases of the NIH (AR063351) and Rutgers University. We thank Drs. Joseph Geissler, George Pellegrino, Stephen Flowers and Chirag Patel, as well as Brian Canter, Mayuri Kinkhabwala, Juby Roy, David Sadegh, Timothy Ngoge, Alexander Kheshvadjian, Joe Lumuti and Luke Fritzky for technical assistance. The manuscript based on this chapter will be submitted for publication with the following author list: Edek A.J. Williams[1], Veronique Douard[2], Keiichiro Sugimoto[3,4], Fabienne Devime[2], Xufei Zhang[2], Kunihiro Kishida[5], Ronaldo P. Ferraris[6], J. Christopher Fritton[1], 1) Department of Biomedical Engineering, Graduate School, Rutgers University, New Brunswick & Department of Orthopaedics, New Jersey Medical School, Rutgers University, Newark, NJ, USA, 2) MICALIS Institute, INRA, AgroParisTech, Université Paris-Saclay, Jouy-en-Josas,

France, 3) Research and Development Center, Nagaoka Co. Ltd., Ibaraki, Osaka, Japan, 4) Center for Research and Development of Bioresources & Department of Clinical Nutrition, College of Health and Human Sciences, Osaka Prefecture University, Habikino, Osaka, Japan, 5) Department of Science and Technology on Food Safety, Kindai University, Wakayama, Japan; 6) Department of Pharmacology and Physiology, New Jersey Medical School, Rutgers University, Newark, NJ, USA. All authors contributions are gratefully acknowledged. Specifically, the contributions of authors were to study design (EW, VD, RF, JF), data collection (EW, KS, FD, XZ, KK), data analysis and interpretation (EW, VD, RF, JF), writing of first draft (EW), and critical editing of the final version of the manuscript (VD, RF, JF).

Chapter 5 : Conclusion

Fructose Effects on Bone Progenitors. Fructose affected the progenitor population of bone-forming cells in KHK-KO mice, but not in Wild-Type mice. A relationship between plasma concentrations of fructose and sclerostin was observed in the KO animals of the feeding experiment. Sclerostin, produced by osteocytes, binds to LRP5/6 and antagonizes the Wnt pathway. An increase in sclerostin production by our mice due to increased fructose would mean decreased bone formation. Sost KO mice have been observed to have increased plasma 1,25VitD3 concentrations due to increased 1α-hydroxylase activation (175). Though we did not observe changes in FGF23, Sost KO mice were also found to have reduced FGF23, the possible cause for increased 1,25VitD3 activation (175).

Osteoblasts share progenitors with multiple connective tissues, particularly adipocytes and the availability of less-differentiated cells determine mature cell numbers (18, 51, 52, 176, 177). I observed within the KHK-KO mice, that fructose feeding reduced the number of available osteogenic precursors. Osteogenic differentiation is characterized by expression of RUNX2, a key transcription factor, and is regulated by the interactions between the Wingless-int (Wnt)/catenin, transforming growth factor-beta (TGF-beta)/bone morphogenetic protein (BMP) signaling. Wnt/Beta Catenin signaling involves the formation of a complex of receptors Wnt and frizzled, conjugated to their ligand, low-density lipoprotein receptor-related protein (LRP5/6). Wnt signal transduction involves stabilizing Beta catenin by inhibiting glycogen synthase kinase 3 (GSK-3) -mediated Beta-catenin phosphorylation. Accumulation of Beta-catenin translocates to the nucleus and activates downstream genes (57, 69). BMPs are a member of the TGF (transforming growth

factor)-Beta superfamily and the 30 BMPs make it the largest subset of the family. TGF-Beta/BMP ligand signal is mediated by heterodimeric receptor serine/threonine protein kinases and the Smad protein family of substrates. Receptor kinases phosphorylate R-Smads (receptor-regulated Smads) and phosphorylated R-Smads then complex with C-Smads (common-mediator Smads). The complex translocates into the nucleus and regulates transcription. BMPs 2 and 7 induce Runx2 and Osterix in mesenchymal stem cells (MSCs) and promotes differentiation (57). Together, Wnt/Beta catenin and TGF-Beta/BMP pathways induce the osteogenic phenotype by modulating RUNX2(CBFA1/AML3). The Runx family has three members, characterized by their runt domain that is a DNA-binding homologue of Drosophila pair-rule gene runt. Runx is co-activated by core binding factor B (Cbfb)/polyoma enhance binding protein 2b (Pebp2b), forming a heterodimer. Runx2 is essential for differentiation of MSCs into osteoblasts and chondrocyte maturation and therefore endochondral ossification. Runx2 triggers the expression of major bone matrix protein genes at an early stage of osteoblast differentiation and sustains a supply of preosteoblasts (57).

Pro-adipogenic *in vitro* culture of pre-adipocytes, 3T3-L1 fibroblasts, decreased expression of Runx2, ALP, OCN, ColIa and osterix (178). Work by other researchers using 3T3-L1 cells have shown a response of fat cells to fructose *in vitro*. 3T3-L1 cells can survive in culture with 5.5mM fructose as the only nutrient. In the cell line, physiological levels (50µM - 550µM) of fructose added to media containing 11.1 mM glucose potentiated adipogenesis and increased storage of lipids (179). Fructose supporting adipocyte differentiation may reduce the pool preosteoblasts. Also, leptin is a cytokine that is

expressed proportionally to the lipid content of adipocytes. Though leptin was not increased in our model, increased leptin production, due to increased fat, could reduce the osteogenic potential through the β2 adrenergic pathway. This could explain the reduction in osteoblasts from the obCFU assay in Chapter 3.

Metabolic Syndrome Endpoints Cause their own Bone Effects. In my feeding experiment, I did not observe great perturbations in insulin, leptin or the gut peptides that were measured. However, fructose can be used in rodent models to create insulin resistance (41, 151, 172, 180-182). A consequence of increased fructose consumption is the development of the metabolic syndrome which includes the development of diabetes, obesity and insulin insensitivity. Diabetes affects bone morphology and mineral density which is caused by reduced insulin production, increased advanced glycation end-products, low bone mass and increased production of inflammatory cytokines.(183). Type-1 diabetes was shown to blunt the pubertal growth spurt in Indian children; leading to increased risk of fracture later in life, as they do not reach peak bone mass.(183)

Along with alteration to bone morphology, type 1 and 2 diabetes have been linked to increased vitamin D deficiency and/or insufficiency in children and adults. Vitamin D activation from 25VitD2 to 1,25VitD3 occurs within the mitochondria of epithelial cells of the proximal tubules. 25VitD2 is typically bound to Vitamin D Binding Protein (VDBP) in plasma. Type-1 diabetes subjects who also had albuminuria had increased VDBP in urine, which could be bound to 25VitD2. Leading to compensatory increases in CYP27b1 production to compensate for decreased levels of precursor (184).

Type-2 diabetes mellitus is a condition that develops from impaired insulin signaling and insulin resistance. Chronic fructose consumption can lead to the development of diabetes in humans and can be used to induce the disease in rodent models. There may be key insights in the progression of diabetes that explain how fructose affects bone. Diabetes leads to alterations in bone cell metabolism, bone matrix composition, and increased rate of fracture and complications arising from fracture (185). Post-menopausal diabetic women have increased fracture risk at several bone sites, despite greater DXA measured bone mineral density, than non-diabetic counterparts. (185-188). Diabetic children have blunted pubertal growth, associated reduced peak bone mass and slender bones. The duration of the diagnosis exacerbates the deleterious effect of diabetes on bone (183).

Like observations in fructose feeding in rodents, vitamin D deficiency has been observed to be concomitant with diabetics in adults and children and T1DM and T2DM. The deficiency has been reported to be independent of diabetic nephropathy and is believed to be related to the expression of LRP2 (megalin) by renal epithelial cells. Megalin is a multiligand receptor for albumin, vitamin binding proteins, lipoproteins, hormones, enzymes and drugs (184, 189). Like other steroid hormones, Vitamin D3 metabolites are lipophilic compounds that are transported by a binding protein. Due to a tight affinity for 25VitD3, only 0.003% of the metabolite is found in the free form (189). Megalin facilitates the vitamin D activation by the reabsorption of 25VitD3-vitamin D binding protein (VDBP) complex in the proximal tubule (189, 190). Megalin and its co-receptor cubilin trigger the endocytosis of 25VitD3-VDBP complex through the glomerular filtrate (184,

189). Once inside the cell, 25VitD3 is released and hydroxylated by 1α-hydroxylase (117, 184, 189). Thus, it is believed that microalbuminuria due to megalin deficiency also causes VDBP bound 25VitD3 to be cleared through the urine and causing a compensatory increase in 1α-hydroxylase activity (184).

Diabetic patients have significantly greater fasting levels of sugars, including fructose, in plasma than healthy individuals. *In vitro* work has demonstrated that fructosylation of proteins by fructose occurs seven times more rapidly than glycation with glucose (35). This raises the susceptibility of advanced glycation end product (AGE) development in long-lasting proteins, such as collagens. Sugar concentrations in plasma cause non-enzymatic modifications to proteins due to Maillard reactions. AGEs occur normally with age, but sugar type and duration and magnitude of exposure determine the rate of AGE development. All reducing sugars can cause AGEs to form, but some sugars are more reactive than others; for example, fructose is more reactive than glucose (191). AGEs cause increased crosslinking in collagens; which alter material properties of tissues and may create brittle bone (188). AGEs are believed involved in the development of diabetes-related fractures (185, 191). AGEs have been shown to induce FGF23 expression in UMR106 rat osteosarcoma cells due to inflammation.

Obesity is a global problem, with an affected 30-45 million children aged 5-17 having a body mass index (BMI) of >2.67 standard deviations. Though fructose isn't the main culprit for this pandemic, it is another endpoint that has been reported to be associated with increase fracture risk in children (192, 193). Compared to non-obese controls, children that

were obese had reduced BMD, when adjusted for body size, age, weight and height (194). A case-control study was conducted in Italy that determined that inactivity was a coincidence for fracture among overweight/obese children (195). They also found that the male control and fracture groups had similar prevalence of obesity, while obese girls were a large proportion of the fracture cases (195).

Fructose Effects Metabolism and Could Affect Vulnerable Populations. There is a population of people with a rare genetic disorder called, Essential benign fructosuria (EBF), that prevents the metabolism of fructose. As the name suggests, it may be an innocuous inborn error of metabolism and is characterized by the intermittent appearance of fructose in the urine (20, 22). The condition was first recognized in 1876 and represents an early recorded case of disordered metabolism (26). When fed dietary fructose, sucrose or sorbitol, those affected present with persistent increased fructose concentration and by excretion of 10-20% of the ingested load in urine (20, 22, 27, 28). EBF is a rare genetic disease and the exact incidence is unclear, due to its perceived innocuity. Lasker (156) estimated the incidence at 1 case in every 130,000 though this may be an overestimate, due to consanguinity of studied populations (22).

The EBF population is modelled by the KHK knockout mouse. We received the Ketohexokinase knockout mouse (KHK-KO) from the RJ Johnson lab, who developed the mouse line. Genetic inhibition of KHK provides a unique approach for ameliorating the effects of fructose on diet (25). To create a KHK-KO selective genetic lesion, an in-frame stop codon was engineered into exon 3a and a region between exons 3c and 7 was deleted.

For positive selection, a floxed neomycin cassette from PGKneobpA-lox was inserted 5' to exon 3a. For negative selection a PGK-DTA cassette was inserted 3' to Khk (27). KHK-KO animals are outwardly healthy and indistinguishable from their wild-type littermates. KHK-KO animals are able to mate and carry normal-sized litters to full-term (27). The mouse model was published in 2010 and has made significant contributions to understanding fructose metabolism. Through the KHK-KO model, GLUT5 activation has been discovered to be KHK-dependent (196). KHK-KO mice have been shown to be protected from developing metabolic syndrome and fatty liver when on a high fructose diet (141). KHK-KO animals have been used to show that fructose induces proinflammatory changes in the proximal tubule in a KHK-dependent manner (23). Knocking out KHK in B6 mice does not affect adaptive responses of the intestine to absorb calcium from diet (197). The work presented within is novel, as it is the first examination of the bone phenotype of this model.

Though EBF is believed to be benign, we found that in our mouse model, ingestion of the equivalent of a human load of fructose resulted almost immediately in decreased body mass. Fructose effects were not observed in WT mice which exhibited no increase in plasma fructose. Both genotypes had similar calorie consumption regardless of type of sugar. The differences we observed in bone phenotype found when feeding fructose to KHK-KO mice has not been reported in clinical presentations of the disease. Future clinical studies of EBF may find value in examining possible effects on height and serum Vitamin D.

Suggested Ways to Ameliorate Fructose Effects on Bone. Fructose use as a primary sweetener may continue to trend upward and the optimal thing for humans to do, is to make wise decisions regarding its use. In fact, fructose may not be all bad, as its low glycemic index makes it the preferred sweetener for diabetics. Also, fructose has been shown to facilitate memory. Injection of fructose at 320 mg/kg body weight enhanced cognitive function in rats (198). Messier et al, measured cognitive behavior, by a bar pressing in mice, and found that 3 months of fructose feeding enhanced task training (199). In addition to moderate use of fructose and other additive sweeteners, there may be additional steps that could be taken.

To overcome the reductions to Vitamin D activation would be to supplement with exogenous Vitamin D. 1,25VitD3 concentrations in the kidney maintain elevated levels after treatment in normal mice, indicating that supplementation may have sustained effects on the target tissue (110). Previously, Douard et al found that Vitamin D supplementation prevented deleterious reductions in calcium transport due to fructose (200).

Summary of work. The experiments described within evaluated the effects of fructose at doses that did not cause metabolic disruption. The two primary studies (Chapters 3 and 4) address the questions of whether fructose ingestion or metabolism affects bone. The concrete finding is that fructose feeding and pump implantation both elevate fructose concentrations in KHK-KO animals. At 20%, fructose was not significantly increased in WT mice; however, pump implantation uniformly elevated the sugar concentrations in the

plasma. This is valuable for future studies that wish to evaluate the effects of fructose concentration between genotypes and want precise control of serum fructose.

Experiment 1 confirmed previous findings from fructose feeding in mice, such as a reduction in CYP27b1 expression. It also revealed that fructose concentration had a strong relationship with observed changes to bone parameters. Though 1,25-Vitamin D3 was not measured, the assumed reduction in active Vitamin D could be the driving factor for bone alteration. Also, the trabecular bone of KHK-KO mice fed fructose responded with increased bone volume. To briefly describe the bone of KHK-KO mice fed fructose, they were shorter, narrower and had increased trabecular bone; however, these morphological changes did not change the mechanical properties of the bone as measured.

Experiment 2 is a valuable proof of concept for the use of osmotic pumps to alter plasma fructose. The calcium-restriction had the greatest effect on bone parameters, though some effects were observed in either calcium replete or calcium deficient populations. Low-calcium diet increased bone formation parameters in this experiment, which was not observed in dynamic histomorphometry of bones from the work presented in Chapter 2.

Future Approaches. Future work should examine fructose feeding effects on bone expression of CYP27B1. Bone cells have the machinery to activate vitamin D for paracellular signaling (201-203). In human trabecular biopsies, CYP27b1 expression strongly and significantly correlated with bone marker genes for: transcription factors (NFATC1, RUNX2, MSX-2, HIF1α); osteoclastic factors (CTR, TRAP, CA2, TWEAK); and osteoblastic factors (OPN, DMP1) and a response to hypoxia, exposing strong relationships between CYP27b1, CYP24a1 and HIF1α (201).

A large-scale experiment that studies fructose-feeding at multiple timepoints and at varying concentrations would reveal the discreet effects on growth. We observed a decrease in body weight in the KHK-KO mice during the first 4 weeks of our feeding experiment. We evaluated the bones of mice at 8- and 12- weeks of age, growth impediments at earlier ages could be corrected as the animals adjust to their new diets. It would be interesting if there existed a window for fructose feeding to have its greatest effect on growth.

Human health is benefited by the microbiome, through the digestion of resistant starches, synthesis of vitamins, and modulating our immunity (204). The gut-microbiome consists of trillions of individual cells with 150-fold more genes than those expressed by their human hosts (205-207). With the advent of high-throughput sequencing techniques, researchers can characterize these microbes. By clustering the 16s rRNA sequences of colonic samples microbe populations are segregated into operational taxonomic units (OTU) (204); of which, thousands have been observed in humans (208). The most abundant phylotypes found in human and rodent gut microbiomes are the firmicutes, followed by

Bacteroidetes, and proteobacteria (209, 210). This diverse population produce short-chain fatty acids (SCFA) by anaerobically digesting whatever is not absorbed from the upper intestines. The human colon normally produces a concentration of 50-100mmol/L, mainly composed of acetate, propionate and butyrate (204).

Alterations in the gut microbiome are associated with malnutrition, inflammatory bowel disease, obesity and metabolic diseases, which are known to be associated with increased fracture risk (211). Du et al found that IBD patients had increased CYP27b1 expression locally and that antibiotics removed this adaptive response, which was due to a lack of TNF-α production (212). It has been recently discovered that the absence of the gut microbiome is coincident of higher bone mass in germ-free mice (206, 207). The proposed mechanism is a reduction in inflammatory cytokines that are known to activate immune cells, including osteoclast precursors. Another proposed mechanism is that the acidic environment, created by SCFAs prevents the creation of larger mineral complexes and allows for greater intestinal absorption of minerals like calcium. (205, 213).

Fructose is absorbed from the gut as readily as it is present in the gut; however, a portion of a fructose-load makes it to the large intestines where the gut microbiota resides. A high intake of simple sugars can affect the microenvironment. Hansen et al fed 30% Fructose, glucose or sucrose to rats for 5-weeks and observed an increase in caecal pH and a decrease in concentrations of acetic acid and propionic acid. (214). Du Luccia et al fed 30% fructose and glucose to rats for 8 weeks and found that fructose increased non-esterified fatty acids and plasma TNF-α (209). Remarkably they were able to reverse completely or partly these

effects with antibiotics, that killed the resident microbiome or antibiotics with fecal transplant (209). At the class level, Clostridia are the most abundant, followed by bacilli in control and fructose fed animals and they found that fructose altered the abundance of several genii's OTUs (Table 5-1) (209).

Phylum	Class	Order	Family	Genus	Fructose Effect
Bacteroidetes	Bacteroidia	Bacteroidales	Bacteroidaceae	Bacteroides	↓
Firmicutes	Bacilli	Lactobacillales	Lactobacillacaeae	Lactobacillus	↓
	Clostridia	Clostridiales	Clostridiaceae	Clostridium	↓
			Lachnospiraceae	Coprococcus	↑
				Rosburia	↑
			Peptococcacaee	Rct4-4	↑
			Ruminococcacae	Ruminococcus	↑
		Coriobacteriales	Coriobacteriaceae		↑
	Eysipelotrichia	Erysipelotrichales	Coprobacillaceae	Coprobacillus	↑

Table 5-1: Effects of fructose feeding on the different populations of gut flora in rats after 8 weeks. (209)

Fructose as a complex oligosaccharide has been shown to promote bone health. Fructooligosaccharide (FOS) has been shown to increase calcium absorption in rats (215) as well as in adolescents (216). FOS has also been reported to increase femoral trabecular volume in rats (217) and OVX mice (218). These works cite the SCFA mechanism of action of the decreased pH facilitating more efficient mineral transport. Measuring serum fructose of FOS fed animals would reveal if distal gut breakdown of FOS by bacteria could cause direct fructose affects. Additionally, observing the effects of fructose compared to FOS

would indicate if the microbiota's access to fructose drives the effects seen in fructose-feeding studies.

This work highlights the nuances of fructose consumption. Fructose is a natural sugar and mammals, mice and humans included, digest the sugar without difficulty. Fructose perturbs the calcium response. However, with adequate calcium, fructose does little to cause detriment to calcium stasis and bone quality. Differences in serum concentrations of fructose within KHK-KO reveal potential mechanisms for action. Under low serum concentrations of fructose (<100µM), regardless of method of administration (feeding, osmotic pump) bone parameters remained at or near baseline. However, at fructose concentrations near 1mM there were marked changes in the architecture of the metaphysis and the numbers of progenitors that can be expanded with *in vitro* culture.

Appendices

A1 The Laboratory Mouse (Mus musculus)

Mice have been a member of our immediate environment for many centuries. Mice and rats, members of the family muridae, were spread with man and his commerce from their origin in Asia to the rest of the world (174). Mice turned from vermin to valuable research tool with the 19th century curiosity of European zoologists that bred mice for aesthetic traits (174). Clarence Cook Little created the first inbred strain of mice, named dbr (or DBA) in the early 1900s. Little received mice from Miss A.E.C. Lathrop and mated littermate's female 57 and male 52 (Figure A1-1). The creation of the C57BL and C57BR strains, by the early 1920s, arose from segregating their progeny by black and brown coat colors respectively. Standardized mice strains have been used for laboratory research for over a century. Outbred strains selected for coat color were interbred by intensive brother-sister mating to create homozygous inbred strains. A strain is considered inbred when there have been 20 or more consecutive generations of brother-sister/parent-offspring mating (174). By the turn of the millennium, there were 450 known inbred strains (219). Genetic diversity, within an inbred strain, is improved upon by pen breeding and 3 animals can yield scores within 3 generations when a single male sires progeny with two or more females, typically with brother-sister, or cousin pairings. Homozygous populations can be created by taking two strains (P1, P2) with distinct traits creating a F1 generation. The F1 generation of heterozygous animals are created and intercrossed with one another, to create a second hybrid F2 generation. Selection of homozygous animals from the F2 generation produces two first generation backcross generations (B1 and B2) (174).

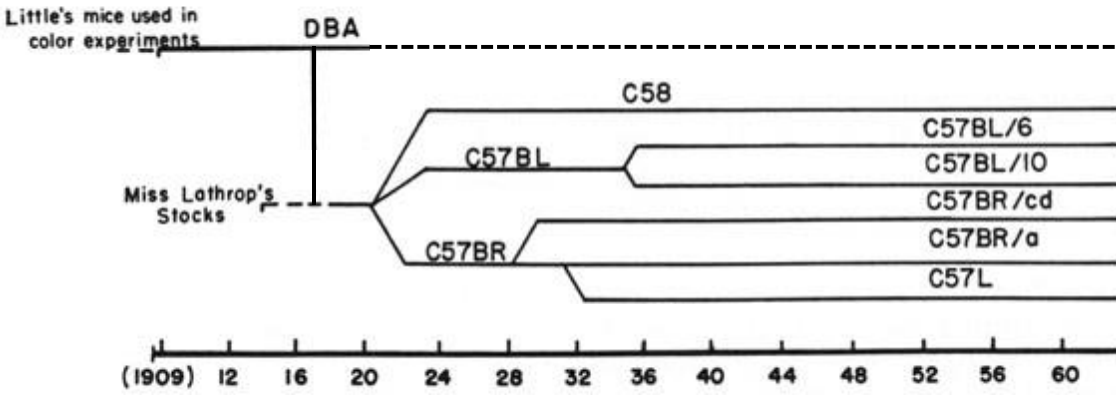

Figure A1-1: Timeline of C57BL/6 mouse development from the mating of Little's DBA mice with Miss Lathrop's mice in 1917.

There is variability in the susceptibility of different mouse strains to diet-induced obesity. B6 mice have the T1R3 taste receptor and have an affinity to sweet (220). In an examination of four mice strains (AKR, 129P3, B6, FVB) given 10% and 34% sugar solutions, sucrose was a greater inducer of obesity and fructose was only effective in producing obesity in 34% solution (220). High-fat diets throughout life shorten the lifespan of B6 mice (174). Fructose is no more obesogenic than sucrose in some rat and inbred mouse strains (220).

The C57BL/6 (B6) mouse has been used extensively in bone research and has been thoroughly characterized, genetically and phenotypically. Young mice can be weaned after 3 weeks of age and they become sexually mature at 4 to 5 weeks of age (174). The mean and median life span of C57BL/6 mice have been reported as 539 (174) and 901(219) days, respectively, for males, making the B6 mouse an attractive model for aging studies, including osteoporosis (219). Most mice strains achieve peak bone mass at 4-6 months of

age (219). In mice, longitudinal growth slows at the growth plates, but does not completely fuse and disappear (219).

MICE ARE A POWERFUL MODEL FOR UNDERSTANDING BONE PHYSIOLOGY BUT HAVE LIMITED EXPLANATORY POWER WHEN EXTRAPOLATING MECHANISMS TO THE HUMAN CONDITION. UNLIKE HUMANS, LONGITUDINAL GROWTH AND BONE ACQUISITION CONTINUES AFTER SEXUAL MATURITY (219). CANCELLOUS BONE TURNOVER IN MICE IS APPROXIMATELY 0.7% (222) PER DAY IN THE DISTAL FEMUR, COMPARED TO THE 0.1% TURNOVER IN THE ILIAC CREST OF HUMANS (219). THE ABSENCE OF HAVERSIAN	**HUMAN**	**MOUSE**

SYSTEMS IN MURINE CORTICAL BONE MAKE IT DIFFICULT TO MODEL THE REMODELING SEEN IN HUMANS. IN HUMANS THE LIFESPAN OF THE BMU IS 6-9 MONTH, WHILE OSTEOBLASTS IN RODENTS ARE ACTIVE FOR A SHORTER PERIOD OF TIME (219). INCREASED BONE TURNOVER AND HIGHER METABOLIC RATES REQUIRE THAT MICE BE ADMINISTERED HIGHER DOSES OF BIOLOGICAL AGENTS (219).PARAMETER

Longitudinal bone growth	Ceases at sexual maturity	Slow growth after sexual maturity
Cancellous bone turnover	~0.1% per day (iliac crest)	~0.7% per day (distal femur)
Life span of bone multicellular unit	6–9 mo	~2 wk
Osteonal bone remodeling	Present	Absent

Table A.1-1: Comparisons between mouse and human bone physiology. Adapted from (219)

A2 Alzet Osmotic Pumps

One approach to determining the direct effects of fructose on peripheral tissues would be to consider fructose loads as a drug dosage. Oral administration of drugs can have poor pharmokinetics, with gastrointestinal absorption being either too fast or too slow (223). Drug absorption depends on factors such as physico-chemical properties of the drug, physiological factors such as: presence or absence of food, GI motility or pH of the GI tract (173). Additionally, with most of fructose being metabolized by the liver and kidneys, constant levels of plasma fructose can be difficult to maintain.

Osmotic pumps belong to a class of rate-controlled systems providing continuous delivery and offer a set of distinct advantages over traditional drug dosing regimens (Table A.2-1).

PROS AND CONS OF OSMOTIC PUMPS

Advantages	Disadvantages
• Ability to implant into multiple species • Small Form Factor • Reliable-Predictable Delivery • Variety in Reservoir size, delivery rate and duration of infusion • Delivery is not affected by eating	• Invasive implantation • Risk of infection • Pump may not work • May cause irritation or ulcer due to saturated solution or drug

Table A.2-1: Osmotic pumps provide advantages to traditional drug dosing regimens with minor drawbacks.

These devices use the principle of osmosis, the flow along the concentration gradient when two solutions of different solute concentrations are separated by a semi-permeable membrane. This leads to a hydrostatic pressure difference across the semi-permeable

membrane, causing an oppositely directed flow of solvents. Osmosis was first observed in 1748 by Abbe Nollet then the idea expounded on in 1877 by Pfeffer, using semi-permeable membranes to separate sugar solution from water and in 1886 by Van't Hoff (173). According to Van't Hoff equations, the osmotic pressure of a solution is proportional to solute concentration and temperature (173, 223). Osmotic pressure

$$\pi = i * \frac{n}{V} * R * T = i * C * R * T$$

Where *n* is the number of moles of solute (mol), V is the volume of solution (L), C stands for the corresponding solute concentration (mol/L), R is the molar gas constant (8314 $Jmol^{-1}K^{-1}$) and T the absolute temperature (K). Van't Hoff factor (i) represents the number of moles of solute dissolved in a solution per mole of added solid solute. When α being the degree of dissociation and ν the number ions, a solute can dissociate into I molecules according to the following equation:

$$i = 1 + \alpha * (\nu - 1) \text{ (1)}$$

The net flow rate of solvent can be described by the following equation

$$\frac{dV}{dt} = K * A * (\sigma * \Delta\pi - \Delta P) \text{ (2)}$$

Where dV/dt stands for the volumetric net flow rate of solvent across the semi permeable membrane, K is the permeability of the semi permeable membrane with respect to the solvent, A is the surface area of the semi-permeable membrane and σ is its osmotic reflection coefficient. The reflection coefficient describes the leakage of solute through semi-permeable membranes and is ideally equal to one. The osmotic pressure difference across the semi-permeable membrane is Δπ. ΔP stands for the hydrostatic pressure difference between the two sites of the semi-permeable membrane. The effective drug

release rate is dm/dt and can be derived from the volume flow rate of liquid drug solution dV/dt as:

$$\frac{dm}{dt} = \frac{dV}{dt} * C \quad (3)$$

Where C stands for the drug concentration of the dispensed solution (223).

Fructose and sodium chloride (NaCl) have similar osmotic pressures (335atm and 356atm, respectively), however saline is a better osmotogen than fructose due to its lower solubility (36.1 G/100g H2O and 79.0g/100g H2O for NaCl and fructose, respectively) and higher density (2.17g/cm3 and 1.59g/cm3, for NaCl and fructose, respectively) (173). Therefore, less volume of osmotic agent is needed to displace a given volume of drug.

The Rose-Nelson pump (224) developed by Australian scientists in 1955 for drug delivery in sheep, is recognized as the pioneer in osmotic pump drug delivery (223, 225, 226). In 1970, Higuchi and Theeuwes developed another variant of the Rose-Nelsom pump, consisting of a ridged housing of semipermeable membrane. The drug is loaded into the device only prior to application. The release from the device is governed by the salt used in the salt chamber and the permeability characteristics of the outer membrane. The Alzet osmotic pumps are of the Higuchi and Theeuwes format (225).

The Alzet osmotic pumps are among the most prominent examples of miniature osmotic pumps (223, 226). ALZET pumps are cylindrically shaped and comprise of a collapsible reservoir made of impermeable thermoplastic hydrocarbon elastomer surrounded by a coating of osmotic driving agent. A cannula working as flow moderator is inserted after

filling and doesn’t begin release until environmental fluids enters the reservoir (223). The work within Chapter 4 utilized ALZET 1004 model rodent pumps with an infusion rate of 0.11 µL/hr.

Blood volume in adult mice has been estimated at 5.5 mL / 100g of body weight. Short-term compensation for blood loss is achieved by dilation of liver, spleen and vascular tree, so the fluid flow to the heart is constant (174).

A3 Gut Hormones

Ghrelin, an octanoylated 28-amino acid peptide produced by cells in the stomach, signals the hypothalamus to interpret hunger and increase food intake.(4, 35, 134, 136). Ghrelin is primarily produced by the oxyntic cells in the gastric mucosa. Acylation of the serine amino acid at position 3 by a molecule of n-octanoyl allows for the protein to cross the blood-brain barrier (35, 136). Once in the brain, ghrelin binds to the growth hormone secretagogue receptor (GHSR) (35, 136). In humans, ghrelin levels rise with increasing subjective hunger and peak at the time of voluntary food consumption and decrease after a meal (35). Ghrelin modulates energy homeostasis by stimulating the expression of the genes encoding NPY an AgRP and by binding to the presynaptic terminals of NPY and POMC neurons (35, 134, 136). In humans, ghrelin increases almost 2-fold immediately after a meal and subsequently falls postprandially (136). This results in a net orexigenic effect, functionally diametric to that produced by leptin (35, 134).

Inflammatory cytokines produced by adipose tissue TNF-α and IL-6 are involved in energy homeostasis. TNF-α is a cytokine that is involved in the metabolic disturbances of chronic inflammation (134). Adipose tissue is both a source of and a target for TNF-α, and is overexpressed in obese rodents and humans (134). Circulating levels of IL-6 are proportional to adipose mass and the magnitude of insulin resistance (134). These cytokine, TNF-α, IL-6, modulate the expression of neurotransmitters involved in the control of energy homeostasis, favoring anorexia and energy expenditure (134).

The incretin effect is a phenomenon characterized by the higher insulin response to orally administered glucose to intravenous glucose (134). Incretin peptides glucagon-like protein 1 (GLP-1) and glucose-dependent insulinotropic polypeptide (GIP) are key mediators of the effects of small intestinal glucose on gastric emptying, appetite and insulin release (227). GIP, once known as gastric inhibitory polypeptide, was the first incretin identified (134). GIP is mainly secreted by K cells in the duodenum and jejunum in response to nutrient intake (134, 136). GIP regulates insulin secretion, stimulates β-cell proliferation and mass expansion, and stimulates glucagon secretion (134, 136). In adipocytes, GIP promotes lipoprotein lipase activity and fatty acid synthesis (136). GLP-1 is a 29-amino acid amidated peptide produced by entero-endocrine L-cells in the distal ileum and colon (134, 136). GLP-1 traverses the blood-brain barrier and targets the GLP-1 receptors in the cerebral cortex, GnRH rich regions of the hypothalamus, pituitary, caudate putamen and cerebellum to enhance satiety (136). As the only other incretin, GLP-1 is responsible for as much as 50% of post-prandial insulin secretion. GLP-1 is insulinotropic, participates in regulating gastric motility, islet β-cell neogenesis, neuronal plasticity and suppression of plasma glucagon (134). ATP-sensitive K^+ (K_{ATP}) channels play an important role in glucose-induced insulin secretion, along with hexokinase in pancreatic β-cells. It is believed that GLP-1 and GIP secretion from the L- and K-cells, respectively, utilize K_{ATP} and hexokinase in a similar fashion (228).

Peptide YY (PYY) is a 36-amino acid gut hormone so called after the tyrosine residues at each terminus of the peptide that belongs to the NPY family (134). PYY is produced mainly by L-cells of the distal gut, localized to the ileum and colon (134). PYY crosses the blood-

brain barrier and acts through the Y2 receptors of hypothalamic NPY neurons, inhibiting them (136). Thus, PYY decreases food intake.

A4 Protocols

A4.1 Blood Collection

Objective Blood was collected to measure concentrations of fructose and bone and gut analytes. It is imperative to minimize the rupture of red blood cells, and coagulation of the sample. Minimizing both, tubes are coated with EDTA and care is taken during aspiration. The serum is separated by centrifugation and frozen until analyzed. Serum was diluted with acetyl nitrile and distilled water for fructose HPLC, and bone and gut Milliplex.

Materials

- EDTA Treated 1.5 ml Eppendorf tube
- >21 gage needle or lancet
- Isoflurane
- Ketamine
- Gauze

A4.1.1 Eppendorf Tube Preparation

- Add 1.5 mL of 0.5M EDTA to Eppendorf tubes, let tubes sit for 5 minutes. Aspirate extra liquid (can be re-used). Let tubes dry (uncapped) overnight under ventilated hood.

A4.1.2 Cardiac Puncture

1. 1- to 3-ml syringe with 23- to 25-G needle.
2. Anesthetize the mouse; place in dorsal recumbency.
3. Insert needle just below and slightly to the left of the xiphoid cartilage at the base of the sternum, at a 15 - 20° angle.

4. Advance needle slowly, applying slight negative pressure on the barrel of the syringe. Aspirate gently until blood flow ceases.
5. Ensure death by cervical dislocation/aortic dissection when collection is complete.

A4.1.3 Post-Draw Handling

- Centrifuge samples for 15 minutes at 3,000 RPM (1500 x g) at 4°C. Separate serum and store at -20°C

A4.2 Fructose Preparation

Objective: I used an Alzet Model 1004 Osmotic Pump to elevate the concentration of fructose in blood. I calculated that 4.9544 µg x BW of fructose was the desired amount of fructose desired to be dispensed per hour. I based this on an estimated mouse blood volume of ~5.5mL/100g body weight (BW) or 55uL/g BW. I wanted to create a 0.5 mMol solution in mouse serum, thus 4.9544 µg of fructose must be present in serum for every g BW. At an infusion rate of 0.11uL/hr; the reservoir solution needs to be 250 mM per g BW.

Materials

- D-Fructose
- 0.9% Saline
- 50 mL Conical Tube

A4.2.1 Stock Solution Preparation

- Add 10mL of fructose to 18.02g of fructose in a 50mL conical tube.
- Invert until solution is homogenous.
- Store at 20°C

A4.2.2 Dose Preparation

To create an appropriate concentration of fructose for infusion, dilute 10M stock with saline according to rubric below.

Weight	**5 g**	**10 g**	**15 g**	**20 g**	**25 g**	**30 g**
10 M Stock FRC	12.5 µL	25 µL	37.5 µL	50 µL	62.5 µL	75 µL
Saline	87.5 µL	75 µL	62.5 µL	50 µL	37.5 µL	25 µL

A4.3Alzet Pump Surgery

Overview: To elevate the level of fructose in mice, without adding the sugar to the diet or drinking water, I chose to administer fructose via osmotic pump. These are rate-controlled devices that release the sugar continuously for an extended period. The model I chose releases fructose at a rate of 0.11µL/hr for 4-weeks which was a duration of time that would only require two surgeries during the 8-week study.

Materials:

- 1x - Alzet Pump Reservoir [Model #1004]
- 1x - Alzet Pump Flow Moderator
- 1mL Syringe
- 1x Filling tube
- Fructose solution
- Scale
- Weighing Boat/Container
- Isoflurane vaporizer station
- Nair
- Gauze
- Reflex Wound Clips
- Ophthalmic Lubricating Gel
- 0.125% (1.25 mg/ml) Bupivacaine

A4.3.1 Prep (12-2 hours before):

- **Body Weight:** Body weights are used to determine dosage of fructose and Bupivacaine. Place scale and weighing container into hood. Place mouse into weighing boat and record weight.
- **Pump Preparation:** Mix appropriate concentration for infusion. Weigh the empty pump together with flow moderator. Attach a filling tube to a syringe and draw up the room temperature solution. It is essential that the syringe be free of air bubbles. With the flow moderator removed, hold the pump upright and insert the filling tube through the opening of the pump until it can go no further. Slowly push the plunger of the syringe, holding the pump in an upright position. When the solution appears at the outlet, stop filling and carefully remove the tube. Wipe off the excess solution and insert the flow moderator until the cap is flush with the top of the pump. The insertion of the flow moderator will displace some of the solution; this overflow should be wiped off. Weigh the filled pump with the flow moderator in place. The difference in the weights will give the net weight of the solution loaded. For most aqueous solutions, weight (mg) and volume (µL) is 1:1. The fill volume should be more than 90% of the reservoir volume [100 µL]. If not, there may be some air trapped inside the pump. Evacuate the incorrectly filled pump and refill. If pump is prepared overnight, prime pump by storing in saline.

A4.3.2 Handling

- Sedate mouse with 3% isoflurane either in gas chamber or via nose cone. Make sure to notify the appropriate person that nebulizer is needed. Place ophthalmic lubricating gel over eyes. Shave approximately 30mm x 20mm area of fur right

above the scapula. Use Nair to remove fine hairs. Sterilize the surgical field with 70% ethanol/isopropanol. Draw preoperative blood on the left cheek. Inject with no more than 2 mg/kg body weight of 0.1% Bupivacaine solution and allow 5-15 minutes for onset of medication.

A4.3.3 Surgery

- Make a mid-scapular incision [5-15mm] adjacent to the site of pump placement. Insert hemostat into the incision, spread the subcutaneous tissue by opening and closing the hemostat. The pocket should be large enough to allow free movement, about 1 cm longer than the pump [1.1cm+1]; pump should not rest immediately beneath the incision. Insert a filled pump into the pocket, delivery port first. Close the wound with 1-2 wound clips or 1-2 stitches.

A4.4 Genotyping

Overview: To identify the genotype during breeding, I used the ear clippings used to create identifying marks on the animal to extract DNA for PCR and gel electrophoresis.

Materials

- Mouse Ear Punch
- 5X PCRBIO Rapid Extract Buffer A (Lysis Buffer)
- 10X PCRBIO Rapid Extract Buffer B (Protease Containing Buffer)
- 2x PCRBIO HS Taq Mix Red
- DEPC Water
- 1.5 mL Eppendorf tubes
- Ice
- 0.2mL PCR tubes
- Primers
    - A1F (forward): GGGAGGGGTCCAAAGTATTACC
    - neof2 (forward): CGGTAGAATTTCGACGACCT
    - A2R (reverse): AGAATGTTGGCGGAGGTCA

A4.4.1 DNA Extraction

Summary of manufacturers protocol

1. Setup extraction reaction with ear clippings in PCRBIO Extract Buffers A and B and DEPC water.
2. Incubate at 75°C for 5 minutes and then 95°C for 10 minutes
3. Dilute with DEPC water and centrifuge;

A4.4.2 PCR

1. Once the DNA is extracted, it is put through PCR which includes the primers neo2 f2, A2R, and AIF, with neo2 f2 specific to KO mice, AIF specific to wild type mice, and A2R common to both.
2. Setup PCR reaction with Taq Mix primers, DEPC water and extracted material.
3. Incubate at 95°C for 1-2 minutes then for 40 cycles: Denature at 95°C for 15 seconds, anneal at 55-65°C for 15 seconds and extend for 1-90 seconds.

PCR products are run on a 2.2% agarose gel.

A4.4.3 Gel Preparation

Materials:

- 1X TAE Buffer (Tris-Acetic Acid-EDTA)
- Agarose powder
- E-Z Cast Gel mold
- Ethidium Bromide

Small gels are used for up to two rows of 6-12 samples.

Large gels are used for up to two rows of 12-24 samples.

To create 2.2% small gel:

1. Add 50mL of TAE buffer with 1.1 grams of agarose powder.
2. Microwave in 250mL glass bottle or larger for 1-2minutes; until powder has dissolved completely.
3. Let cool in bottle for 15-20 minutes before adding 3 μL of ethidium bromide.

4. Pour gel into assembled E-Z Cast gel mold.
5. Allow gel to set, (if not using the gel right away, place in refrigerator and wrap in aluminum foil; with lane combs still in place).
6. To create 2.2% large gel, multiply reagent quantities by 3X (i.e. 150mL TAE; 3.3 grams agarose; 9 μL ethidium bromide).

A4.4.4 Gel Electrophoresis

1. Fill electrophoresis tub, with gel in place, to fill line with 1X TAE buffer.
2. Add 3 μL of loading dye to 10 μL aliquot of PCR products.
3. On the left most well add 1 μL (orange) or 10 μL (blue) DNA ladder. Each row should have at least one ladder.
4. Add 10 μL of PCR product to well, in desired order.
5. Run gel at 90 volts for 30-45 minutes.
6. Observe gel under UV light and capture image.

A4.5 Intestine Dissection

Overview: To understand the effects of fructose feeding on the gene expression of mouse intestine I extracted and dissected the gastrointestinal tract. Samples were flash frozen and stored at 80°C.

Materials:

- Eppendorf Tubes
- Gauze
- PBS
- Pefabloc: 100 mg/mL soln *store @ +4C or aliquot and freeze @ -20C*
- Aprotinin: 25 mg/2.5mL soln *store @ +4C or aliquot and freeze @ -20C*
- DPPIV
- EDTA-Treated tube/Venosafe

Procedure:

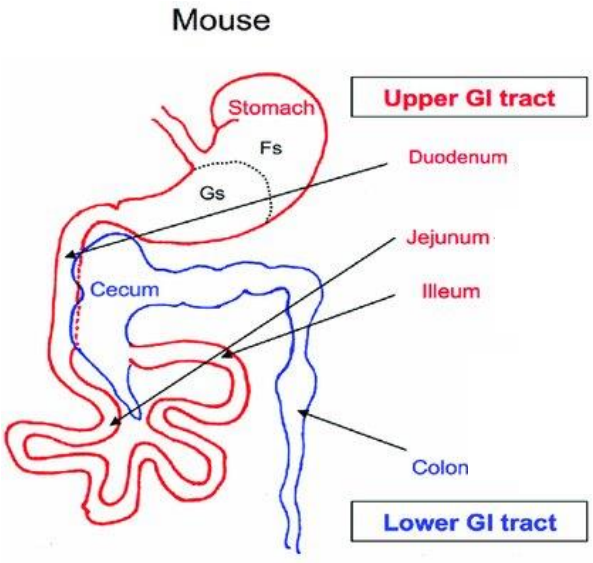

Figure A.4.5-1: Schematic of mouse gastrointestinal anatomy. Intestinal components were resected and frozen.

Stomach -> Duodenum -> Jejunum -> Ileum -> Cecum-> Colon

1. Before sacrifice add 70 μL aprotinin, 40 μL pefabloc and 40 μL DPPIV. Keep at +4°C.
2. Duodenum: 10 cm section; 0.5 cm frozen, remainder opened and scraped for protein and mRNA.
3. Jejunum: 10 cm section; 0.5 cm frozen, remainder opened and scraped for protein and mRNA.
4. Ileum: 10 cm section; 1.0 cm IHC, 0.5 cm frozen, remainder opened and scraped for protein and mRNA.
5. Cecum: opened and scraped for protein and mRNA
6. Colon: 1.0 cm IHC, 0.5 cm frozen, remainder opened and scraped for protein and mRNA.

A4.6 µCT

Overview: Femurs were evaluated by µ-computed tomography for density and morphology.

Materials:

- Long Bones
- Bruker Skyscan 1172
- 0.5mm Aluminum filter
- Multiple Bone Holder
- Density calibration phantoms (0.25 g/cm^3 and 0.75 g/cm^3)
- Saline
- 6 – well cell culture plates

Procedure:

1. Set X-Ray current and voltage to 120 µA, 80 keV respectively
2. Set voxel size to 8 µm
3. Install 0.5 mm aluminum filter
4. Thaw bones in 6 – well plate filled with room temperature saline
5. Place 5-bones into custom holder, fill with saline and secure with Styrofoam
6. Place density calibration phantoms (0.25 and 0.75 g/cm^3) and saline into designated parts of custom holder
7. Cover holder with parafilm
8. Perform an over-sized scan; with consecutive 2000x1150 pixel images taken 180° at 0.6° steps.

9. Bones were then returned to saline soaked gauze and stored frozen (-20° C) prior to mechanical testing.
10. Reconstruct scan using the packaged software, nRecon, which uses the Feldkamp algorithm, make sure multiple scans are aligned and make post scan adjustments.
11. Analyze reconstructed scans using CTAn
12. Create regions of interest for Trabecular (Tb) and cortical (Ct) bones at set distances from the distal growth plate. Tb regions of interest (ROIs) were hand drawn at the marrow / endosteal border, starting 0.25 mm below the growth plate and were 3.9 mm in depth along the femur length. Ct midshaft ROI began 2.15 mm distal to the growth plate and were 0.43 mm in depth along the femur.
13. Measure: Trabecular: thickness (Tb.Th), spacing (Tb.Sp) number (Tb.N), pattern factor (Tb.Pf) and BMD; and Cortical: thickness (Ct.Th), area (Ct.Ar), and moments of inertia (Ct.MMI), and medullary area (or marrow, Ma.Ar). Cortical area fractions (Ct.Ar/Tt.Ar and Ma.Ar/Tt.Ar), were calculated, where Tt, or total, equals Ma.Ar + Ct.Ar.

A4.7 3-Point Bending

Overview: Bending test determines if fructose contributes to alterations in mechanical properties. Three-point bending determines the energy required to fracture cortical bone.

Materials:

- Bose Electroforce Test Bench
- 6.5 mm 3-point span
- 6.5 mm alignment gage
- Long Bones
- 6 – well culture plates
- Saline

Procedure:

1. Install 6.5 mm span and align upper anvil and lower supports using 6.5 mm alignment gage.
2. Remove frozen samples from -80°C freezer, keep on ice until an hour before mechanical loading.
3. Thaw frozen bones in 6 – well plate well filled with room temperature saline.
4. Remove bone from gauze and place on lower span, with the right support at the base of the trochanter.
5. Load bone at displacement control rate of 0.05mm per second.
6. Load bone until fractured.
7. Collect data and upload into MATLAB code

A4.8 MATLAB program for analyzing 3-Point Bending Data

```
%% Structural Analysis V. 1.1a
% Updated 05/31/16
% Created By Edek Williams to analyze monotonic data
% Modified 07/15/16 by Chris Fritton
function Structural_AnalysisV_1_1
%% Functions
function filename = GetFile1(varargin)
[filename, ~, ~] = uigetfile('*.txt','Pick Raw Data File');
end
function [ElapsedTime,Disp,Load,Axialcmd] = ReadFunc1(filename,
startRow, endRow)
    %IMPORTFILE Import numeric data from a text file as column vectors.
    %   [ELAPSEDTIME,SCANTIME,DISP,LOAD] = IMPORTFILE(FILENAME) Reads
data from
    %   text file FILENAME for the default selection.
    %
    %   [ELAPSEDTIME,SCANTIME,DISP,LOAD] = IMPORTFILE(FILENAME,
STARTROW,
    %   ENDROW) Reads data from rows STARTROW through ENDROW of text
file
    %   FILENAME.
    %
    % Example:
    %   [ElapsedTime,ScanTime,Disp,Load] = importfile('42116_A1
04212016 033113_std.TXT',1, 2716);
    %
    %    See also TEXTSCAN.

    % Auto-generated by MATLAB on 2016/05/03 14:02:27

    %% Initialize variables
    delimiter = ',';
    if nargin<=2
        startRow = 1;
        endRow = inf;
    end

    %% Read columns of data as strings:
    % For more information, see the TEXTSCAN documentation.
    formatSpec = '%q%q%q%q%q%[^\n\r]';

    %% Open the text file.
    fileID = fopen(filename,'r');

    %% Read columns of data according to format string.
    % This call is based on the structure of the file used to generate
this
    % code. If an error occurs for a different file, try regenerating
the code
    % from the Import Tool.
    textscan(fileID, '%[^\n\r]', startRow(1)-1, 'WhiteSpace', '',
'ReturnOnError', false);
```

```
    dataArray = textscan(fileID, formatSpec, endRow(1)-startRow(1)+1,
'Delimiter', delimiter, 'ReturnOnError', false);
    for block=2:length(startRow)
        frewind(fileID);
        textscan(fileID, '%[^\n\r]', startRow(block)-1, 'WhiteSpace',
'', 'ReturnOnError', false);
        dataArrayBlock = textscan(fileID, formatSpec, endRow(block)-
startRow(block)+1, 'Delimiter', delimiter, 'ReturnOnError', false);
        for col=1:length(dataArray)
            dataArray{col} = [dataArray{col};dataArrayBlock{col}];
        end
    end


    %% Close the text file.
    fclose(fileID);

    %% Convert the contents of columns containing numeric strings to
numbers.
    % Replace non-numeric strings with NaN.
    raw = repmat({''},length(dataArray{1}),length(dataArray)-1);
    for col=1:length(dataArray)-1
        raw(1:length(dataArray{col}),col) = dataArray{col};
    end

    numericData = NaN(size(dataArray{1},1),size(dataArray,2));
    for col=[1,2,3,4]
        % Converts strings in the input cell array to numbers. Replaced
non-numeric
        % strings with NaN.
           rawData = dataArray{col};
        for row=1:size(rawData, 1);
            % Create a regular expression to detect and remove non-
numeric prefixes and
            % suffixes.
            regexstr =
'(?<prefix>.*?)(?<numbers>([-]*(\d+[\,]*)+[\.]{0,1}\d*[eEdD]{0,1}[-
+]*\d*[i]{0,1})|([-]*(\d+[\,]*)*[\.]{1,1}\d+[eEdD]{0,1}[-
+]*\d*[i]{0,1}))(?<suffix>.*)';
            try

                result = regexp(rawData{row}, regexstr, 'names');
                numbers = result.numbers;

                % Detected commas in non-thousand locations.
                invalidThousandsSeparator = false;
                if any(numbers==',');
                    thousandsRegExp = '^\d+?(\,\d{3})*\.{0,1}\d*$';
                    if isempty(regexp(thousandsRegExp, ',', 'once'));
                        numbers = NaN;
                        invalidThousandsSeparator = true;
                    end
                end

                % Convert numeric strings to numbers.
```

```
                if ~invalidThousandsSeparator;
                    numbers = textscan(strrep(numbers, ',', ''), '%f');
                    numericData(row, col) = numbers{1};
                    raw{row, col} = numbers{1};
                end
            catch
            end
        end
    end


    %% Exclude rows with non-numeric cells
    I = ~all(cellfun(@(x) (isnumeric(x) || islogical(x)) &&
~isnan(x),raw),2); % Find rows with non-numeric cells
    raw(I,:) = [];

    %% Allocate imported array to column variable names
    ElapsedTime = cell2mat(raw(:, 1));
    Disp = cell2mat(raw(:, 2));
    scan = size(Disp); scan = scan(1);
    tf = 0.05*(scan/200); %calculate end time scan length / sample rate
    t = linspace(0,tf,scan);
    Disp = -t;
    Load = cell2mat(raw(:, 3));
    Axialcmd = cell2mat(raw(:, 4));

end

function [d, p, dc, pc] = LoadandGraph1(Disp,Load)
rawD = (Disp - (Disp(1,1)));
rawP = (Load - (Load(1,1)));
d = -1 * rawD;
p = -1 * rawP;

maxX = max(d);
maxY = max(p);
maxY = ceil(maxY);
figure(1);
plot(d,p,'.');

xlim([0,maxX]);
ylim([0,maxY]);
brush on
pause
dc = ans(:,1);
pc = ans(:,2);
end
function [ds, ps] = smoothing1(dc,pc)

scan = size(dc); scan = scan(1);
tf = 0.05*(scan/200); %calculate end time scan length / sample rate
t = linspace(0,tf,scan);

ds = transpose(t);
p = polyfit(ds,pc,4);
```

```
ps4 = polyval(p,ds);

p = polyfit(ds,pc,5);
ps5 = polyval(p,ds);

p = polyfit(ds,pc,6);
ps6 = polyval(p,ds);

p = polyfit(ds,pc,7);
ps7 = polyval(p,ds);

p = polyfit(ds,pc,8);
ps8 = polyval(p,ds);

p = polyfit(ds,pc,9);
ps9 = polyval(p,ds);

scrsz = get(groot,'ScreenSize');

figure('MenuBar','none','Name','9th Order
Polynomial','NumberTitle','off','Position',[200+2*scrsz(4)/3 100
scrsz(4)/3 scrsz(4)/3]);
plot(ds,pc,'.'); axis([0 inf 0 inf]);
hold on
plot(ds,ps9,'r.');

figure('MenuBar','none','Name','8th Order
Polynomial','NumberTitle','off','Position',[200+2*scrsz(4)/3 scrsz(3)/3
scrsz(4)/3 scrsz(4)/3]);
plot(ds,pc,'.'); axis([0 inf 0 inf]);
hold on
plot(ds,ps8,'r.')

figure('MenuBar','none','Name','7th Order
Polynomial','NumberTitle','off','Position',[150+scrsz(4)/3 100
scrsz(4)/3 scrsz(4)/3]);
plot(ds,pc,'.'); axis([0 inf 0 inf]);
hold on
plot(ds,ps7,'r.')

figure('MenuBar','none','Name','6th Order
Polynomial','NumberTitle','off','Position',[150+scrsz(4)/3 scrsz(3)/3
scrsz(4)/3 scrsz(4)/3]);
plot(ds,pc,'.'); axis([0 inf 0 inf]);
hold on
plot(ds,ps6,'r.')

figure('MenuBar','none','Name','5th Order
Polynomial','NumberTitle','off','Position',[100 100 scrsz(4)/3
scrsz(4)/3]);
plot(ds,pc,'.'); axis([0 inf 0 inf]);
hold on
plot(ds,ps5,'r.')
```

```
figure('MenuBar','none','Name','4th Order
Polynomial','NumberTitle','off','Position',[100 scrsz(3)/3 scrsz(4)/3
scrsz(4)/3]);
plot(ds,pc,'.'); axis([0 inf 0 inf]);
hold on
plot(ds,ps4,'r.')

fit = 0;

while (fit < 4 || fit > 9);
    fit = input('What is the polynomial order number (4,5,6,7,8 or 9)
of the best fit? ');
end

if isequal(fit,4);
    ps = ps4;
elseif isequal(fit,5);
    ps = ps5;
elseif isequal(fit,6);
    ps = ps6;
elseif isequal(fit,8);
    ps = ps8;
elseif isequal(fit,9);
    ps = ps9;
else ps = ps7;
end

figure('Name','Chosen Polynomial Fit','NumberTitle','off');
plot(ds,pc,'.');
hold on
plot(ds,ps,'r.');

end
function [off,xyp,m,yp] = monofindyield1(ds,pc,pcr)
con=0;
    while (isequal(con,0));
    hold on
brush on
pause %wait for user input
x = ans(:,1); %get x-value of selection
[~,Imin] = min(x);[~,Imax] = max(x);
y = ans(:,2); %get y-value of selection
clear ans
szx = size(x); %create variable to measure size of selection
szx = szx(1); %only the first value
szdc = size(ds);
szdc = szdc(1);


[rr,m,b] = regression(x,y,'one');
b; rr^2
off = (ds*(m*.9))+b; %find intersect of 10% stiffness loss

maxY = max(pc);
maxY = ceil(maxY);
```

```
[~,Imax] = max(pc);

%%Close all figures
set(groot,'ShowHiddenHandles','on')
c = get(groot,'Children');
delete(c)

figure('Name','Slope Grid','NumberTitle','off');

plot(ds,ds*m-1,'r-');
xlim([0,ds(Imax)]);
ylim([0,maxY]);
hold on
plot(ds,ds*m-2,'r-')
plot(ds,ds*m-3,'r-')
plot(ds,ds*m-4,'r-')
plot(ds,ds*m-5,'r-')
plot(ds,ds*m-6,'r-')
plot(ds,ds*m-7,'r-')
plot(ds,ds*m-8,'r-')
plot(ds,ds*m-9,'r-')
plot(ds,ds*m-10,'r-')
plot(ds,ds*m-11,'r-')
plot(ds,ds*m-12,'r-')
plot(ds,ds*m,'r-')
plot(ds,ds*m+1,'r-')
plot(ds,ds*m+2,'r-')
plot(ds,ds*m+3,'r-')
plot(ds,ds*m+4,'r-')
plot(ds,ds*m+5,'r-')
plot(ds,ds*m+6,'r-')
plot(ds,ds*m+7,'r-')
plot(ds,ds*m+8,'r-')
plot(ds,ds*m+9,'r-')
plot(ds,ds*m+10,'r-')
plot(ds,ds*m+11,'r-')
plot(ds,ds*m+12,'r-')
plot(ds,pc,'g.');

fig = gcf;
fig.PaperPositionMode = 'auto';
print('SlopeGrid','-dpng','-r0')

con = input('Has the correct max slope been chosen (0 = no, 1 = yes or
CR)? ');
    end

set(groot,'ShowHiddenHandles','on')
c = get(groot,'Children');
delete(c)

figure('Name','Fit and Offset','NumberTitle','off');
hold on
plot(ds,off,'r-')
plot(ds,pc,'g.')
```

```
maxY = max(pc);

maxY = ceil(maxY);
ylim([0,maxY]);

fig = gcf;
fig.PaperPositionMode = 'auto';
print('FitAndOffset','-dpng','-r0')

brush on
pause

xyp = mean(ans(:,1));
yyp = mean(ans(:,2));

yp = find(ds >= xyp,1,'first');
end

function [data] = collectvars1(dc,pc,m,pcr,yp)
%% Stress Values
loadmax = max(pc);
[~,I] = max(pc);
loady = pc(yp);

%% Strain Values
dismax = dc(I);
dispy = dc(yp);
dispmax = max(dc);
disppyd = dispmax-dispy;

stiffness = m;
stiffoff = m * 0.9;

%% Work Values
szx = size(dc);
szx = szx(1);
smprate = 200; %hz
loadrate = 0.05; %mm/sec
lineardisp = (szx/smprate) * loadrate; %theoretical max displacement
dlin = linspace(0,lineardisp,szx); %linear displacement vector
wtot = dlin(2) * trapz(pc);
wy = dlin(2) * trapz(pc(1:yp));
wpyd =  wtot-wy;

%% Print Values
name = input('What is the sample name?','s');
Load_ult = num2str(loadmax);
Disp_ult = num2str(dismax);
Load_yd = num2str(loady);
Disp_max = num2str(dispmax);
Disp_yd = num2str(dispy);
Disp_pyd = num2str(disppyd);
Stiffness = num2str(stiffness);
Stiffoff = num2str(stiffoff);
```

```
w_tot = num2str(wtot);
w_yd = num2str(wy);
w_pyd = num2str(wpyd);
Val = {Load_ult Disp_ult Load_yd Disp_max Disp_yd Disp_pyd Stiffness...
    Stiffoff w_tot w_yd w_pyd};
data = horzcat(name, Val);
[name, Val]
end
function Writer1(data)
%% Write File
fid = fopen([date 'Mech_RESULTS.csv'],'a+');
while ftell(fid) == 0
    Para = {'Name' 'Load_ult' 'Disp_ult' 'Load_yd' 'Disp_max' 'Disp_yd'
'Disp_pyd'...
        'Stiffness' 'Stiffoff' 'w_tot' 'w_yd' 'w_pyd'};

    N = size(Para);
    for ii = 1:N(1,2)
        if ii == N(1,2)
            fprintf(fid,'%s \n', Para{1,ii});
        else
            fprintf(fid,'%s', Para{1,ii});
            fprintf(fid,', ');
        end
    end
end



    [M,N] = size(data);
    for ii = 1:M
        for jj = 1
            fprintf(fid, '%s, ', data{ii,jj});
        end
        for jj = 2:(N - 1)
            fprintf(fid, '%s, ', data{ii,jj});
        end
        for jj = N
            fprintf(fid, '%s, ', data{ii,jj});
        end
        fprintf(fid,'\n');
    end
        fclose(fid);
end
%% Intialize Program
%. closes and clears all... restart counter will be used when reset
button is implemented .%
close all;
clc;

 %% Get File Name
    filename = GetFile1;
    %% Read File
    [~, Disp, Load, ~] = ReadFunc1(filename);
    %% Rectify and Get Cropped Section
    [~, ~, dc, pc] = LoadandGraph1(Disp, Load);
    [ds, ps] = smoothing1(dc, pc);
```

```
    pcr = ps;
    dc = ds;
    pc = ps;

    %% Yield Point
    [~,~,m,yp] = monofindyield1(dc,pc,pcr);

    %% Create Variables
    [data] = collectvars1(dc,pc,m,pcr,yp);

    %% Write Variables
    Writer1(data)

end
```

A4.9 Matlab code for Multiple Analysis of Variance (ANOVA)

```
clc %% Clears Previous results/Initalizes Command Window
%% create structure 'stats' that contains the ANOVA results
[~,~,stats] = anovan(B,{Calcium
Sugar},'model','interaction','varnames',...
    {'Calcium', 'Sugar'});
%% POST HOC Tests
%%Bonferroni post-hoc test
'Bonferroni'
[c,~,~,gnames] = multcompare(stats,'Dimension',[1
2],'CType','bonferroni','Alpha',0.01)
%%Tukey post-hoc test
'Tukey'
[c,~,~,gnames] = multcompare(stats,'Dimension',[1
2],'CType','hsd','Alpha',0.01)
%%Fisher post-hoc test
'Fisher'
[c,~,~,gnames] = multcompare(stats,'Dimension',[1
2],'CType','lsd','Alpha',0.01)
```

A5 Experimental Design

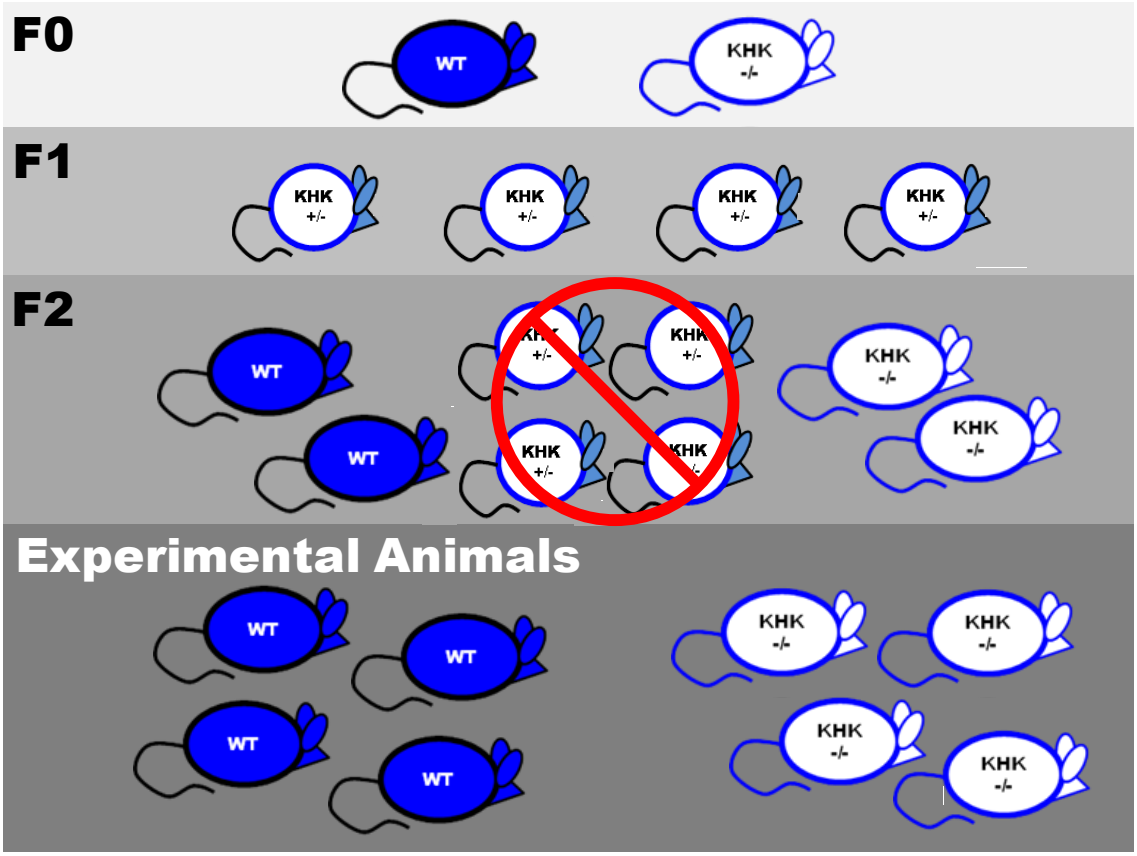

Figure A.5-1 Breeding strategy to create experimental animals. 1 KHK-KO male was paired with 2 WT females (F0). The heterozygous progeny (F1) were used to create the homozygous parents (F2) for the experimental animals. Heterozygous F2 animals were culled.

Study Timeline: Fructose and genotype effects.

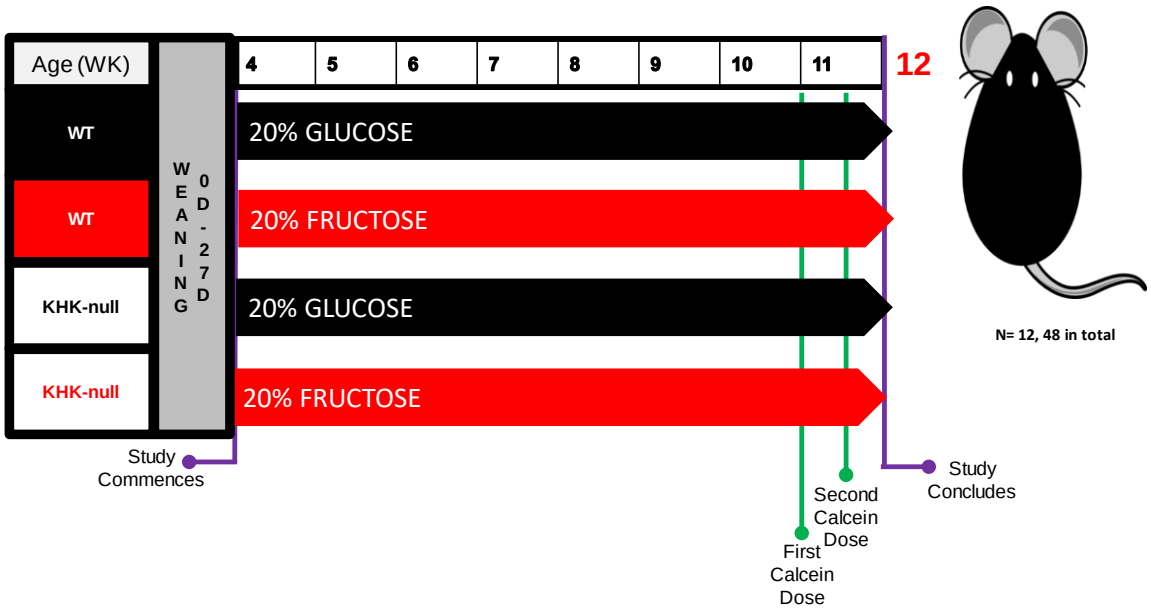

Figure A.5-2 Experimental design for feeding experiment

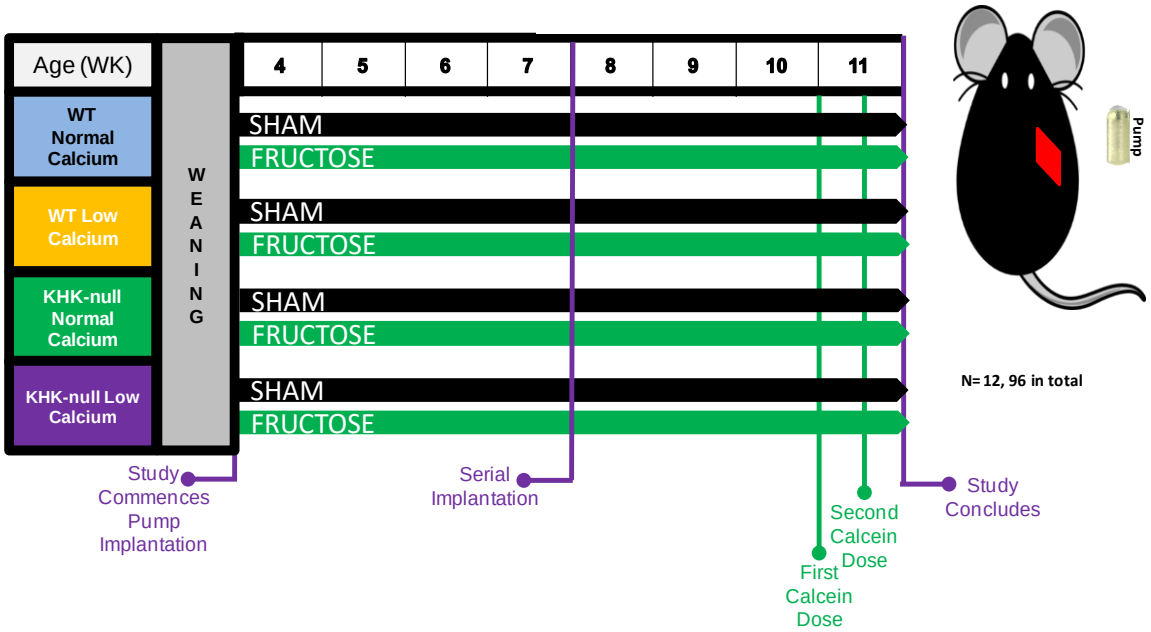

Figure A.5-3 Experimental design for pump experiment

A6 Diets

	GLU		FRU	
	gm%	kcal%	gm%	kcal%
Protein	21	20	21	20
Carbohydrate	64	64	64	64
Fat	7	16	7	16
Total	-	100	-	100
kcal/gm	4.03		4.03	
Ingredients				
Casein, 30 Mesh	200	800	200	800
L-Cystine	3	12	3	12
Corn Starch	329.5	1318	329.5	1318
Maltodextrin	100	400	100	400
Sucrose	-	-	-	-
Dextrose	200	800	-	-
Fructose	-	-	200	800
Cellulose BW 200	50	-	50	-
Corn Oil				
Soybean Oil	70	630	70	630
t-Butylhydroquinone	0.008	0	0.008	0
Mineral Mix S10022G	-	-	-	-
Mineral Mix S10022C	3.5	0	3.5	0
Calcium Carbonate	12.495	0	12.495	0
Potassium Phosphate, Monobasic	6.86	0	6.86	0
Potassium Citrate	2.4773	0	2.4773	0
Sodium Chloride	2.59	0	2.59	0
Vitamin Mix V10037	-	-	-	-
Vitamin Mix V10037C	1	4	1	4
Choline Bitartrate	2.5	0	2.5	0
Total	983.93	3964	983.93	3964

Ca%	0.5	-	0.5	-
P%	0.32	-	0.32	-
K%	0.36	-	0.36	-
Na%	0.1	-	0.1	-

Table A.6-1 20% Dextrose and 20% Fructose Diets for Experiment 1

	Normal Calcium		**Restricted Calcium**	
	gm%	kcal%	gm%	kcal%
Protein	21	20	21	20
Carbohydrate	64	64	64	64
Fat	7	16	7	16
Total	-	100	-	100
kcal/gm	4.03		4.03	
Ingredients				
Casein, 30 Mesh	200	800	200	800
L-Cystine	3	12	3	12
Corn Starch	329.5	1318	329.5	1318
Maltodextrin	100	400	100	400
Sucrose	-	-	-	-
Dextrose	200	800	200	800
Fructose	-	-	-	-
Cellulose BW 200	50	-	50	-
Corn Oil				
Soybean Oil	70	630	70	630
t-Butylhydroquinone	0.008	0	0.008	0
Mineral Mix S10022G	-	-	-	-
Mineral Mix S10022C	3.5	0	3.5	0
Calcium Carbonate	12.495	0	12.495	0
Potassium Phosphate, Monobasic	6.86	0	6.86	0

Potassium Citrate	2.4773	0	2.4773	0
Sodium Chloride	2.59	0	2.59	0
Vitamin Mix V10037	-	-	-	-
Vitamin Mix V10037C	1	4	1	4
Choline Bitartrate	2.5	0	2.5	0
Total	983.93	3964	983.93	3964
Ca%	0.5	-	0.02	-
P%	0.32	-	0.32	-
K%	0.36	-	0.36	-
Na%	0.1	-	0.1	-

Table A.6-2 Normal Calcium (0.5) and Calcium Restricted (0.02) Diet for Experiment 2

A7 qtPCR Primers

Gene	**Accession n°**	**Direction**	**Primer sequence 3' → 5'**	**Probe size (Pb)**	**Annealing temp**
Gut					
GLUT5 (*Slc2a5*)	NM_019741	Forward Reverse	agagcaacgatggaggaaaa ccagagcaaggaccaatgtc	62	59
KHK (*Khk*)	NM_008439	Forward Reverse	Tgtcctttccttgcttggag aagtcagccaccaggaagtc	84	59
CaBP9k (*S100g*)	NM_009789	Forward Reverse	Aaatatgcagccaaggaagg cagctccttaaagagattgtcca	126	59
TRPV6 (*Trpv6*)	NM_022413	Forward Reverse	Gctgatggctgtggtaattct gggatcctctgtctggaaaa	67	59
THP1 (*Tph1*)	NM_009414	Forward Reverse	Cacagttcagatcccctctaca gaacgtggcctaggagttca	63	59
Actin beta (*Actb)*	NM_007393	Forward Reverse	Ctaaggccaaccgtgaaaag accagaggcatacagggaca	104	59
Kidney					
CYP24A1	NM_009996	Forward Reverse	cctgggacaccattttcaa caaaggaaatccgcacca	88	60
CYP27B1	NM_010009	Forward Reverse	agtggggaatgtgacagagc ggagagcgtattggataccg	61	60
Klotho	NM_013823	Forward Reverse	gtgacagccaatggaatcg cgcaaagtagccacaaagg	135	60

TRPV5	NM_001007572	Forward Reverse	cctggatgctgctataatgct tgtgcagtgcagtctgaccta	95	60
Napi2a (Slc34a1)	NM_011392	Forward Reverse	agacacaacagaggcttc cacaaggaggataagacaag	181	60
G6Pase	NM_008061	Forward Reverse	ttaccaagactcccaggactg gagctgttgctgtagtagtcg	228	60
GLUT5	NM_019741	Forward Reverse	atcgctgcctttggctcatcct agcagcgtcaaggtgaaggact	143	60
KHK	NM_008439	Forward Reverse	tcctgcactgtcctttccttg gccctcaatgtggatccactt	285	60
CaBP9k	Same as Gut			126	60

Table A.7-1: Sequences of primers used for qtPCR of duodenum, jejunum and kidney.

References

1. Eaton SB, Konner M. Paleolithic nutrition. A consideration of its nature and current implications. N Engl J Med. 1985;312(5):283-9. doi: 10.1056/NEJM198501313120505. PubMed PMID: 2981409.
2. Council NR. Diet and Health: Implications for Reducing Chronic Disease Risk. Washington, DC: The National Academies Press; 1989. 768 p.
3. Ng SW, Slining MM, Popkin BM. Use of caloric and noncaloric sweeteners in US consumer packaged foods, 2005-2009. J Acad Nutr Diet. 2012;112(11):1828-34 e1-6. doi: 10.1016/j.jand.2012.07.009. PubMed PMID: 23102182; PMCID: PMC3490437.
4. Lindqvist A, Baelemans A, Erlanson-Albertsson C. Effects of sucrose, glucose and fructose on peripheral and central appetite signals. Regul Pept. 2008;150(1-3):26-32. doi: 10.1016/j.regpep.2008.06.008. PubMed PMID: 18627777.
5. Douard V, Ferraris RP. The role of fructose transporters in diseases linked to excessive fructose intake. J Physiol. 2013;591(2):401-14. doi: 10.1113/jphysiol.2011.215731. PubMed PMID: 23129794; PMCID: PMC3577529.
6. Cordain L, Eaton SB, Sebastian A, Mann N, Lindeberg S, Watkins BA, O'Keefe JH, Brand-Miller J. Origins and evolution of the Western diet: health implications for the 21st century. The American Journal of Clinical Nutrition. 2005;81:341-54.
7. Milne DB, Nielsen FH. The Interaction Between Dietary Fructose and Magnesium Adversely Affects Macromineral Homeostasis in Men. Journal of the American College of Nutrition. 2000;19(1):31-7.
8. Levi B, Werman MJ. Long-Term Fructose Consumption Accelerates Glycation and Several Age-Related Variables in Male Rats. J Nutr. 1998;128:1442-9.
9. Fitch C, Keim KS, Academy of N, Dietetics. Position of the Academy of Nutrition and Dietetics: use of nutritive and nonnutritive sweeteners. J Acad Nutr Diet. 2012;112(5):739-58. doi: 10.1016/j.jand.2012.03.009. PubMed PMID: 22709780.
10. Company TC-C. Coca-Cola Freestyle Dispenser Users Manual. FCC-ID2010. p. 4.
11. Havel PJ. Dietary Fructose: Implications for Dysregulation of Energy Homeostasis and Lipid/Carbohydrate Metabolism. Nutr Rev. 2005;63(5):133-57. doi: 10.1301/nr.2005.may.133-157.
12. Basciano H, Federico L, Adeli K. Fructose, insulin resistance, and metabolic dyslipidemia. Nutrition & metabolism. 2005;2(1):5. doi: 10.1186/1743-7075-2-5. PubMed PMID: 15723702; PMCID: 552336.
13. Mellor KM, Wendt IR, Ritchie RH, Delbridge LM. Fructose diet treatment in mice induces fundamental disturbance of cardiomyocyte Ca^{2+} handling and myofilament responsiveness. American Journal of Physiology: Heart and Circulatory Physiology. 2012;302:H964-H72. doi: 10.1152/ajpheart.00797.2011.-High.
14. Laughlin MR. Normal roles for dietary fructose in carbohydrate metabolism. Nutrients. 2014;6(8):3117-29. doi: 10.3390/nu6083117. PubMed PMID: 25100436; PMCID: PMC4145298.
15. Moran TH. Fructose and satiety. J Nutr. 2009;139(6):1253S-6S. doi: 10.3945/jn.108.097956. PubMed PMID: 19403706.
16. Bizeau ME, Pagliassotti MJ. Hepatic adaptations to sucrose and fructose. Metabolism. 2005;54(9):1189-201. doi: 10.1016/j.metabol.2005.04.004. PubMed PMID: 16125531.

17. Augustin R. The protein family of glucose transport facilitators: It's not only about glucose after all. IUBMB life. 2010;62(5):315-33. doi: 10.1002/iub.315. PubMed PMID: 20209635.
18. Ohara H, Tamayama T, Maemura K, Kanbara K, Hayasaki H, Abe M, Watanabe M. Immunocytochemical demonstration of glucose transporters in epiphyseal growth plate chondrocytes of young rats in correlation with autoradiographic distribution of 2-deoxyglucose in chondrocytes of mice. Acta histochemica. 2001;103(4):365-78. doi: 10.1078/0065-1281-00604. PubMed PMID: 11700943.
19. Haradahira T, Tanaka A, Maeda M, Kanazawa Y, Ichiya Y-I, Masuda K. Radiosynthesis, Rodent Biodistribution, and Metabolism of 1-Deoxy-1-[^{18}F]Fluoro-D-Fructose. Nucl Med Biol. 1995;22(6):719-25.
20. Hayward BE, Bonthron DT. Structure and alternative splicing of the ketohexokinase gene. European journal of biochemistry. 1998;257(1):85-91. PubMed PMID: 9799106.
21. Diggle CP, Shires M, Leitch D, Brooke D, Carr IM, Markham AF, Hayward BE, Asipu A, Bonthron DT. Ketohexokinase: expression and localization of the principal fructose-metabolizing enzyme. The journal of histochemistry and cytochemistry : official journal of the Histochemistry Society. 2009;57(8):763-74. doi: 10.1369/jhc.2009.953190. PubMed PMID: 19365088; PMCID: 2713076.
22. Bonthron DT, Brady N, Donaldson IA, Steinmann B. Molecular basis of essential fructosuria: molecular cloning and mutational analysis of human ketohexokinase (fructokinase). Hum Mol Genet. 1994;3(9):1627-31. PubMed PMID: 7833921.
23. Cirillo P, Gersch MS, Mu W, Scherer PM, Kim KM, Gesualdo L, Henderson GN, Johnson RJ, Sautin YY. Ketohexokinase-dependent metabolism of fructose induces proinflammatory mediators in proximal tubular cells. Journal of the American Society of Nephrology : JASN. 2009;20(3):545-53. doi: 10.1681/ASN.2008060576. PubMed PMID: 19158351; PMCID: 2653686.
24. Marek G, Pannu V, Shanmugham P, Pancione B, Mascia D, Crosson S, Ishimoto T, Sautin YY. Adiponectin resistance and proinflammatory changes in the visceral adipose tissue induced by fructose consumption via ketohexokinase-dependent pathway. Diabetes. 2015;64(2):508-18. doi: 10.2337/db14-0411. PubMed PMID: 25187370.
25. Raushel FM, Cleland WW. The substrate and anomeric specificity of fructokinase. The Journal of biological chemistry. 1973;248(23):8174-7. PubMed PMID: 4356621.
26. Asipu A, Hayward BE, O'Reilly J, Bonthron DT. Properties of normal and mutant recombinant human ketohexokinases and implications for the pathogenesis of essential fructosuria. Diabetes. 2003;52(9):2426-32. PubMed PMID: 12941785.
27. Diggle CP, Shires M, McRae C, Crellin D, Fisher J, Carr IM, Markham AF, Hayward BE, Asipu A, Bonthron DT. Both isoforms of ketohexokinase are dispensable for normal growth and development. Physiol Genomics. 2010;42A(4):235-43. doi: 10.1152/physiolgenomics.00128.2010. PubMed PMID: 20841500.
28. Trinh CH, Asipu A, Bonthron DT, Phillips SE. Structures of alternatively spliced isoforms of human ketohexokinase. Acta crystallographica Section D, Biological crystallography. 2009;65(Pt 3):201-11. doi: 10.1107/S0907444908041115. PubMed PMID: 19237742; PMCID: 2651755.

29. Iizuka K. The Role of Carbohydrate Response Element Binding Protein in Intestinal and Hepatic Fructose Metabolism. Nutrients. 2017;9(2). doi: 10.3390/nu9020181. PubMed PMID: 28241431; PMCID: PMC5331612.
30. Sugimoto K, Hosotani T, Kawasaki T, Nakagawa K, Hayashi S, Nakano Y, Inui H, Yamanouchi T. Eucalyptus leaf extract suppresses the postprandial elevation of portal, cardiac and peripheral fructose concentrations after sucrose ingestion in rats. J Clin Biochem Nutr. 2010;46(3):205-11. doi: 10.3164/jcbn.09-93. PubMed PMID: 20490315; PMCID: PMC2872225.
31. Coss-Bu JA, Sunehag AL, Haymond MW. Contribution of galactose and fructose to glucose homeostasis. Metabolism. 2009;58(8):1050-8. doi: 10.1016/j.metabol.2009.02.018. PubMed PMID: 19481772; PMCID: PMC2730655.
32. Le MT, Frye RF, Rivard CJ, Cheng J, McFann KK, Segal MS, Johnson RJ, Johnson JA. Effects of high-fructose corn syrup and sucrose on the pharmacokinetics of fructose and acute metabolic and hemodynamic responses in healthy subjects. Metabolism. 2012;61(5):641-51. doi: 10.1016/j.metabol.2011.09.013. PubMed PMID: 22152650; PMCID: PMC3306467.
33. Bjorkman O, Felig P. Role of the kidney in the metabolism of fructose in 60-hour fasted humans. Diabetes. 1982;31(6 Pt 1):516-20. PubMed PMID: 6130022.
34. Aoyama M, Isshiki K, Kume S, Chin-Kanasaki M, Araki H, Araki S, Koya D, Haneda M, Kashiwagi A, Maegawa H, Uzu T. Fructose induces tubulointerstitial injury in the kidney of mice. Biochem Biophys Res Commun. 2012;419(2):244-9. doi: 10.1016/j.bbrc.2012.02.001. PubMed PMID: 22342673.
35. Lustig RH. Fructose: metabolic, hedonic, and societal parallels with ethanol. J Am Diet Assoc. 2010;110(9):1307-21. doi: 10.1016/j.jada.2010.06.008. PubMed PMID: 20800122.
36. Kong MF, Chapman I, Goble E, Wishart J, Wittert G, Morris H, Horowitz M. Effects of oral fructose and glucose on plasma GLP-1 and appetite in normal subjects. Peptides. 1999;20(5):545-51. PubMed PMID: 10465505.
37. Yau AM, McLaughlin J, Gilmore W, Maughan RJ, Evans GH. The Acute Effects of Simple Sugar Ingestion on Appetite, Gut-Derived Hormone Response, and Metabolic Markers in Men. Nutrients. 2017;9(2). doi: 10.3390/nu9020135. PubMed PMID: 28216550; PMCID: PMC5331566.
38. Kuhre RE, Gribble FM, Hartmann B, Reimann F, Windelov JA, Rehfeld JF, Holst JJ. Fructose stimulates GLP-1 but not GIP secretion in mice, rats, and humans. Am J Physiol Gastrointest Liver Physiol. 2014;306(7):G622-30. doi: 10.1152/ajpgi.00372.2013. PubMed PMID: 24525020; PMCID: PMC3962593.
39. Gersch MS, Mu W, Cirillo P, Reungjui S, Zhang L, Roncal C, Sautin YY, Johnson RJ, Nakagawa T. Fructose, but not dextrose, accelerates the progression of chronic kidney disease. American journal of physiology Renal physiology. 2007;293(4):F1256-61. doi: 10.1152/ajprenal.00181.2007. PubMed PMID: 17670904.
40. Anton SD, Martin CK, Han H, Coulon S, Cefalu WT, Geiselman P, Williamson DA. Effects of stevia, aspartame, and sucrose on food intake, satiety, and postprandial glucose and insulin levels. Appetite. 2010;55(1):37-43. doi: 10.1016/j.appet.2010.03.009. PubMed PMID: 20303371; PMCID: PMC2900484.
41. Felice JI, Gangoiti MV, Molinuevo MS, McCarthy AD, Cortizo AM. Effects of a metabolic syndrome induced by a fructose-rich diet on bone metabolism in rats.

Metabolism. 2014;63(2):296-305. doi: 10.1016/j.metabol.2013.11.002. PubMed PMID: 24355623.
42. Wuest M, Trayner BJ, Grant TN, Jans HS, Mercer JR, Murray D, West FG, McEwan AJ, Wuest F, Cheeseman CI. Radiopharmacological evaluation of 6-deoxy-6-[18F]fluoro-D-fructose as a radiotracer for PET imaging of GLUT5 in breast cancer. Nucl Med Biol. 2011;38(4):461-75. doi: 10.1016/j.nucmedbio.2010.11.004. PubMed PMID: 21531283.
43. Tsanzi E, Fitch CW, Tou JC. Effect of consuming different caloric sweeteners on bone health and possible mechanisms. Nutr Rev. 2008;66(6):301-9. doi: 10.1111/j.1753-4887.2008.00037.x. PubMed PMID: 18522618.
44. Kontulainen SA, Hughes JM, Macdonald HM, Johnston JD. The biomechanical basis of bone strength development during growth. Med Sport Sci. 2007;51:13-32. doi: 10.1159/000103002. PubMed PMID: 17505117.
45. Rauch F, Travers R, Glorieux FH. Cellular activity on the seven surfaces of iliac bone: a histomorphometric study in children and adolescents. J Bone Miner Res. 2006;21(4):513-9. doi: 10.1359/jbmr.060108. PubMed PMID: 16598370.
46. Bonewald L. Mechanosensation and Transduction in Osteocytes. Bonekey Osteovision. 2006;3(10):7-15.
47. Alves RD, Demmers JA, Bezstarosti K, van der Eerden BC, Verhaar JA, Eijken M, van Leeuwen JP. Unraveling the human bone microenvironment beyond the classical extracellular matrix proteins: a human bone protein library. J Proteome Res. 2011;10(10):4725-33. doi: 10.1021/pr200522n. PubMed PMID: 21892838.
48. Delgado-Calle J, Arozamena J, Garcia-Renedo R, Garcia-Ibarbia C, Pascual-Carra MA, Gonzalez-Macias J, Riancho JA. Osteocyte deficiency in hip fractures. Calcif Tissue Int. 2011;89(4):327-34. doi: 10.1007/s00223-011-9522-0. PubMed PMID: 21874545.
49. Pi M, Quarles LD. Novel bone endocrine networks integrating mineral and energy metabolism. Curr Osteoporos Rep. 2013;11(4):391-9. doi: 10.1007/s11914-013-0178-8. PubMed PMID: 24193547; PMCID: PMC4011556.
50. Aubin J. Advances in the osteoblast lineage. Biochemistry and Cell Biology. 1998;76(6):899-910.
51. Bonucci E, Mocetti P, Silvestrini G, Ballanti P, Zalza S, Fortin M, Nanci A. The osteoblastic phenotype in calcium-depleted and calcium-repleted rats: a structural and histomorphometric study. Japanese Society of Electron Microscopy. 2001;50(4):333-47.
52. Elefteriou F, Yang X. Genetic mouse models for bone studies--strengths and limitations. Bone. 2011;49(6):1242-54. doi: 10.1016/j.bone.2011.08.021. PubMed PMID: 21907838; PMCID: 3331798.
53. Lian J, Stein G. Development of the Osteoblast Pheontype: Molecular Mechanisms Mediating Osteoblast Growth and Differentiation. The Iowa Orthopaedic Journal. 1995;15:118-40.
54. Bonjour JP. Calcium and phosphate: a duet of ions playing for bone health. J Am Coll Nutr. 2011;30(5 Suppl 1):438S-48S. PubMed PMID: 22081690.
55. Dallas SL, Bonewald LF. Dynamics of the transition from osteoblast to osteocyte. Ann N Y Acad Sci. 2010;1192:437-43. doi: 10.1111/j.1749-6632.2009.05246.x. PubMed PMID: 20392270; PMCID: PMC2981593.

56. Mc Garrigle MJ, Mullen CA, Haugh MG, Voisin MC, McNamara LM. Osteocyte differentiation and the formation of an interconnected cellular network in vitro. European cells & materials. 2016;31:323-40. PubMed PMID: 27215740.
57. Datta HK, Ng WF, Walker JA, Tuck SP, Varanasi SS. The cell biology of bone metabolism. J Clin Pathol. 2008;61(5):577-87. doi: 10.1136/jcp.2007.048868. PubMed PMID: 18441154.
58. Barragan-Adjemian C, Nicolella D, Dusevich V, Dallas MR, Eick JD, Bonewald LF. Mechanism by which MLO-A5 late osteoblasts/early osteocytes mineralize in culture: similarities with mineralization of lamellar bone. Calcif Tissue Int. 2006;79(5):340-53. doi: 10.1007/s00223-006-0107-2. PubMed PMID: 17115241; PMCID: PMC1802097.
59. Holmbeck K, Bianco P, Pidoux I, Inoue S, Billinghurst RC, Wu W, Chrysovergis K, Yamada S, Birkedal-Hansen H, Poole AR. The metalloproteinase MT1-MMP is required for normal development and maintenance of osteocyte processes in bone. J Cell Sci. 2005;118(Pt 1):147-56. doi: 10.1242/jcs.01581. PubMed PMID: 15601659.
60. Inoue Y, Segawa H, Kaneko I, Yamanaka S, Kusano K, Kawakami E, Furutani J, Ito M, Kuwahata M, Saito H, Fukushima N, Kato S, Kanayama HO, Miyamoto K. Role of the vitamin D receptor in FGF23 action on phosphate metabolism. Biochem J. 2005;390(Pt 1):325-31. doi: 10.1042/BJ20041799. PubMed PMID: 15885032; PMCID: PMC1184586.
61. Perwad F, Zhang MY, Tenenhouse HS, Portale AA. Fibroblast growth factor 23 impairs phosphorus and vitamin D metabolism in vivo and suppresses 25-hydroxyvitamin D-1alpha-hydroxylase expression in vitro. American journal of physiology Renal physiology. 2007;293(5):F1577-83. doi: 10.1152/ajprenal.00463.2006. PubMed PMID: 17699549.
62. Motyl KJ, McCabe LR, Schwartz AV. Bone and glucose metabolism: a two-way street. Arch Biochem Biophys. 2010;503(1):2-10. doi: 10.1016/j.abb.2010.07.030. PubMed PMID: 20682281; PMCID: PMC2946845.
63. Clemens TL, Karsenty G. The osteoblast: an insulin target cell controlling glucose homeostasis. J Bone Miner Res. 2011;26(4):677-80. doi: 10.1002/jbmr.321. PubMed PMID: 21433069.
64. Confavreux CB, Levine RL, Karsenty G. A paradigm of integrative physiology, the crosstalk between bone and energy metabolisms. Mol Cell Endocrinol. 2009;310(1-2):21-9. doi: 10.1016/j.mce.2009.04.004. PubMed PMID: 19376193; PMCID: PMC3667507.
65. Lanske B, Densmore MJ, Erben RG. Vitamin D endocrine system and osteocytes. BoneKEy reports. 2014;3:494. Epub 2014/03/08. doi: 10.1038/bonekey.2013.228. PubMed PMID: 24605211; PMCID: 3944125.
66. Buenzli PR, Sims NA. Quantifying the osteocyte network in the human skeleton. Bone. 2015;75:144-50. doi: 10.1016/j.bone.2015.02.016. PubMed PMID: 25708054.
67. Hannah KM, Thomas CD, Clement JG, De Carlo F, Peele AG. Bimodal distribution of osteocyte lacunar size in the human femoral cortex as revealed by micro-CT. Bone. 2010;47(5):866-71. doi: 10.1016/j.bone.2010.07.025. PubMed PMID: 20691298.
68. Weinstein RS, Manolagas SC. Apoptosis and osteoporosis. Am J Med. 2000;108(2):153-64. PubMed PMID: 11126309.
69. Bonewald LF, Johnson ML. Osteocytes, mechanosensing and Wnt signaling. Bone. 2008;42(4):606-15. doi: 10.1016/j.bone.2007.12.224. PubMed PMID: 18280232; PMCID: PMC2349095.

70. Di Nisio A, De Toni L, Speltra E, Rocca MS, Taglialavoro G, Ferlin A, Foresta C. Regulation of Sclerostin Production in Human Male Osteocytes by Androgens: Experimental and Clinical Evidence. Endocrinology. 2015;156(12):4534-44. doi: 10.1210/en.2015-1244. PubMed PMID: 26393301.
71. Knothe Tate ML, Niederer P, Knothe U. In vivo tracer transport through the lacunocanalicular system of rat bone in an environment devoid of mechanical loading. Bone. 1998;22(2):107-17. PubMed PMID: 9477233.
72. Vashishth D, Gibson G, Kimura J, Schaffler MB, Fyhrie DP. Determination of bone volume by osteocyte population. The Anatomical record. 2002;267(4):292-5. doi: 10.1002/ar.10114. PubMed PMID: 12124907.
73. Vashishth D, Verborgt O, Divine G, Schaffler MB, Fyhrie DP. Decline in osteocyte lacunar density in human cortical bone is associated with accumulation of microcracks with age. Bone. 2000;26(4):375-80. doi: 10.1016/S8756-3282(00)00236-2. PubMed PMID: 10719281.
74. Cashman KD. Milk Minerals (including trace elements) and bone health. International Dairy Journal 2006:1389-98.
75. Tucker KL. Vegetarian diets and bone status. Am J Clin Nutr. 2014;100 Suppl 1:329S-35S. doi: 10.3945/ajcn.113.071621. PubMed PMID: 24898237.
76. Foundation NO. 54 Million Americans Affected by Osteoporosis and Low Bone Mass. 2014.
77. Raff MC, Durand B, Gao FB. Cell number control and timing in animal development: the oligodendrocyte cell lineage. The International journal of developmental biology. 1998;42(3):263-7. PubMed PMID: 9654007.
78. Zhang Q, Riddle RC, Clemens TL. Bone and the regulation of global energy balance. J Intern Med. 2015;277(6):681-9. doi: 10.1111/joim.12348. PubMed PMID: 25597336; PMCID: PMC4446154.
79. Mackie EJ, Ahmed YA, Tatarczuch L, Chen KS, Mirams M. Endochondral ossification: how cartilage is converted into bone in the developing skeleton. Int J Biochem Cell Biol. 2008;40(1):46-62. doi: 10.1016/j.biocel.2007.06.009. PubMed PMID: 17659995.
80. Sissons HA, Kember NF. Longitudinal bone growth of the human femur. Postgrad Med J. 1977;53(622):433-7. PubMed PMID: 917957; PMCID: PMC2496732.
81. Russell M, Breggia A, Mendes N, Klibanski A, Misra M. Growth hormone is positively associated with surrogate markers of bone turnover during puberty. Clin Endocrinol (Oxf). 2011;75(4):482-8. doi: 10.1111/j.1365-2265.2011.04088.x. PubMed PMID: 21535073; PMCID: PMC3722873.
82. Parfitt AM. Misconceptions (1): epiphyseal fusion causes cessation of growth. Bone. 2002;30(2):337-9. PubMed PMID: 11856639.
83. Rizzoli R. Nutrition: its role in bone health. Best Pract Res Clin Endocrinol Metab. 2008;22(5):813-29. doi: 10.1016/j.beem.2008.08.005. PubMed PMID: 19028358.
84. Perry RJ, Farquharson C, Ahmed SF. The role of sex steroids in controlling pubertal growth. Clin Endocrinol (Oxf). 2008;68(1):4-15. doi: 10.1111/j.1365-2265.2007.02960.x. PubMed PMID: 17645565.
85. Courtland HW, Sun H, Beth-On M, Wu Y, Elis S, Rosen CJ, Yakar S. Growth hormone mediates pubertal skeletal development independent of hepatic IGF-1 production.

J Bone Miner Res. 2011;26(4):761-8. doi: 10.1002/jbmr.265. PubMed PMID: 20928887; PMCID: PMC3179330.
86. Mauras N, Bishop K, Welch S. Growth hormone action in puberty: effects by gender. Growth Horm IGF Res. 2007;17(6):463-71. doi: 10.1016/j.ghir.2007.04.011. PubMed PMID: 17566776.
87. Rizzoli R. Nutritional aspects of bone health. Best Pract Res Clin Endocrinol Metab. 2014;28(6):795-808. doi: 10.1016/j.beem.2014.08.003. PubMed PMID: 25432353.
88. Matar M, Al-Shaar L, Maalouf J, Nabulsi M, Arabi A, Choucair M, Tamim H, El-Hajj Fuleihan G. The Relationship Between Calciotropic Hormones, IGF-1, and Bone Mass Across Pubertal Stages. J Clin Endocrinol Metab. 2016;101(12):4860-70. doi: 10.1210/jc.2016-3071. PubMed PMID: 27676398.
89. Fritton JC, Emerton KB, Sun H, Kawashima Y, Mejia W, Wu Y, Rosen CJ, Panus D, Bouxsein M, Majeska RJ, Schaffler MB, Yakar S. Growth hormone protects against ovariectomy-induced bone loss in states of low circulating insulin-like growth factor (IGF-1). J Bone Miner Res. 2010;25(2):235-46. doi: 10.1359/jbmr.090723. PubMed PMID: 19619004; PMCID: PMC3153382.
90. Valerio G, Galle F, Mancusi C, Di Onofrio V, Colapietro M, Guida P, Liguori G. Pattern of fractures across pediatric age groups: analysis of individual and lifestyle factors. BMC Public Health. 2010;10:656. doi: 10.1186/1471-2458-10-656. PubMed PMID: 21034509; PMCID: PMC2987399.
91. Handel MN, Heitmann BL, Abrahamsen B. Nutrient and food intakes in early life and risk of childhood fractures: a systematic review and meta-analysis. Am J Clin Nutr. 2015;102(5):1182-95. doi: 10.3945/ajcn.115.108456. PubMed PMID: 26447151.
92. Goulding A. Risk factors for fractures in normally active children and adolescents. Med Sport Sci. 2007;51:102-20. doi: 10.1159/000103007. PubMed PMID: 17505122.
93. Clark EM. The epidemiology of fractures in otherwise healthy children. Curr Osteoporos Rep. 2014;12(3):272-8. doi: 10.1007/s11914-014-0227-y. PubMed PMID: 24973964.
94. Kodama Y, Miyakoshi N, Linkhart TA, Wergedal J, Srivastava A, Beamer W, Donahue LR, Rosen C, Baylink DJ, Farley J. Effects of dietary calcium depletion and repletion on dynamic determinants of tibial bone volume in two inbred strains of mice. Bone. 2000;27(3):445-52. PubMed PMID: 10962358.
95. Mangels AR. Bone nutrients for vegetarians. Am J Clin Nutr. 2014;100 Suppl 1:469S-75S. doi: 10.3945/ajcn.113.071423. PubMed PMID: 24898231.
96. Centeno V, de Barboza GD, Marchionatti A, Rodriguez V, Tolosa de Talamoni N. Molecular mechanisms triggered by low-calcium diets. Nutrition research reviews. 2009;22(2):163-74. Epub 2009/10/20. doi: 10.1017/S0954422409990126. PubMed PMID: 19835652.
97. Blair H, Schlesinger P, Huang C, Zaidi M. Calcium Signalling and Calcium Transport in Bone Disease. Subcell Biochem. 2007;45:539,62.
98. Heaney R, Abrams S, Dawson-Hughes B, Looker A, Marcus R, Matkovic V, Weaver C. Peak Bone Mass. Osteoporosis International. 2000;11:985-1009.
99. Miller G, Anderson JJ. The Role of Calcium In Prevention of Chronic Diseases. Journal of the American College of Nutrition. 1999;18(5):371S-2S.
100. Miller G, Jarvis J, McBean L. The Importance of Meeting Calcium Needs with Foods. Journal of the American College of Nutrition. 2001;20(2):168S-85S.

101. Zhu K, Prince RL. Calcium and bone. Clinical biochemistry. 2012;45(12):936-42. doi: 10.1016/j.clinbiochem.2012.05.006. PubMed PMID: 22609892.
102. Renkema KY, Alexander RT, Bindels RJ, Hoenderop JG. Calcium and phosphate homeostasis: concerted interplay of new regulators. Annals of medicine. 2008;40(2):82-91. Epub 2008/02/23. doi: 10.1080/07853890701689645. PubMed PMID: 18293139.
103. Haussler MR, Whitfield GK, Kaneko I, Haussler CA, Hsieh D, Hsieh JC, Jurutka PW. Molecular mechanisms of vitamin D action. Calcif Tissue Int. 2013;92(2):77-98. doi: 10.1007/s00223-012-9619-0. PubMed PMID: 22782502.
104. Juppner H. Phosphate and FGF-23. Kidney international Supplement. 2011(121):S24-7. Epub 2011/02/25. doi: 10.1038/ki.2011.27. PubMed PMID: 21346724; PMCID: 3257051.
105. Kirchner S, Muduli A, Casirola D, Prum K, Douard V, Ferraris RP. Luminal fructose inhibits rat intestinal sodium-phosphate cotransporter gene expression and phosphate uptake. The American Journal of Clinical Nutrition. 2008;87:1028-38.
106. Kornak U. Animal models with pathological mineralization phenotypes. Joint, bone, spine : revue du rhumatisme. 2011;78(6):561-7. doi: 10.1016/j.jbspin.2011.03.020. PubMed PMID: 21550285.
107. Dror DK, Allen LH. Dairy product intake in children and adolescents in developed countries: trends, nutritional contribution, and a review of association with health outcomes. Nutr Rev. 2014;72(2):68-81. doi: 10.1111/nure.12078. PubMed PMID: 24330063.
108. Nieves JW. Osteoporosis: the role of micronutrients. The American Journal of Clinical Nutrition. 2005;81(Suppl):1232S-9S.
109. Fleet JC, Schoch RD. Molecular mechanisms for regulation of intestinal calcium absorption by vitamin D and other factors. Crit Rev Clin Lab Sci. 2010;47(4):181-95. doi: 10.3109/10408363.2010.536429. PubMed PMID: 21182397; PMCID: 3235806.
110. Chow EC, Quach HP, Vieth R, Pang KS. Temporal changes in tissue 1alpha,25-dihydroxyvitamin D3, vitamin D receptor target genes, and calcium and PTH levels after 1,25(OH)2D3 treatment in mice. Am J Physiol Endocrinol Metab. 2013;304(9):E977-89. doi: 10.1152/ajpendo.00489.2012. PubMed PMID: 23482451.
111. Forrest KY, Stuhldreher WL. Prevalence and correlates of vitamin D deficiency in US adults. Nutr Res. 2011;31(1):48-54. doi: 10.1016/j.nutres.2010.12.001. PubMed PMID: 21310306.
112. Brommage R, Neuman WF. Mechanism of mobilization of bone mineral by 1,25-dihydroxyvitamin D3. American Journal of Physiology: Endocrinology. 1979;237(2):E113-E20.
113. Christakos S, Dhawan P, Porta A, Mady LJ, Seth T. Vitamin D and intestinal calcium absorption. Mol Cell Endocrinol. 2011;347(1-2):25-9. doi: 10.1016/j.mce.2011.05.038. PubMed PMID: 21664413; PMCID: 3405161.
114. Williams E, Bajaj D, Douard V, Sabbagh Y, Ferraris R, Fritton JC, editors. Relationships between the mechanical quality of bone and FGF23 levels in mice challenged by fructose and calcium modified diets. . Annual Meeting of the American Society of Biomechanics; 2013; Omaha, NE.
115. Douard V, Sabbagh Y, Lee J, Patel C, Kemp FW, Bogden JD, Lin S, Ferraris RP. Excessive fructose intake causes 1,25-(OH)2D3-dependent inhibition of intestinal and renal calcium transport in growing rats. Am J Physiol Endocrinol Metab. 2013. Epub

2013/04/11. doi: 10.1152/ajpendo.00582.2012. PubMed PMID: 23571713; PMCID: 3680696.
116. Douard V, Asgerally A, Sabbagh Y, Sugiura S, Shapses SA, Casirola D, Ferraris RP. Dietary fructose inhibits intestinal calcium absorption and induces vitamin D insufficiency in CKD. Journal of the American Society of Nephrology : JASN. 2010;21(2):261-71. doi: 10.1681/ASN.2009080795. PubMed PMID: 19959720; PMCID: 2834550.
117. Chesney RW. Interactions of vitamin D and the proximal tubule. Pediatr Nephrol. 2016;31(1):7-14. doi: 10.1007/s00467-015-3050-5. PubMed PMID: 25618772.
118. Douard V, Patel C, Lee J, Tharabenjasin P, Williams E, Fritton JC, Sabbagh Y, Ferraris RP. Chronic high fructose intake reduces serum 1,25 (OH)2D3 levels in calcium-sufficient rodents. PLoS One. 2014;9(4):e93611. doi: 10.1371/journal.pone.0093611. PubMed PMID: 24718641; PMCID: 3981704.
119. Black RE, Williams SM, Jones IE, Goulding A. Children who avoid drinking cow milk have low dietary calcium intakes and poor bone health. Am J Clin Nutr. 2002;76(3):675-80. PubMed PMID: 12198017.
120. Bolland MJ, Leung W, Tai V, Bastin S, Gamble GD, Grey A, Reid IR. Calcium intake and risk of fracture: systematic review. BMJ. 2015;351:h4580. doi: 10.1136/bmj.h4580. PubMed PMID: 26420387; PMCID: PMC4784799.
121. Lemay DG, Lynn DJ, Martin WF, Neville MC, Casey TM, Rincon G, Kriventseva EV, Barris WC, Hinrichs AS, Molenaar AJ, Pollard KS, Maqbool NJ, Singh K, Murney R, Zdobnov EM, Tellam RL, Medrano JF, German JB, Rijnkels M. The bovine lactation genome: insights into the evolution of mammalian milk. Genome Biol. 2009;10(4):R43. doi: 10.1186/gb-2009-10-4-r43. PubMed PMID: 19393040; PMCID: PMC2688934.
122. Pereira PC. Milk nutritional composition and its role in human health. Nutrition. 2014;30(6):619-27. doi: 10.1016/j.nut.2013.10.011. PubMed PMID: 24800664.
123. Kalkwarf HJ, Khoury JC, Lanphear BP. Milk intake during childhood and adolescence, adult bone density, and osteoporotic fractures in US women. Am J Clin Nutr. 2003;77(1):257-65. PubMed PMID: 12499350.
124. Baran D, Sorensen A, Grimes J, Lew R, Karellas A, Johnson B, Roche J. Dietary modification with dairy products for preventing vertebral bone loss in premenopausal women: a three-year prospective study. J Clin Endocrinol Metab. 1990;70(1):264-70. doi: 10.1210/jcem-70-1-264. PubMed PMID: 2294135.
125. Bonjour JP, Carrie AL, Ferrari S, Clavien H, Slosman D, Theintz G, Rizzoli R. Calcium-enriched foods and bone mass growth in prepubertal girls: a randomized, double-blind, placebo-controlled trial. J Clin Invest. 1997;99(6):1287-94. doi: 10.1172/JCI119287. PubMed PMID: 9077538; PMCID: PMC507944.
126. Goulding A, Rockell JE, Black RE, Grant AM, Jones IE, Williams SM. Children who avoid drinking cow's milk are at increased risk for prepubertal bone fractures. J Am Diet Assoc. 2004;104(2):250-3. doi: 10.1016/j.jada.2003.11.008. PubMed PMID: 14760576.
127. Davidsson L. Minerals and trace elements in infant nutrition. Acta Paediatr Suppl. 1994;83(395):38-42. PubMed PMID: 8025358.
128. Winzenberg T, Shaw K, Fryer J, Jones G. Effects of calcium supplementation on bone density in healthy children: meta-analysis of randomised controlled trials. BMJ.

2006;333(7572):775. doi: 10.1136/bmj.38950.561400.55. PubMed PMID: 16980314; PMCID: PMC1602024.
129. Weber J-M. Energy Cycle in Vertebrates. eLS: John Wiley & Sons, Ltd; 2001.
130. Daci E, van Cromphaut S, Bouillon R. Mechanisms influencing bone metabolism in chronic illness. Horm Res. 2002;58 Suppl 1:44-51. doi: 10.1159/000064758. PubMed PMID: 12373014.
131. Shapiro IM, Srinivas V. Metabolic consideration of epiphyseal growth: survival responses in a taxing environment. Bone. 2007;40(3):561-7. doi: 10.1016/j.bone.2006.09.030. PubMed PMID: 17157572; PMCID: PMC1941712.
132. Komarova SV, Ataullakhanov FI, Globus RK. Bioenergetics and mitochondrial transmembrane potential during differentiation of cultured osteoblasts. Am J Physiol Cell Physiol. 2000;279(4):C1220-9. doi: 10.1152/ajpcell.2000.279.4.C1220. PubMed PMID: 11003602.
133. Frikha-Benayed D, Basta-Pljakic J, Majeska RJ, Schaffler MB. Regional differences in oxidative metabolism and mitochondrial activity among cortical bone osteocytes. Bone. 2016;90:15-22. doi: 10.1016/j.bone.2016.05.011. PubMed PMID: 27260646; PMCID: PMC4970923.
134. Lancha A, Fruhbeck G, Gomez-Ambrosi J. Peripheral signalling involved in energy homeostasis control. Nutrition research reviews. 2012;25(2):223-48. doi: 10.1017/S0954422412000145. PubMed PMID: 23174510.
135. Mobasheri A. Glucose: an energy currency and structural precursor in articular cartilage and bone with emerging roles as an extracellular signaling molecule and metabolic regulator. Front Endocrinol (Lausanne). 2012;3:153. doi: 10.3389/fendo.2012.00153. PubMed PMID: 23251132; PMCID: PMC3523231.
136. Comninos AN, Jayasena CN, Dhillo WS. The relationship between gut and adipose hormones, and reproduction. Hum Reprod Update. 2014;20(2):153-74. doi: 10.1093/humupd/dmt033. PubMed PMID: 24173881.
137. Martos-Moreno GA, Chowen JA, Argente J. Metabolic signals in human puberty: effects of over and undernutrition. Mol Cell Endocrinol. 2010;324(1-2):70-81. doi: 10.1016/j.mce.2009.12.017. PubMed PMID: 20026379.
138. Takeda S, Elefteriou F, Levasseur R, Liu X, Zhao L, Parker KL, Armstrong D, Ducy P, Karsenty G. Leptin regulates bone formation via the sympathetic nervous system. Cell. 2002;111(3):305-17. PubMed PMID: 12419242.
139. Cheng HL, Amatoury M, Steinbeck K. Energy expenditure and intake during puberty in healthy nonobese adolescents: a systematic review. Am J Clin Nutr. 2016;104(4):1061-74. doi: 10.3945/ajcn.115.129205. PubMed PMID: 27629054.
140. Patel C, Sugimoto K, Douard V, Shah A, Inui H, Yamanouchi T, Ferraris RP. Effect of dietary fructose on portal and systemic serum fructose levels in rats and in KHK-/- and GLUT5-/- mice. Am J Physiol Gastrointest Liver Physiol. 2015;309(9):G779-90. doi: 10.1152/ajpgi.00188.2015. PubMed PMID: 26316589; PMCID: 4628968.
141. Le MT, Lanaspa MA, Cicerchi CM, Rana J, Scholten JD, Hunter BL, Rivard CJ, Randolph RK, Johnson RJ. Bioactivity-Guided Identification of Botanical Inhibitors of Ketohexokinase. PLoS One. 2016;11(6):e0157458. doi: 10.1371/journal.pone.0157458. PubMed PMID: 27322374; PMCID: PMC4913896.
142. Dempster DW, Compston JE, Drezner MK, Glorieux FH, Kanis JA, Malluche H, Meunier PJ, Ott SM, Recker RR, Parfitt AM. Standardized nomenclature, symbols, and

units for bone histomorphometry: a 2012 update of the report of the ASBMR Histomorphometry Nomenclature Committee. J Bone Miner Res. 2013;28(1):2-17. doi: 10.1002/jbmr.1805. PubMed PMID: 23197339; PMCID: 3672237.
143. Douard V, Suzuki T, Sabbagh Y, Lee J, Shapses S, Lin S, Ferraris RP. Dietary fructose inhibits lactation-induced adaptations in rat 1,25-(OH)(2)D(3) synthesis and calcium transport. FASEB J. 2012;26(2):707-21. doi: 10.1096/fj.11-190264. PubMed PMID: 22038050; PMCID: 3290445.
144. Persson P, Gagnemo-Persson R, Hakanson R. The effect of high or low dietary calcium on bone and calcium homeostasis in young male rats. Calcif Tissue Int. 1993;52(6):460-4. PubMed PMID: 8369995.
145. Viguet-Carrin S, Hoppler M, Membrez Scalfo F, Vuichoud J, Vigo M, Offord EA, Ammann P. Peak bone strength is influenced by calcium intake in growing rats. Bone. 2014;68:85-91. doi: 10.1016/j.bone.2014.07.029. PubMed PMID: 25102437.
146. Replogle RA, Li Q, Wang L, Zhang M, Fleet JC. Gene-by-diet interactions influence calcium absorption and bone density in mice. J Bone Miner Res. 2014;29(3):657-65. doi: 10.1002/jbmr.2065. PubMed PMID: 23955923.
147. Kasukawa Y, Baylink DJ, Wergedal JE, Amaar Y, Srivastava AK, Guo R, Mohan S. Lack of insulin-like growth factor I exaggerates the effect of calcium deficiency on bone accretion in mice. Endocrinology. 2003;144(11):4682-9. doi: 10.1210/en.2003-0745. PubMed PMID: 12960002.
148. Malik VS, Popkin BM, Bray GA, Despres JP, Willett WC, Hu FB. Sugar-sweetened beverages and risk of metabolic syndrome and type 2 diabetes: a meta-analysis. Diabetes Care. 2010;33(11):2477-83. doi: 10.2337/dc10-1079. PubMed PMID: 20693348; PMCID: PMC2963518.
149. Ma D, Jones G. Soft drink and milk consumption, physical activity, bone mass, and upper limb fractures in children: a population-based case-control study. Calcif Tissue Int. 2004;75(4):286-91. doi: 10.1007/s00223-004-0274-y. PubMed PMID: 15549642.
150. Wyshak G, Frisch RE. Carbonated beverages, dietary calcium, the dietary calcium/phosphorus ratio, and bone fractures in girls and boys. J Adolesc Health. 1994;15(3):210-5. PubMed PMID: 8075091.
151. Felice JI, Schurman L, McCarthy AD, Sedlinsky C, Aguirre JI, Cortizo AM. Effects of fructose-induced metabolic syndrome on rat skeletal cells and tissue, and their responses to metformin treatment. Diabetes Res Clin Pract. 2017;126:202-13. doi: 10.1016/j.diabres.2017.02.011. PubMed PMID: 28259010.
152. Tsanzi E, Light HR, Tou JC. The effect of feeding different sugar-sweetened beverages to growing female Sprague-Dawley rats on bone mass and strength. Bone. 2008;42(5):960-8. doi: 10.1016/j.bone.2008.01.020. PubMed PMID: 18328797.
153. Yarrow JF, Toklu HZ, Balaez A, Phillips EG, Otzel DM, Chen C, Wronski TJ, Aguirre JI, Sakarya Y, Tumer N, Scarpace PJ. Fructose consumption does not worsen bone deficits resulting from high-fat feeding in young male rats. Bone. 2016;85:99-106. doi: 10.1016/j.bone.2016.02.004. PubMed PMID: 26855373; PMCID: 4801515.
154. Bass EF, Baile CA, Lewis RD, Giraudo SQ. Bone quality and strength are greater in growing male rats fed fructose compared with glucose. Nutr Res. 2013;33(12):1063-71. doi: 10.1016/j.nutres.2013.08.006. PubMed PMID: 24267046.
155. Scriver CR. The metabolic and molecular bases of inherited disease. 6th ed. New York: McGraw-Hill, Health Professions Division; 1989.

156. Lasker M. Essential Frutosuria. Human Biology. 1941;13:51-63.
157. Patel C, Douard V, Yu S, Tharabenjasin P, Gao N, Ferraris RP. Fructose-induced increases in expression of intestinal fructolytic and gluconeogenic genes are regulated by GLUT5 and KHK. Am J Physiol Regul Integr Comp Physiol. 2015;309(5):R499-509. doi: 10.1152/ajpregu.00128.2015. PubMed PMID: 26084694; PMCID: 4591376.
158. Ishimoto T, Lanaspa MA, Le MT, Garcia GE, Diggle CP, Maclean PS, Jackman MR, Asipu A, Roncal-Jimenez CA, Kosugi T, Rivard CJ, Maruyama S, Rodriguez-Iturbe B, Sanchez-Lozada LG, Bonthron DT, Sautin YY, Johnson RJ. Opposing effects of fructokinase C and A isoforms on fructose-induced metabolic syndrome in mice. Proc Natl Acad Sci U S A. 2012;109(11):4320-5. doi: 10.1073/pnas.1119908109. PubMed PMID: 22371574; PMCID: PMC3306692.
159. Sugimoto K, Yamanouchi T. Assays of fructose in experimental nutrition. In: Preedy VR, editor. Dietary Sugars: Chemistry, Analysis, Function and Effects. 3 ed2012. p. 464-83.
160. Schindelin J, Arganda-Carreras I, Frise E, Kaynig V, Longair M, Pietzsch T, Preibisch S, Rueden C, Saalfeld S, Schmid B, Tinevez JY, White DJ, Hartenstein V, Eliceiri K, Tomancak P, Cardona A. Fiji: an open-source platform for biological-image analysis. Nat Methods. 2012;9(7):676-82. doi: 10.1038/nmeth.2019. PubMed PMID: 22743772; PMCID: 3855844.
161. Schmittgen TD, Livak KJ. Analyzing real-time PCR data by the comparative C(T) method. Nat Protoc. 2008;3(6):1101-8. PubMed PMID: 18546601.
162. Jang C, Hui S, Lu W, Cowan AJ, Morscher RJ, Lee G, Liu W, Tesz GJ, Birnbaum MJ, Rabinowitz JD. The Small Intestine Converts Dietary Fructose into Glucose and Organic Acids. Cell Metab. 2018;27(2):351-61 e3. doi: 10.1016/j.cmet.2017.12.016. PubMed PMID: 29414685.
163. Laron Z. Essential benign fructosuria. Arch Dis Child. 1961;36:273-7. PubMed PMID: 13759156; PMCID: PMC2012767.
164. Hirota Y, Nakagawa K, Mimatsu S, Sawada N, Sakaki T, Kubodera N, Kamao M, Tsugawa N, Suhara Y, Okano T. Nongenomic effects of 1alpha,25-dihydroxyvitamin D3 on cartilage formation deduced from comparisons between Cyp27b1 and Vdr knockout mice. Biochem Biophys Res Commun. 2017;483(1):359-65. doi: 10.1016/j.bbrc.2016.12.139. PubMed PMID: 28025137.
165. Panda DK, Miao D, Bolivar I, Li J, Huo R, Hendy GN, Goltzman D. Inactivation of the 25-hydroxyvitamin D 1alpha-hydroxylase and vitamin D receptor demonstrates independent and interdependent effects of calcium and vitamin D on skeletal and mineral homeostasis. The Journal of biological chemistry. 2004;279(16):16754-66. doi: 10.1074/jbc.M310271200. PubMed PMID: 14739296.
166. Panda DK, Miao D, Tremblay ML, Sirois J, Farookhi R, Hendy GN, Goltzman D. Targeted ablation of the 25-hydroxyvitamin D 1alpha -hydroxylase enzyme: evidence for skeletal, reproductive, and immune dysfunction. Proc Natl Acad Sci U S A. 2001;98(13):7498-503. doi: 10.1073/pnas.131029498. PubMed PMID: 11416220; PMCID: 34697.
167. Miller WL, Portale AA. Vitamin D 1 alpha-hydroxylase. Trends Endocrinol Metab. 2000;11(8):315-9. PubMed PMID: 10996526.

168. Miller WL. Genetic disorders of Vitamin D biosynthesis and degradation. J Steroid Biochem Mol Biol. 2017;165(Pt A):101-8. doi: 10.1016/j.jsbmb.2016.04.001. PubMed PMID: 27060335.
169. Petkovich M, Jones G. CYP24A1 and kidney disease. Curr Opin Nephrol Hypertens. 2011;20(4):337-44. doi: 10.1097/MNH.0b013e3283477a7b. PubMed PMID: 21610497.
170. Jatkar A, Kurland IJ, Judex S. Diets High in Fat or Fructose Differentially Modulate Bone Health and Lipid Metabolism. Calcif Tissue Int. 2017;100(1):20-8. doi: 10.1007/s00223-016-0205-8. PubMed PMID: 27832314; PMCID: 5217484.
171. Ritze Y, Bardos G, D'Haese JG, Ernst B, Thurnheer M, Schultes B, Bischoff SC. Effect of high sugar intake on glucose transporter and weight regulating hormones in mice and humans. PLoS One. 2014;9(7):e101702. doi: 10.1371/journal.pone.0101702. PubMed PMID: 25010715; PMCID: PMC4092057.
172. Tran LT, Yuen VG, McNeill JH. The fructose-fed rat: a review on the mechanisms of fructose-induced insulin resistance and hypertension. Mol Cell Biochem. 2009;332(1-2):145-59. doi: 10.1007/s11010-009-0184-4. PubMed PMID: 19536638.
173. Gupta BP, Thakur N, Jain NP, Banweer J, Jain S. Osmotically controlled drug delivery system with associated drugs. J Pharm Pharm Sci. 2010;13(4):571-88. PubMed PMID: 21486532.
174. Roscoe B. Jackson Memorial Laboratory., Green EL. Biology of the laboratory mouse. 2d ed. New York,: Blakiston Division; 1966. xii, 706 p. p.
175. Ryan ZC, Ketha H, McNulty MS, McGee-Lawrence M, Craig TA, Grande JP, Westendorf JJ, Singh RJ, Kumar R. Sclerostin alters serum vitamin D metabolite and fibroblast growth factor 23 concentrations and the urinary excretion of calcium. Proc Natl Acad Sci U S A. 2013;110(15):6199-204. doi: 10.1073/pnas.1221255110. PubMed PMID: 23530237; PMCID: PMC3625358.
176. Lode A, Bernhardt A, Gelinsky M. Cultivation of human bone marrow stromal cells on three-dimensional scaffolds of mineralized collagen: influence of seeding density on colonization, proliferation and osteogenic differentiation. Journal of tissue engineering and regenerative medicine. 2008;2(7):400-7. doi: 10.1002/term.110. PubMed PMID: 18756590.
177. Caplan A. Adult Mesenchymal Stem Cells for Tissue Engineering Versus Regenerative Medicine. Journal of Cellular Physiology. 2007;213:341-7. doi: 10.1002/jcp.21200
10.1002/JCP.
178. Liu LF, Shen WJ, Zhang ZH, Wang LJ, Kraemer FB. Adipocytes decrease Runx2 expression in osteoblastic cells: roles of PPARgamma and adiponectin. J Cell Physiol. 2010;225(3):837-45. doi: 10.1002/jcp.22291. PubMed PMID: 20589837.
179. Legeza B, Balazs Z, Odermatt A. Fructose promotes the differentiation of 3T3-L1 adipocytes and accelerates lipid metabolism. FEBS Lett. 2014;588(3):490-6. doi: 10.1016/j.febslet.2013.12.014. PubMed PMID: 24374344.
180. Patel J, Iyer A, Brown L. Evaluation of the chronic complications of diabetes in a high fructose diet in rats. Indian J Biochem Biophys. 2009;46(1):66-72. PubMed PMID: 19374256.
181. Aydin S, Aksoy A, Aydin S, Kalayci M, Yilmaz M, Kuloglu T, Citil C, Catak Z. Today's and yesterday's of pathophysiology: biochemistry of metabolic syndrome and

animal models. Nutrition. 2014;30(1):1-9. doi: 10.1016/j.nut.2013.05.013. PubMed PMID: 24290591.
182. Islam MS, Venkatesan V. Experimentally-Induced Animal Models of Prediabetes and Insulin Resistance: A Review. Acta Pol Pharm. 2016;73(4):827-34. PubMed PMID: 29648707.
183. Parthasarathy LS, Khadilkar VV, Chiplonkar SA, Zulf Mughal M, Khadilkar AV. Bone status of Indian children and adolescents with type 1 diabetes mellitus. Bone. 2016;82:16-20. doi: 10.1016/j.bone.2015.04.050. PubMed PMID: 25956533.
184. Thrailkill KM, Jo CH, Cockrell GE, Moreau CS, Fowlkes JL. Enhanced excretion of vitamin D binding protein in type 1 diabetes: a role in vitamin D deficiency? J Clin Endocrinol Metab. 2011;96(1):142-9. doi: 10.1210/jc.2010-0980. PubMed PMID: 20943786; PMCID: 3038488.
185. Stolzing A, Sellers D, Llewelyn O, Scutt A. Diabetes induced changes in rat mesenchymal stem cells. Cells, tissues, organs. 2010;191(6):453-65. Epub 2010/02/05. doi: 10.1159/000281826. PubMed PMID: 20130391.
186. Schwartz AV, Sellmeyer DE, Ensrud KE, Cauley JA, Tabor HK, Schreiner PJ, Jamal SA, Black DM, Cummings SR. Older women with diabetes have an increased risk of fracture: a prospective study. J Clin Endocrinol Metab. 2001;86(1):32-8. Epub 2001/03/07. doi: 10.1210/jcem.86.1.7139. PubMed PMID: 11231974.
187. Schwartz AV. Diabetes Mellitus: Does it Affect Bone? Calcif Tissue Int. 2003;73(6):515-9. Epub 2003/10/01. doi: 10.1007/s00223-003-0023-7. PubMed PMID: 14517715.
188. Leslie WD, Rubin MR, Schwartz AV, Kanis JA. Type 2 diabetes and bone. J Bone Miner Res. 2012;27(11):2231-7. Epub 2012/10/02. doi: 10.1002/jbmr.1759. PubMed PMID: 23023946.
189. Nykjaer A, Dragun D, Walther D, Vorum H, Jacobsen C, Herz J, Melsen F, Christensen EI, Willnow TE. An endocytic pathway essential for renal uptake and activation of the steroid 25-(OH) vitamin D3. Cell. 1999;96(4):507-15. PubMed PMID: 10052453.
190. Reinke DC, Kogawa M, Barratt KR, Morris HA, Anderson PH, Atkins GJ. Evidence for altered osteoclastogenesis in splenocyte cultures from Cyp27b1 knockout mice. J Steroid Biochem Mol Biol. 2016;164:353-60. doi: 10.1016/j.jsbmb.2015.11.015. PubMed PMID: 26639637.
191. Schalkwijk CG, Stehouwer CD, van Hinsbergh VW. Fructose-mediated non-enzymatic glycation: sweet coupling or bad modification. Diabetes/metabolism research and reviews. 2004;20(5):369-82. doi: 10.1002/dmrr.488. PubMed PMID: 15343583.
192. Goulding A, Grant AM, Williams SM. Bone and body composition of children and adolescents with repeated forearm fractures. J Bone Miner Res. 2005;20(12):2090-6. doi: 10.1359/JBMR.050820. PubMed PMID: 16294262.
193. Goulding A, Taylor RW, Jones IE, McAuley KA, Manning PJ, Williams SM. Overweight and obese children have low bone mass and area for their weight. Int J Obes Relat Metab Disord. 2000;24(5):627-32. PubMed PMID: 10849586.
194. Dimitri P, Wales JK, Bishop N. Fat and bone in children: differential effects of obesity on bone size and mass according to fracture history. J Bone Miner Res. 2010;25(3):527-36. doi: 10.1359/jbmr.090823. PubMed PMID: 19778184.

195. Valerio G, Galle F, Mancusi C, Di Onofrio V, Guida P, Tramontano A, Ruotolo E, Liguori G. Prevalence of overweight in children with bone fractures: a case control study. BMC Pediatr. 2012;12:166. doi: 10.1186/1471-2431-12-166. PubMed PMID: 23088687; PMCID: PMC3502372.
196. Patel C, Douard V, Yu S, Gao N, Ferraris RP. Transport, metabolism, and endosomal trafficking-dependent regulation of intestinal fructose absorption. FASEB J. 2015;29(9):4046-58. doi: 10.1096/fj.15-272195. PubMed PMID: 26071406; PMCID: 4550372.
197. Tharabenjasin P, Douard V, Patel C, Krishnamra N, Johnson RJ, Zuo J, Ferraris RP. Acute interactions between intestinal sugar and calcium transport in vitro. Am J Physiol Gastrointest Liver Physiol. 2014;306(1):G1-12. doi: 10.1152/ajpgi.00263.2013. PubMed PMID: 24177030.
198. Rodriguez WA, Horne CA, Mondragon AN, Phelps DD. Comparable dose-response functions for the effects of glucose and fructose on memory. Behav Neural Biol. 1994;61(2):162-9. PubMed PMID: 8204081.
199. Messier C, Whately K, Liang J, Du L, Puissant D. The effects of a high-fat, high-fructose, and combination diet on learning, weight, and glucose regulation in C57BL/6 mice. Behav Brain Res. 2007;178(1):139-45. doi: 10.1016/j.bbr.2006.12.011. PubMed PMID: 17222919.
200. Douard V, Sabbagh Y, Lee J, Patel C, Kemp FW, Bogden JD, Lin S, Ferraris RP. Excessive fructose intake causes 1,25-(OH)(2)D(3)-dependent inhibition of intestinal and renal calcium transport in growing rats. Am J Physiol Endocrinol Metab. 2013;304(12):E1303-13. doi: 10.1152/ajpendo.00582.2012. PubMed PMID: 23571713; PMCID: 3680696.
201. Ormsby RT, Findlay DM, Kogawa M, Anderson PH, Morris HA, Atkins GJ. Analysis of vitamin D metabolism gene expression in human bone: evidence for autocrine control of bone remodelling. J Steroid Biochem Mol Biol. 2014;144 Pt A:110-3. doi: 10.1016/j.jsbmb.2013.09.016. PubMed PMID: 24120913.
202. Zhou S, LeBoff MS, Glowacki J. Vitamin D metabolism and action in human bone marrow stromal cells. Endocrinology. 2010;151(1):14-22. doi: 10.1210/en.2009-0969. PubMed PMID: 19966181; PMCID: PMC2803155.
203. Geng S, Zhou S, Glowacki J. Effects of 25-hydroxyvitamin D(3) on proliferation and osteoblast differentiation of human marrow stromal cells require CYP27B1/1alpha-hydroxylase. J Bone Miner Res. 2011;26(5):1145-53. doi: 10.1002/jbmr.298. PubMed PMID: 21542014; PMCID: PMC3179303.
204. Zhu L, Baker RD, Baker SS. Gut microbiome and nonalcoholic fatty liver diseases. Pediatr Res. 2015;77(1-2):245-51. doi: 10.1038/pr.2014.157. PubMed PMID: 25310763.
205. Weaver CM. Diet, gut microbiome, and bone health. Curr Osteoporos Rep. 2015;13(2):125-30. doi: 10.1007/s11914-015-0257-0. PubMed PMID: 25616772; PMCID: PMC4996260.
206. Ohlsson C, Sjogren K. Effects of the gut microbiota on bone mass. Trends Endocrinol Metab. 2015;26(2):69-74. doi: 10.1016/j.tem.2014.11.004. PubMed PMID: 25497348.
207. Sjogren K, Engdahl C, Henning P, Lerner UH, Tremaroli V, Lagerquist MK, Backhed F, Ohlsson C. The gut microbiota regulates bone mass in mice. J Bone Miner Res.

2012;27(6):1357-67. doi: 10.1002/jbmr.1588. PubMed PMID: 22407806; PMCID: PMC3415623.
208. Arumugam M, Raes J, Pelletier E, Le Paslier D, Yamada T, Mende DR, Fernandes GR, Tap J, Bruls T, Batto JM, Bertalan M, Borruel N, Casellas F, Fernandez L, Gautier L, Hansen T, Hattori M, Hayashi T, Kleerebezem M, Kurokawa K, Leclerc M, Levenez F, Manichanh C, Nielsen HB, Nielsen T, Pons N, Poulain J, Qin J, Sicheritz-Ponten T, Tims S, Torrents D, Ugarte E, Zoetendal EG, Wang J, Guarner F, Pedersen O, de Vos WM, Brunak S, Dore J, Meta HITC, Antolin M, Artiguenave F, Blottiere HM, Almeida M, Brechot C, Cara C, Chervaux C, Cultrone A, Delorme C, Denariaz G, Dervyn R, Foerstner KU, Friss C, van de Guchte M, Guedon E, Haimet F, Huber W, van Hylckama-Vlieg J, Jamet A, Juste C, Kaci G, Knol J, Lakhdari O, Layec S, Le Roux K, Maguin E, Merieux A, Melo Minardi R, M'Rini C, Muller J, Oozeer R, Parkhill J, Renault P, Rescigno M, Sanchez N, Sunagawa S, Torrejon A, Turner K, Vandemeulebrouck G, Varela E, Winogradsky Y, Zeller G, Weissenbach J, Ehrlich SD, Bork P. Enterotypes of the human gut microbiome. Nature. 2011;473(7346):174-80. doi: 10.1038/nature09944. PubMed PMID: 21508958; PMCID: PMC3728647.
209. Di Luccia B, Crescenzo R, Mazzoli A, Cigliano L, Venditti P, Walser JC, Widmer A, Baccigalupi L, Ricca E, Iossa S. Rescue of Fructose-Induced Metabolic Syndrome by Antibiotics or Faecal Transplantation in a Rat Model of Obesity. PLoS One. 2015;10(8):e0134893. doi: 10.1371/journal.pone.0134893. PubMed PMID: 26244577; PMCID: PMC4526532.
210. Tian G, Wu X, Chen D, Yu B, He J. Adaptation of gut microbiome to different dietary nonstarch polysaccharide fractions in a porcine model. Mol Nutr Food Res. 2017;61(10). doi: 10.1002/mnfr.201700012. PubMed PMID: 28586175.
211. Guss JD, Horsfield MW, Fontenele FF, Sandoval TN, Luna M, Apoorva F, Lima SF, Bicalho RC, Singh A, Ley RE, van der Meulen MC, Goldring SR, Hernandez CJ. Alterations to the Gut Microbiome Impair Bone Strength and Tissue Material Properties. J Bone Miner Res. 2017;32(6):1343-53. doi: 10.1002/jbmr.3114. PubMed PMID: 28244143; PMCID: PMC5466506.
212. Du J, Wei X, Ge X, Chen Y, Li YC. Microbiota-Dependent Induction of Colonic Cyp27b1 Is Associated With Colonic Inflammation: Implications of Locally Produced 1,25-Dihydroxyvitamin D3 in Inflammatory Regulation in the Colon. Endocrinology. 2017;158(11):4064-75. doi: 10.1210/en.2017-00578. PubMed PMID: 28938443.
213. Younes H, Demigne C, Remesy C. Acidic fermentation in the caecum increases absorption of calcium and magnesium in the large intestine of the rat. Br J Nutr. 1996;75(2):301-14. PubMed PMID: 8785206.
214. Hansen M, Baunsgaard D, Autrup H, Vogel UB, Moller P, Lindecrona R, Wallin H, Poulsen HE, Loft S, Dragsted LO. Sucrose, glucose and fructose have similar genotoxicity in the rat colon and affect the metabolome. Food Chem Toxicol. 2008;46(2):752-60. doi: 10.1016/j.fct.2007.09.110. PubMed PMID: 17988776.
215. Morohashi T, Sano T, Ohta A, Yamada S. True calcium absorption in the intestine is enhanced by fructooligosaccharide feeding in rats. J Nutr. 1998;128(10):1815-8. doi: 10.1093/jn/128.10.1815. PubMed PMID: 9772155.
216. van den Heuvel EG, Muys T, van Dokkum W, Schaafsma G. Oligofructose stimulates calcium absorption in adolescents. Am J Clin Nutr. 1999;69(3):544-8. doi: 10.1093/ajcn/69.3.544. PubMed PMID: 10075343.

217. Takahara S, Morohashi T, Sano T, Ohta A, Yamada S, Sasa R. Fructooligosaccharide consumption enhances femoral bone volume and mineral concentrations in rats. J Nutr. 2000;130(7):1792-5. doi: 10.1093/jn/130.7.1792. PubMed PMID: 10867052.
218. Ohta A, Uehara M, Sakai K, Takasaki M, Adlercreutz H, Morohashi T, Ishimi Y. A combination of dietary fructooligosaccharides and isoflavone conjugates increases femoral bone mineral density and equol production in ovariectomized mice. J Nutr. 2002;132(7):2048-54. doi: 10.1093/jn/132.7.2048. PubMed PMID: 12097691.
219. Jilka RL. The relevance of mouse models for investigating age-related bone loss in humans. J Gerontol A Biol Sci Med Sci. 2013;68(10):1209-17. doi: 10.1093/gerona/glt046. PubMed PMID: 23689830; PMCID: PMC3779631.
220. Glendinning JI, Breinager L, Kyrillou E, Lacuna K, Rocha R, Sclafani A. Differential effects of sucrose and fructose on dietary obesity in four mouse strains. Physiol Behav. 2010;101(3):331-43. doi: 10.1016/j.physbeh.2010.06.003. PubMed PMID: 20600198; PMCID: PMC2930118.
221. Bachmanov AA, Reed DR, Beauchamp GK, Tordoff MG. Food intake, water intake, and drinking spout side preference of 28 mouse strains. Behav Genet. 2002;32(6):435-43. PubMed PMID: 12467341; PMCID: PMC1397713.
222. Weinstein RS, Jilka RL, Parfitt AM, Manolagas SC. Inhibition of osteoblastogenesis and promotion of apoptosis of osteoblasts and osteocytes by glucocorticoids. Potential mechanisms of their deleterious effects on bone. J Clin Invest. 1998;102(2):274-82. doi: 10.1172/JCI2799. PubMed PMID: 9664068; PMCID: PMC508885.
223. Herrlich S, Spieth S, Messner S, Zengerle R. Osmotic micropumps for drug delivery. Adv Drug Deliv Rev. 2012;64(14):1617-27. doi: 10.1016/j.addr.2012.02.003. PubMed PMID: 22370615.
224. Rose S, Nelson JF. A continuous long-term injector. Aust J Exp Biol Med Sci. 1955;33(4):415-9. PubMed PMID: 13269346.
225. Keraliya RA, Patel C, Patel P, Keraliya V, Soni TG, Patel RC, Patel MM. Osmotic drug delivery system as a part of modified release dosage form. ISRN Pharm. 2012;2012:528079. doi: 10.5402/2012/528079. PubMed PMID: 22852100; PMCID: PMC3407637.
226. Santus G, Baker RW. Osmotic Drug Delivery: A Review of the Patient Literature. Journal of Controlled Release. 1995;35:1-21.
227. Chaikomin R, Wu KL, Doran S, Meyer JH, Jones KL, Feinle-Bisset C, Horowitz M, Rayner CK. Effects of mid-jejunal compared to duodenal glucose infusion on peptide hormone release and appetite in healthy men. Regul Pept. 2008;150(1-3):38-42. doi: 10.1016/j.regpep.2008.02.006. PubMed PMID: 18396340.
228. Seino Y, Ogata H, Maekawa R, Izumoto T, Iida A, Harada N, Miki T, Seino S, Inagaki N, Tsunekawa S, Oiso Y, Hamada Y. Fructose induces glucose-dependent insulinotropic polypeptide, glucagon-like peptide-1 and insulin secretion: Role of adenosine triphosphate-sensitive K(+) channels. J Diabetes Investig. 2015;6(5):522-6. doi: 10.1111/jdi.12356. PubMed PMID: 26417408; PMCID: PMC4578490.

Acknowledgement of Previous Publications

Several sections of this dissertation and related research have been published in peer-reviewed journals and/or presented at scientific conferences.

Peer- reviewed journal publications:

Williams, EAJ, Douard, V, Sugimoto, K, Inui, H, Devime, F, Zhang, X, Kishida, K, Ferraris, RP, Fritton, JC, "Bone growth is influenced by fructose in adolescent male mice lacking ketohexokinase (khk)," *Calcified Tissue International*, 2019 (submitted)

Zhang, X, Grosfeld, A, Williams, EAJ, Vasiliauskas, D, Barretto, S, Smith, L, Devime, F, Philippe, C, Mariadassou, M, Melchior, C, Gourcerol, G, Dourmap, N, Blottiere, MH, Heberden, C, Gerard, P, Rehfeld, JF, Ferraris, RP, Fritton, JC, Ellero-Simatos, S, Douard, V, "Fructose malabsorption induces cholecystokinin (ckk) expression in the ileum and ceacum by changing microbiota composition and metabolism," *The FASEB Journal*, accepted (February 19, 2019).

Nguyen, KH, Xu, F, Flowers, S, Williams, EAJ, Fritton, JC, Moran, E, "SWI/SNF mediated lineage determination in mesenchymal stem cells confers resistance to osteoporosis," *Stem Cells*, 33(10):3028, 2015. http://dx.doi.org/10.1002/stem.2064

Rutgers SOAR: https://doi.org/doi:10.7282/T3NC647V

Douard, V, Patel, C, Lee, J, Tharabenjasin, P, Williams, EAJ, Fritton, JC, Sabbagh, Y, Ferraris, RP, "Chronic high-fructose intake reduces serum 1,25 (OH)2D3 levels in calcium sufficient rodents," *PLOS ONE*, 9(4):e93611, 2014. http://dx.doi.org/10.1371/journal.pone.0093611

Rutgers SOAR: https://doi.org/doi:10.7282/T30P132H

Conference presentations:

Geissler, JR, Ball, JR, Williams, EAJ, Allen, MR, Burr, DB, Fritton, JC, "Long-term alendronate exacerbates the effects of aging on the dynamic mechanical properties of cortical bone tissue," Annual Meeting, Austin, TX, *Transactions of the Orthopaedic Research Society*, Presentation Number:45:0341, 2019. https://www.ors.org/Transactions/65/0341

Zhang, X, Williams, EAJ, Devime, F, Maximin, E, Mariadassou, M, Abraham, A, Blottiere, H, Heberden, C, Ferraris, RP, Fritton, JC, Douard, V, "Fructose malabsorption regulates the identity of the L-cells by activating cck expression in those cells in the distal gastrointestinal tract," Club d'Etudes des Cellules Epitheliales Digestives, Marseille, Provence, France, 2018.

Williams, EAJ, Sugimoto, K, Douard, V, Ferraris, RP, Fritton, JC, "Bone morphology and mechanical properties in mice challenged with low calcium and high fructose diets," 5th Annual Musculoskeletal Repair and Regeneration Symposium, Albert Einstein College of

Medicine, Bronx, NY, 2016. http://www.einstein.yu.edu/departments/orthopaedic-surgery/symposium/5/

Flowers, S, Nguyen, KH, Xu, F, Himelman, E, Williams, EAJ, Fritton, JC, Moran, E, "SWI/SNF-mediated lineage determination in mesenchymal stem cells confers resistance to osteoporosis," American Society for Bone and Mineral Research Annual Meeting, Seattle, WA, *Journal of Bone and Mineral Research*, MO0211, 2015. http://www.asbmr.org/education/2015-abstracts

Williams, EAJ, Douard, V, Lomuti, JM, Ferraris, R, Fritton, JC, "Fructose upregulates FGF23 expression in MC3T3 pre-osteoblasts," Annual Meeting, New Orleans, LA, *Transactions of the Orthopaedic Research Society*, 39:0560, 2014. https://www.ors.org/Transactions/60/0560.pdf

Conference presentations (continued, † denotes an award):

Williams, EAJ, Bajaj, D, Douard, V, Sabbagh, Y, Ferraris, R, Fritton, JC, "Relationships between the mechanical quality of bone and FGF23 levels in mice challenged by fructose and calcium modified diets," Annual Meeting of the American Society of Biomechanics, Omaha, NE, 2013. http://www.asbweb.org/conferences/2013/abstracts/392.pdf

†Williams, EAJ, Douard, V, Bajaj, D, Sabbagh, Y, Ferraris, R, Fritton, JC, "Relationships between cortical bone quality and serum FGF23 in growing mice challenged by low calcium and high fructose in the diet," American Society for Bone and Mineral Research Annual Meeting, Baltimore, MD, *Journal of Bone and Mineral Research*, SA0052, 2013. Poster chosen for MARC Award. http://www.asbmr.org/education/2013-abstracts

Williams, EAJ, Douard, V, Bajaj, D, Sabbagh, Y, Ferraris, R, Fritton, JC, "Relationships between cortical bone mechanical quality and serum in mice challenged by low calcium and high fructose diet," 2nd Annual Musculoskeletal Repair and Regeneration Symposium, Albert Einstein College of Medicine, Bronx, NY, 2013. http://www.einstein.yu.edu/departments/orthopaedic-surgery/symposium/2/

Williams, EAJ, Douard, V, Bajaj, D, Sabbagh, Y, Ferraris, R, Fritton, JC, "Low calcium and high fructose diet diminish the quality of circumferential long-bone growth," 39th Annual Northeast Bioengineering Conference, Syracuse, NY, 227-8, 2013. http:\\doi.org\10.1109/NEBEC.2013.109

†Williams, EAJ, Bajaj, D, Sabbagh, Y, Douard, V, Ferraris, R, Fritton, JC, "Low calcium and high fructose diet diminish the quality of circumferential long-bone growth," American Society for Bone and Mineral Research Annual Meeting, Minneapolis, MN, *Journal of Bone and Mineral Research,* MO0032, 2012. Poster chosen for MARC Award. http://www.asbmr.org/education/2012-abstracts